OCS Study
BOEM 2018-010

Modeling At-Sea Density of Marine Birds to Support Atlantic Marine Renewable Energy Planning

Final Report

US Department of the Interior
Bureau of Ocean Energy Management
Office of Renewable Energy Programs

BOEM
Bureau of Ocean Energy Management

OCS Study
BOEM 2018-010

Modeling At-Sea Density of Marine Birds to Support Atlantic Marine Renewable Energy Planning

Final Report

Authors

Arliss J. Winship, Brian P. Kinlan, Timothy P. White, Jeffery B. Leirness, John Christensen

Prepared under NCCOS IAA MOA-2013-046-8696, BOEM OCS Study 2018-010, and NCCOS BOEM IAA M13PG00005
by
U.S. Department of Commerce
National Oceanic and Atmospheric Administration
National Ocean Service
National Centers for Coastal Ocean Science
Marine Spatial Ecology Division
Biogeography Branch
1305 East-West Hwy, SSMC-4, N/SCI-1
Silver Spring, MD 20910

Published by
U.S. Department of the Interior
Bureau of Ocean Energy Management
Office of Renewable Energy Programs
June 2018

DISCLAIMER

This study was funded, in part, by the US Department of the Interior, Bureau of Ocean Energy Management (BOEM), Environmental Studies Program, Washington, DC, through Inter-Agency Agreement Number M13PG00005 with the US Department of Commerce, National Oceanic and Atmospheric Administration, National Ocean Service, National Centers for Coastal Ocean Science, Silver Spring, MD. This report has been technically reviewed by BOEM and it has been approved for publication. The views and conclusions contained in this document are those of the authors and should not be interpreted as representing the opinions or policies of the US Government, nor does mention of trade names or commercial products constitute endorsement or recommendation for use.

REPORT AVAILABILITY

To download a PDF file of this Environmental Studies Program report, go to the US Department of the Interior, Bureau of Ocean Energy Management, Environmental Studies Program Information System website and search on OCS Study BOEM 2018-010. You may request the report from the BOEM Office of Renewable Energy Programs. The contact information is:

U.S. Department of the Interior
Bureau of Ocean Energy Management
Office of Renewable Energy Programs
45600 Woodland Road, VAM-OREP
Sterling, VA 20166

CITATION

A.J. Winship, B.P. Kinlan, T.P. White, J.B. Leirness, and J. Christensen. 2018. Modeling At-Sea Density of Marine Birds to Support Atlantic Marine Renewable Energy Planning: Final Report. U.S. Department of the Interior, Bureau of Ocean Energy Management, Office of Renewable Energy Programs, Sterling, VA. OCS Study BOEM 2018-010. x+67 pp.

ABOUT THE COVER

Cover photo (Herring Gull) courtesy of David Pereksta (BOEM). Used with permission.

ACKNOWLEDGEMENTS

We thank the many scientists who collected and contributed the survey data analyzed in this study. We are grateful to Allan O'Connell, Mark Wimer, Allison Sussman, Tim Jones, Kaycee Coleman, Kyle Dettloff, and Robert Fowler for processing and providing the data in the Northwest Atlantic Seabird Catalog (formerly Avian Compendium) database and to Carina Gjerdrum (Canadian Wildlife Service, Environment and Climate Change Canada) for providing the Eastern Canada Seabirds at Sea survey data. We thank Peter Cornillon, Michael Coyne, Peter Miller, and Matthew Poti for providing and helping with the processing of environmental predictor data. We thank Robert Rankin for initial development of the modeling framework and computer code, and we thank Zhifa Liu for execution of the models on high performance computing systems. We are grateful to Todd Callaghan, Andrew Gilbert, Carina Gjerdrum, Wing Goodale, Holly Goyert, Christopher Haney, Kevin Powers, Caleb Spiegel, and David Wiley for helpful feedback on the maps that improved this report. We thank David Bigger and Mary Boatman for comments and suggestions that improved this report. This project was funded by the Bureau of Ocean Energy Management (BOEM) through Intra-agency Agreement M11PG00059 with the United States Geological Survey (USGS) and Inter-agency Agreement M13PG00005 with the U.S. Department of Commerce, National Oceanic and Atmospheric Administration, National Ocean Service, National Centers for Coastal Ocean Science (NCCOS), and by the United States Geological Survey through Inter-agency Agreement G13PG00008 with NCCOS. Arliss Winship, Timothy White, and Jeffery Leirness were supported by NOAA Contracts No. DG133C07NC0616 and EA-133C-14-NC-1384 with CSS, Inc. (formerly CSS-Dynamac).

Executive Summary

Marine birds have the potential to be affected by human activities in the ocean environment such as offshore wind energy development. This report describes a project that developed maps of the spatial distributions of marine bird species in U.S. Atlantic Outer Continental Shelf (OCS) waters that can be used to aid ocean planning in the region and guide future data collection efforts.

Sighting survey data from over three decades contained in the 'Northwest Atlantic Seabird Catalog' database, along with Eastern Canada Seabirds at Sea data from Canadian Wildlife Service, Environment and Climate Change Canada, were analyzed to derive seasonal maps of the spatial distributions of 47 marine bird species in U.S. Atlantic OCS and adjacent waters from Florida to Maine.

Spatial predictive modeling was applied to the survey data to account for spatial and temporal heterogeneity in survey effort, platform, and protocol. An ensemble machine-learning technique, component-wise boosting of hierarchical zero-inflated count models, was used to relate the relative density of each species to multiple spatial and temporal predictor variables while accounting for survey heterogeneity and the aggregated nature of sightings. Dynamic spatial environmental predictor variables were formulated as long-term climatologies. The modeling technique allowed for complex non-linear relationships between response and predictor variables and interacting effects among predictors. Bootstrapping was used to derive estimates of the uncertainty in model predictions.

Model predictions are presented as seasonal maps of the relative density of each study species throughout the study area. The maps were reviewed by experts with experience and knowledge of marine birds in the study area and their comments were incorporated in this report. The maps indicate where species are likely to be more or less abundant. The analysis was not designed to estimate the actual number of individuals/density of a given species that would be expected in any location, so the maps should not be interpreted that way. Also, the maps represent the spatial distributions of birds averaged over time (e.g., across days within a season and across years for a given season). The analysis was not designed to provide predictions of the density of birds that would be expected in a specific location at a specific date or time, so the maps should also not be interpreted that way.

Two indications of the uncertainty associated with the model predictions are provided. First, a hatched overlay is included on the maps of predicted relative density to indicate areas with no survey effort. Model predictions in areas with no survey effort should be interpreted with extreme caution. Predictions in these areas were often questionable or unrealistic, so we recommend additional field surveys in these areas to validate the model predictions. Second, estimates of the precision of model predictions are presented as maps of the coefficient of variation (CV) of predicted relative density. Less precise predictions (i.e., higher CV) should be interpreted with more caution. The maps of predicted relative density should always be considered in conjunction with these two indications of uncertainty.

The relative importance of different predictor variables is also presented, indicating which variables most influenced the predicted distributions for each species in each season. While the primary objective of this study was not to determine the ecological drivers and mechanisms behind the spatial distributions of marine bird species in the study area, our model results may provide useful hypotheses for future studies aimed more at ecological inference.

Modeling At-Sea Density of Marine Birds to Support Atlantic Marine Renewable Energy Planning: Final Report

Contents

List of Figures

List of Tables

List of Appendices

Abbreviations and Acronyms

AMO	Atlantic Multidecadal Oscillation
AUC	area under the ROC curve
BOEM	Bureau of Ocean Energy Management
CV	coefficient of variation
CWS-ECCC	Canadian Wildlife Service, Environment and Climate Change Canada
ECSAS	Eastern Canada Seabirds at Sea
ID	identity
MEI	Multivariate El Niño-Southern Oscillation Index
NAO	North Atlantic Oscillation
NOAA	National Oceanic and Atmospheric Administration
OCS	Outer Continental Shelf
PDE	percent deviance explained
RISAMP	Rhode Island Ocean Special Area Management Plan
RMSE	root mean square error
ROC	receiver operating characteristic
SD	standard deviation
SE	standard error
SST	sea surface temperature
TNI	Trans-Niño Index
USGS	United States Geological Survey
USFWS	United States Fish and Wildlife Service
ZINB	zero-inflated negative binomial
ZIP	zero-inflated Poisson

1. Introduction

Marine birds spend much of their time in coastal waters and on the open ocean. As a result, these species have the potential to be affected by human activities in the marine environment such as offshore wind energy development. A prerequisite for quantifying that potential is knowledge of the spatial distributions of marine birds at sea. This report describes a project aimed at producing maps of the spatial distributions of marine bird species in U.S. Atlantic Outer Continental Shelf (OCS) waters (Fig. 1) that can be used to inform marine spatial planning in the region.

Some of the best available information about the at-sea distributions of marine birds comes from visual sighting and photographic surveys conducted aboard boats and aircraft. For U.S. Atlantic OCS waters many data from past sighting surveys have been compiled in the 'Northwest Atlantic Seabird Catalog', hereinafter referred to as the Catalog. The Catalog was originally developed by the U.S. Geological Survey (USGS) Patuxent Wildlife Research Center as the 'Compendium of Avian Occurrence Information for the Continental Shelf waters along the Atlantic Coast of the U.S.' (O'Connell et al. 2009). The Catalog is currently maintained by the U.S. Fish and Wildlife Service (USFWS). The project described here analyzed sighting data from the Catalog along with sighting data from Eastern Canada Seabird at Sea surveys (ECSAS) by Canadian Wildlife Service, Environment and Climate Change Canada (CWS-ECCC) to derive maps of the spatial distributions of 47 marine bird species in U.S. Atlantic OCS and adjacent waters from Florida to Maine.

The survey data analyzed represent numerous surveys spanning nearly four decades. Survey coverage and intensity was highly variable geographically and temporally. Furthermore, a range of survey platforms, observers, and protocols were used. This heterogeneity complicates the quantification of the at-sea distribution of marine birds from these data, and biases simple data summaries. To deal with this heterogeneity, the project described here employed spatial predictive modeling. An ensemble machine-learning technique was used to model counts of each species as a function of multiple predictor variables while accounting for heterogeneous survey effort. The fitted models were then used to predict the spatial distribution of relative density of each species throughout the study area.

The distributions of marine birds at sea are a result of interactions between their behavior (e.g., foraging) and the environment. Atmospheric and oceanographic features and processes across a range of spatial and temporal scales influence the environmental conditions and prey availability experienced by marine birds, and thus ultimately determine their at-sea distributions. The spatial predictive modeling framework employed here relied on a wide suite of spatial and temporal environmental predictor variables to explain and predict the distributions of marine birds. In particular, static environmental variables (e.g., bathymetry) and long-term climatologies of dynamic environmental variables (e.g., sea surface temperature) were considered to explain spatial patterns of relative density.

The project described here was designed to provide broad-scale spatial information that can be used to guide future data collection efforts and aid marine spatial planning in the region. It is important to note that the results presented in this report represent the spatial distributions of birds averaged over time. The project was not designed to provide precise predictions of the actual number of individuals of a given species that would be expected in a specific location at a specific time. The project was also not designed to determine the ecological drivers of marine bird distributions, although the results provide related hypotheses for future research.

2. Methods

2.1 Overview

A statistical modeling framework was used to relate bird sighting data from historical surveys to a range of temporal and spatial environmental predictor variables. The estimated relationships between the counts of birds and the predictor variables were then used to predict the spatial distributions of birds across the entire study area. Separate models were developed for each combination of species and season for which there were sufficient data. Seasons reflected major transitions in environmental conditions in the study region: spring (1 March – 31 May), summer (1 June – 31 August), fall (1 September – 30 November), and winter (1 December – 28/29 February). Note that these seasons do not necessarily align with the timing of migration for individual species. As a result, summer (June-August) and winter (December-February) models may at least partially represent distributions during migration (e.g., Northern Gannet in summer), and spring (March-May) and fall (September-November) models may not be entirely representative of migration per se.

2.2 Survey data

Ninety-two survey datasets were analyzed (Table 1, Appendix A). The majority of the data were obtained from the 'Northwest Atlantic Seabird Catalog' maintained by USFWS through Intra-agency Agreement M14PG00014 with the US Bureau of Ocean Energy Management (BOEM) (Table 1, Appendix A). The Catalog was formerly known as the 'Compendium of Avian Occurrence Information for the Continental Shelf waters along the Atlantic Coast of the U.S.' or 'Avian Compendium', and was originally created and maintained by USGS Patuxent Wildlife Research Center through Intra-agency Agreement M11PG00059 with BOEM. The Catalog is a relational database containing a large number of datasets on the occurrence and distribution of marine birds along the Atlantic coast of the U.S. (O'Connell et al. 2009). These datasets were collected by a range of entities including government agencies, non-governmental organizations, academic researchers, and other individuals.

The quality of the datasets in the Catalog varies from systematic scientific surveys with rigorous sampling protocols to opportunistic sightings. We used only science-quality, geographically-referenced datasets. Opportunistic sighting data (e.g., eBird) often do not have associated quantitative measures of survey effort and often lack explicit information about observed absences. Without data on survey effort it is not possible to determine whether large numbers of sightings reflect high density or simply reflect more survey effort. Without data on observed absences it is not possible to calibrate the estimated probability of occurrence or density. For these reasons opportunistic sighting data were excluded from our analysis. We also excluded data from survey effort where chumming was used to attract birds. We aimed to estimate the typical spatial distributions of birds, therefore we did not use data from survey effort where the local density of birds was intentionally increased temporarily by the survey itself.

Additional survey data were obtained from CWS-ECCC. CWS-ECCC provided ECSAS data from surveys in eastern Canadian and US Atlantic waters. An accidental duplication of data occurred because one of the Catalog datasets (NewEnglandSeamount06) was also included in the ECSAS data; however, the duplicated effort represented only 0.02% of the total surveyed area analyzed so the duplication likely had a negligible impact on our analysis.

The datasets analyzed spanned 1978-2016 with most survey effort occurring from 1978-1988 and from 2002 onward, especially between 2010 and 2014 (Fig. 2). A total of 181,140 km^2 was surveyed with more

survey effort during summer and fall than during winter and spring (Table 1). Most survey effort was in coastal waters and over the continental shelf with much less effort beyond the shelf break (Fig. 3). Survey effort was greatest offshore during the summer and least during the winter. Year-round concentrations of survey effort occurred near the mouths of Delaware Bay and Chesapeake Bay, in Nantucket Sound, and to the southwest of Nantucket Sound. The datasets with the largest combined sample size and widest geographic coverage were collected by Manomet Bird Observatory in coordination with the US National Oceanic and Atmospheric Administration (NOAA) and other cruises between 1978 and 1988 (datasets CSAP and NOAAMBO7880). More recent aerial surveys by USFWS and boat surveys by NOAA as part of the Atlantic Marine Assessment Program for Protected Species (AMAPPS) also covered U.S. Atlantic coastal (aerial) and offshore (boat) waters. Other multi-year survey efforts covered large sections of the coast including NOAA ecosystem monitoring cruises from North Carolina to the Gulf of Maine (datasets EcoMon), pelagic surveys off Georgia, South Carolina, and Florida (dataset GeorgiaPelagic), and the Canadian ECSAS surveys. The remaining datasets are more localized, often from New England and the Gulf of Maine or the mid-Atlantic, but sometimes they had large sample sizes over multiple years (e.g., CapeWind, DOEBRI, HerringAcoustic, MassAudNanAerial, and MassCEC).

The survey data analyzed were counts of birds mainly from aerial and boat-based visual surveys at sea. Three datasets (DOEBRIAerial) represented high-resolution digital video aerial surveys. The original data took the form of species-specific counts along strip transects. The width of the strip transect was reported for most surveys, but for 5 boat-based surveys where it was not, a 300-m wide strip transect was assumed, which is the standard for boat-based seabird surveys (Tasker et al. 1984).

Counts were sometimes recorded continuously, and other times had been binned into discrete transect segments (e.g., 15 minute duration). Binned data were only from boat surveys. If the distance travelled during each transect segment was not available then it was estimated from the duration of the recording period and the vessel speed. The geographic midpoint for each segment was also estimated from the duration of the recording period and the vessel speed and direction. For consistency with the binned data the continuously recorded data were discretized into transect segments of approximately 4 km in length, and counts for each species were summed within each transect segment. Because the length of any given transect was not necessarily divisible by 4 km, any remainder distance was either treated as its own segment (if it was >2 km) or was added to another segment (if it was <2 km). The placement of the resulting short or long segment along a transect was randomized to avoid it always occurring at the end of a transect. Any transects that were originally <6 km in length were treated as single transect segments. The distance travelled during each transect segment was calculated assuming straight-line travel between recorded vessel locations, and the geographic midpoint of each transect segment was calculated as the point along the trackline where half the distance had been travelled. Transect segments <1 km in length were excluded from analysis.

An error in the segmentation of the MassCEC2011-2012, MassCEC2013, and MassCEC2014 datasets was discovered after analysis. The error resulted in the geographic misplacement of sightings. The error was corrected, these datasets were re-processed, and models were re-run for species for which these datasets represented a large proportion of the total count or whose sighting data and model predictions were noticeably affected by the error (Table 2).

The survey datasets analyzed varied in terms of the type of survey platform used, observer identity and expertise, species focus, and environmental conditions. The type of survey platform used (i.e., boat or plane), characteristics of the survey platform (e.g., observation height), detection method (visual or

photographic), and observer expertise all influence the probability that individual birds will be detected and correctly identified to the species level. For some surveys the primary target was marine birds, while for others birds were surveyed along with other components of the ecosystem. Even among bird-focused surveys there was variability in the species of primary focus (e.g., sea ducks). The level of focus on marine birds and specific species also influences the probability that individual birds will be detected and correctly identified. Sighting conditions (e.g., sea state and visibility) can also greatly affect sighting rates. Ideally these factors would be explicitly accounted for in any model of density. Unfortunately, data on many of these factors were not readily available for all of the survey datasets analyzed here. Nevertheless, the analytical framework used attempted to account for this heterogeneity across survey datasets through effects of survey platform type, transect, and survey (see Section 2.4).

It is important to recognize that because the influence of these factors on sighting rates was not modeled explicitly, the spatial distributions of density presented here should be interpreted as relative predictions, not predictions of actual densities.

2.3 Species modeled

Species with ≥100 transect segments with sightings of ≥1 individual in at least one season were selected for analysis. For each of those species, all seasons with ≥50 transect segments with sightings of ≥1 individual were modeled. By these criteria 47 species and 140 species-season combinations were analyzed representing sightings of 2,687,745 individual birds (Table 2). These species represented 13 families. The five species-season combinations with the greatest numbers of transect segments with sightings were Wilson's Storm-Petrel in summer, Herring Gull in fall, Northern Gannet in winter, and Great Shearwater in fall and summer.

2.4 Predictor variables

A wide range of predictor variables were used to model variation in the number of birds counted per transect segment and to predict the spatial distributions of birds throughout the study area (Table 3, Appendix B). Predictor variables fell into one of six categories: survey, temporal, geographic, bathymetric, oceanographic, and atmospheric.

Survey predictor variables were designed to account for variation in counts arising from heterogeneity in the type of survey platform, characteristics of the survey platform (e.g., observation height), observer identity and expertise, species focus, and sighting conditions. These factors influence the probability that individual birds will be detected (e.g., Heinänen et al. 2017) and correctly identified to the species level. Of these factors, only the type of survey platform (boat-visual, aerial-visual, or aerial-photographic) was consistently available for all datasets, and thus was directly usable as a predictor variable. We attempted to account for the effects of the remaining factors through two random-effect predictor variables representing survey identity (ID) and transect ID, respectively. The exact definition of transect ID differed somewhat between datasets, but unique transect IDs generally represented pre-defined survey transects or individual days of effort.

Temporal predictor variables were designed to account for variation in counts over time. Day of the year was used to account for changes in the numbers of birds in the study area over time within a season, for example arising from migratory movements in and out of the study area. Year was used to account for changes in the number of birds in the study area across years, for example arising from changes in population abundance or distributional shifts. Effects of day of the year and year were modeled as smooth

continuous changes over time. Four climate indices (Table 3) were also included as temporal predictor variables to account for variation in counts across years and across months within seasons arising from linkages between the environment and population abundance and distribution. For each climate index two values were included as predictor variables: the value for the month and year of a given transect segment and the value for the same month one year previous.

Geographic predictor variables were designed to account for variation in counts arising from spatial location per se. Projected longitude and latitude were included as predictor variables and their effects were modeled two ways. The first longitude-latitude predictor term allowed for smooth changes in numbers across the study area arising from spatial factors not captured by the other predictor variables (e.g., colonization history). The second longitude-latitude predictor term was formulated using radial basis functions with the intent of capturing some of the spatial autocorrelation in the data after accounting for the effects of other predictor variables. Distance to land was also included as a geographic predictor variable.

Bathymetric predictor variables were designed to account for variation in counts arising from the direct and indirect effects of bathymetry on bird distributions. A depth predictor variable was developed by combining information from six different bathymetric datasets (Table 3). Other bathymetric variables were derived from depth including slope, slope of slope, and planform and profile curvature.

Oceanographic and atmospheric predictor variables were designed to account for variation in counts arising from the direct and indirect effects of the physical state and dynamics of the ocean and air above the ocean as well as biological productivity. Seventeen oceanographic and atmospheric predictor variables were developed from a range of data sources (Table 3). Remote sensing data were used to characterize sea surface height, temperature, chlorophyll-a, turbidity, and wind stress. Other variables were derived from the remotely sensed variables including sea surface height and temperature variability, probabilities of cyclonic and anticyclonic eddy rings, probability of sea surface temperature fronts, wind divergence, and an index of upwelling. Estimates from a data-assimilating ocean dynamics model were used to characterize water currents, and divergence and vorticity were derived from current velocities.

All of the oceanographic and atmospheric variables that we considered are dynamic. We formulated these predictor variables to characterize long-term spatial patterns in average values and variability. Long data time series ranging in length from 10-25 years were used (Table 3). To characterize average values, monthly mean climatologies across years were developed and then integrated to create seasonal climatologies. To characterize variability, standard deviations or probabilities (frequencies) were calculated from the native temporal resolution of the corresponding predictor variables.

Geographic, bathymetric, oceanographic, and atmospheric predictor variables were spatially explicit. Each variable was calculated on a standard study grid with a spatial resolution of 2 km and an oblique Mercator projected coordinate system (origin = 35°N 75°W; azimuth = 40°; scale = 0.9996; NAD83 earth datum). When the native spatial resolution of a predictor variable was finer than that of the study grid, predictor values were averaged within study grid cells. When the native spatial resolution of a predictor variable was similar to or coarser than that of the study grid, bilinear interpolation was used to derive predictor values at the center of study grid cells. Each survey transect segment was matched to the predictor variable values from the study grid cell that contained the midpoint of that segment.

Some of the spatially explicit predictor variables were highly correlated with each other (Table 4). Predictor variables were chosen to avoid correlations >0.9, although summer and fall each had three

pairwise correlations >0.9. Four of the correlations >0.9 involved spatial coordinate variables that were a key structural component of our model. The other two correlations >0.9 were between chlorophyll-a and turbidity and between the mean and standard deviation of sea surface temperature during the summer. Because of the high correlations between some predictor variables, inferences regarding relative variable importance should be made with caution. The accuracy of predictions should be less affected by collinearity among predictor variables.

2.5 Statistical modeling framework

A boosted generalized additive modeling framework (Bühlmann and Hothorn 2007; Hofner et al. 2012) was used to estimate relationships between the numbers of birds counted per transect segment and the predictor variables (Fig. 4). Those relationships were then used to predict the relative density of each species throughout the study area in each season. Our main objective was to provide accurate predictions so we chose a modeling framework that allowed for flexible relationships and multiple interactions between predictor variables while accounting for sampling heterogeneity between and within datasets.

2.5.1 Likelihoods and model components

The number of individuals of a given species counted per transect segment was modeled using zero-inflated Poisson (ZIP; Eq. 1) and zero-inflated negative binomial (ZINB; Eq. 2) likelihoods to account for the overdispersed nature of wildlife count data. Each component/parameter of the likelihood was modeled as a separate function of the predictor variables (Schmid et al. 2008; Mayr et al. 2012). For the ZIP likelihood, the two model components were the probability of an 'extra' zero (p) and the mean of the Poisson distribution (μ):

$$[1] \qquad L(p,\mu;y) = \prod_{i=1}^{n} [p + (1-p)e^{-\mu}]^{I_{y_i}=0} \left[(1-p)\frac{\mu^{y_i}e^{-\mu}}{y_i!}\right]^{I_{y_i}>0}$$

The same components were modeled for the ZINB likelihood in addition to the dispersion parameter of the negative binomial distribution (θ):

$$[2] \qquad L(p,\mu,\theta;y) = \prod_{i=1}^{n} \left[p + (1-p)\left(\frac{\theta}{\theta+\mu}\right)^{\theta}\right]^{I_{y_i}=0} \left[(1-p)\frac{\Gamma(y_i+\theta)}{y_i!\Gamma(\theta)}\left(\frac{\theta}{\theta+\mu}\right)^{\theta}\left(\frac{\mu}{\theta+\mu}\right)^{y_i}\right]^{I_{y_i}>0}$$

The probability of an extra zero (p) was modeled on the logit scale while the mean of the Poisson/negative binomial distribution (μ) and the dispersion parameter of the negative binomial distribution (θ) were modeled on the log scale.

In Eqs 1 and 2, y represents the vector of y_i which represent the total count for transect segment i, n represents the total number of segments, and $I_{y_i=0}$ and $I_{y_i>0}$ are indicators of whether y_i is equal to or greater than zero, respectively (I=1 when the condition is true and I=0 when the condition is false).

2.5.2 Effort offset

To account for variation in the lengths and widths of strip transect segments an effort offset was included in the model. Specifically, the area surveyed per transect segment was used as an effort offset in the μ model component, enforcing a proportional relationship between the area surveyed and the expected number of individuals counted on a transect segment conditional on that segment not being an 'extra' zero

count. Model predictions correspond to counts per 1 km^2 of survey effort and therefore are referred to as density.

2.5.3 Base-learners

Within the boosting framework, each model component was essentially modeled as a function of an ensemble of 'base-learners'. Each base-learner represented a specific functional relationship between a model component and one or more predictor variables. We utilized a suite of base-learners each representing different predictor variables, and different sets of base-learners were employed for different model components (Table 5).

All spatially explicit predictor variables except longitude and latitude were included together in a single tree base-learner. The trees for that learner had a maximum depth of 5, which allowed for interacting effects among the spatially explicit predictor variables. Longitude and latitude appeared in two base learners, and those variables always entered the model as a pair. The remaining survey and temporal predictor variables entered the model individually, either through their own base-learners or in the case of climate indices one at a time through a tree base-learner with a maximum depth of 1. Our model structure did not allow for interactions between temporal and spatial predictor variables.

2.5.4 Stochastic gradient boosting

Stochastic gradient boosting was used to fit models whereby a sub-sample of the data (4/5 during tuning, see Section 2.5.6, or 2/3 otherwise) was fitted in each boosting iteration (Friedman 2002). Rather than re-sampling the data for each boosting iteration, a set of 25 or 50 random sub-samples was created before boosting, and one sub-sample was randomly drawn from this set for each boosting iteration. Mean square error was used to select the base-learner that gave the best fit to the gradient in each boosting iteration.

2.5.5 Boosting offsets

Model component estimates were initialized ('offset' in boosting terminology; Hofner et al. 2012) using one of two methods. The first method was to fit an intercepts-only ZIP or ZINB model with an effort offset to the data ('pscl' package for R; Zeileis et al. 2008, Jackman 2015), then use the estimated intercepts for each component of that model as the boosting offsets. The second method was to fit a simple zero-inflated generalized additive model (Poisson or negative binomial) with an effort offset to the data ('mgcv' and 'pscl' packages for R; Wood 2006, Zeileis et al. 2008, Jackman 2015) and then use the estimated intercepts for each component of that model as the boosting offsets. The model for the second method incorporated effects of projected longitude and latitude through a bivariate thin-plate regression spline with 3 or 4 degrees of freedom.

2.5.6 Tuning of learning rate and number of boosting iterations

A stratified (by transect ID) 5-fold cross-validation approach was used to determine the number of boosting iterations and component-wise learning rates that resulted in the best predictive performance. Three different learning rates were considered for each model component: 0.001, 0.01, and 0.1. For each unique combination of component-wise learning rates (e.g., $3^2 = 9$ for 2 model components) and cross-validation fold, the model was fit to the in-bag data (i.e., 4/5 of the data) and the number of boosting iterations at which the negative log-likelihood of the out-of-bag data (i.e., 1/5 of the data) was minimized was determined. This cross-validation was repeated four times. For each combination of component-wise learning rates the optimal numbers of boosting iterations and their corresponding performance were averaged across cross-validation folds and replicates. Finally, the combination of component-wise learning rates with the best average performance and its corresponding average optimal number of

boosting iterations were identified. The maximum number of boosting iterations allowed was 20,000, so models with an optimal number of boosting iterations near 20,000 should be interpreted with caution as their performance may have improved with additional boosting iterations.

2.5.7 Model selection and performance

Four different models were fitted for each species-season combination. The four models represented all combinations of the two likelihoods (ZIP and ZINB) and the two methods of calculating the boosting offsets (intercept-only model and generalized additive model).

The performance of the four models was evaluated from a suite of nine performance metrics. The first performance metric was percent deviance explained (PDE), which is essentially the percentage of variation in the data explained by the fitted model beyond the amount of variation explained by a simpler model without predictor variables. PDE indicates overall model fit. PDE is somewhat analogous to the more familiar R^2 metric for a linear regression. The second performance metric was the area under the receiver operating characteristic curve (AUC), which indicates how well a model predicts binary data. We calculated AUC by converting the count data to presence/absence data. The AUC metric indicates how well the models predicted the observed presence of a species, but not necessarily how well the models predicted the relative density of a species. The third and fourth performance metrics were the Spearman and Gaussian (Boudt et al. 2012; Bodenhofer et al. 2013) rank correlation coefficients between the observed and predicted data. These metrics indicate how well the model predictions of relative density for each transect segment correlate with the number of individuals counted. The fifth and sixth performance metrics were the median and mean absolute residual error as a percentage of the mean count. The seventh and eighth performance metrics were the median and mean residual error (predicted minus observed) as a percentage of the mean count, referred to as 'bias'. Negative bias values indicate that predicted density was lower than observed, while positive bias values indicate that predicted density was higher than observed. The final performance metric was root mean square error (RMSE), the square root of the average squared residual error.

It is important to recognize that the model performance metrics mainly reflect the statistical fit of the models to the data. They reflect only the data that were analyzed, and they do not reflect the quality of model predictions away from the data. For example, the survey data did not cover the full extent of the study area, so some model predictions are essentially interpolations/extrapolations from data in other parts of the study area. The accuracy of those predictions is not necessarily reflected by the model performance metrics. Nevertheless, the performance metrics give an indication of how accurately a model was able to predict the observed data, and good performance provides a measure of confidence in the modeled distributions, especially within the temporal and spatial coverage of the observed survey data.

The 'best' of the four models for each species-season combination was chosen on the basis of a subset of the performance metrics: PDE, AUC, Gaussian rank correlation, median and mean absolute residual error, and RMSE. The values of each of these performance metrics were ranked across the four models, and the model with the highest sum of ranks across these performance metrics was chosen as the best model. In the case of a tie the model with the highest PDE was chosen.

A small percentage of the 'best' models (4%; 5 models) had highly problematic predictions: Common Eider winter, Dovekie winter, Red Phalarope summer, Roseate Tern fall, and Sooty Shearwater fall. Problems included highly skewed distributions of predicted density across bootstrap replicates and space, flat distributions of predicted density across space, spatial patterns that did not make sense ecologically, and erroneous predicted density values in some bootstrap replicates (e.g., unrealistically high values). The

problematic models for Common Eider, Dovekie, Red Phalarope, and Sooty Shearwater were ZIP models. These species often form large aggregations, which could have contributed to the observed problems, especially with Poisson models that do not allow for overdispersed count data. For three of the five problematic species-season combinations we chose the second best model instead and for two we chose the fourth best model.

2.5.8 Spatial prediction

The final fitted model for each species and season was used to predict relative density throughout the study area. It is important to recognize that the model predictions do not represent actual density. During visual surveys, individual birds may be missed either because they are below the surface of the water (availability bias) or simply because observers failed to notice them (perception bias) (Barlow 2015). The failure to count some individuals biases estimates of density downward relative to actual density. Animal movement can also bias estimates of density. Birds may be attracted or repelled by ships, small boats, and planes biasing estimates upward or downward, respectively. Flying birds can also bias estimates, with the direction of the bias depending on the speed and direction of the animals' movement relative to those of the survey platform (Spear et al. 1999). Furthermore, non-randomized survey data can result in biased estimates of abundance and density in species distribution models (Conn et al. 2017). Our model predictions should only be interpreted as indices of density. The model predictions can be interpreted as being proportional to the expected number of individuals per km^2, but they do not represent the actual expected number of individuals per km^2.

The predicted relative density in a given grid cell corresponds to predictions for a transect segment whose mid-point falls within that grid cell. Spatially explicit predicted values were calculated for each cell of the study grid from the values of the spatially explicit predictor variables for that cell. All other predictor variables were set to their mean values. The predictions integrated the zero-inflated and Poisson/negative binomial components of the likelihood.

2.5.9 Variable importance

While determining the ecological drivers and mechanisms behind the spatial distributions of marine bird species in the study area was not our primary objective, our model results do provide some indication of which variables were most useful for predicting those distributions. Those variables may provide useful starting points for future studies aimed more at ecological inference.

We calculated the relative importance of a given predictor variable in the final fitted models by summing the decrease in the negative log-likelihood in each boosting iteration attributable to that predictor variable. Thus, variable importance reflects the frequency with which a given predictor variable occurred in the selected base-learners across boosting iterations and that variable's ability to explain variation in the data when it was selected. When multiple predictor variables occurred in the selected base-learner for a given boosting iteration, the decrease in the negative log-likelihood was divided evenly among those predictor variables. Relative variable importance was re-scaled so that it summed to 1 across predictor variables.

2.5.10 Uncertainty

Uncertainty in model predictions was estimated using a non-parametric bootstrapping framework. For each bootstrap iteration, the set of unique transect IDs was resampled with replacement, and the data for each transect ID were assigned weights proportional to the frequency of that ID in the sample. These data weights were then applied when fitting the model during that bootstrap iteration. Predictor variables that were not included in the final model were excluded from the bootstrap analysis. Two hundred bootstrap

iterations were conducted producing a sample of predictions from which we calculated means, standard errors (SE), coefficients of variation (CV), 5%, 25%, 50%, 75%, and 95% quantiles, and 50% and 90% confidence interval widths to characterize uncertainty in the predictions. The 50% and 90% confidence intervals were defined as the intervals between the 25% and 75% quantiles and between the 5% and 95% quantiles, respectively.

As with the model performance metrics, the estimated uncertainty in the model predictions is conditional on the model and the data. It does not capture all of the uncertainty associated with our model predictions. Nevertheless, the estimated uncertainty is an important indication of the precision of the model predictions, and it should be an integral consideration when using the model predictions.

The bootstrapped median predictions (50% quantile) were generally better (e.g., smoother density gradients and fewer artifacts) than the bootstrapped mean predictions and the non-bootstrapped predictions, so we chose the bootstrapped median predictions as the best representation of the predicted spatial distributions of relative density.

A small number of bootstrap iterations in seven different models produced unreasonably large predictions in a few grid cells that caused numerical issues when calculating the bootstrapped mean, SE, and CV. These extreme outlying values were removed when calculating these bootstrapped quantities for these models. The models that exhibited this issue were: Brown Pelican winter, Common Eider fall, Great Black-backed Gull winter, Herring Gull winter, Leach's Storm-Petrel spring, Long-tailed Duck spring, and Red-throated Loon winter. All but one of these models were ZIP models suggesting that the issue may have been related to bootstrapping models with that particular likelihood.

2.5.11 Implementation

The analysis was conducted with R 64-bit (R Core Team 2017) version 3.3.3 (or 3.4.4 for model re-runs; see Section 2.2) running under CentOS Linux 7 using custom scripts that relied on multiple existing contributed packages, including 'boot' version 1.3-17 (Canty and Ripley 2015), 'DBI' version 0.6-1 (R-SIG-DB et al. 2017), 'fields' version 8.10 (Nychka et al. 2015), 'gsubfn' version 0.6-6 (Grothendieck 2014a), 'lattice' version 0.20-31 (Sarkar 2008), 'maps' version 3.1.1 (Becker et al. 2016), 'maptools' versions 0.8-36 (Bivand and Lewin-Koh 2015), 'MASS' versions 7.3-42 (Venables and Ripley 2002), 'Matrix' version 1.2-8 (Bates and Maechler 2017), 'mboost' version 2.4-2 (Hothorn et al. 2015), 'mgcv' version 1.8-17 (Wood 2006), 'modeltools' version 0.2-21 (Hothorn et al. 2013), 'mvtnorm' version 1.0-2 (Genz et al. 2014), 'nlme' version 3.1-131 (Pinheiro et al. 2017), 'party' version 1.0-21 (Hothorn et al. 2006), 'pROC' version 1.8 (Robin et al. 2011), 'proto' version 0.3-10 (Grothendieck et al. 2012), 'pscl' version 1.4.9 (Jackman 2015), 'raster' version 2.4-15 (Hijmans 2015), 'reshape' version 0.8.5 (Wickham 2007), 'rgdal' version 1.0-4 (Bivand et al. 2015), 'rgeos' version 0.3-11 (Bivand and Rundel 2015), 'rococo' version 1.1.2 (Bodenhofer et al. 2013), 'RSQLite' version 1.0.0 (Müller et al. 2014), 'sandwich' version 2.3-3 (Zeileis 2006), 'sp' version 1.1-1 (Pebesma and Bivand 2005), 'spam' version 1.3-0 (Furrer and Sain 2010), 'sqldf' version 0.4-10 (Grothendieck 2014b), 'stabs' version 0.5-1 (Hofner and Hothorn 2015), 'strucchange' version 1.5-1 (Zeileis et al. 2002), 'VGAM' version 0.9-8 (Yee 2015), and 'zoo' version 1.8-0 (Zeileis and Grothendieck 2005).

2.6 Map display

Spatial predictions within the study area are displayed as a pair of maps for each species and season (Fig. 5). Seasons were defined as spring (March-May), summer (June-August), fall (September-November), and winter (December-February). The first map for each species and season displays the predicted

relative density (bootstrapped median predictions), and the second map displays the CV of predicted relative density, both at a 2-km spatial resolution. The first map also contains an inset map of observed relative density: the total count divided by the total area surveyed at a 10-km spatial resolution.

Color spectrums are employed to visualize spatial variation in values across the study area. For relative density the colors range from blue (lower density) to red (higher density), and for the CV the colors range from light brown (lower CV, more precise) to dark brown (higher CV, less precise). The number ranges corresponding to each color are indicated in the map legends. The break points between the number ranges were evenly distributed on the natural log scale. To emphasize the relative nature of the model predictions, the number ranges displayed in the legend of each predicted relative density map were re-scaled by dividing them by the maximum predicted value for that map. Thus, predicted relative density values on each map range from 0-1, representing the lowest to the highest predicted relative density for that map. For the inset observed density maps, values greater than the maximum predicted value were included in the highest legend category. We encourage others making maps from the model predictions provided by this project to similarly re-scale the legends to emphasize the relative nature of the predictions and to prevent misinterpretation of the predictions as actual density.

Both maps also display a hatched overlay indicating areas without survey effort at a 10-km spatial resolution. Model predictions in areas without survey effort are essentially extrapolations and should be interpreted with extreme caution. We recommend additional field surveys in these areas to validate model predictions.

2.7 Expert review of maps

We solicited feedback on the accuracy of the maps from 44 experts with experience and knowledge of marine birds in the study area. These experts were from a range of organizations including federal and state government agencies, academic institutions, non-profits, and consultants. We received comments from nine of these experts, and their feedback was incorporated into this report.

2.8 Predicted proportional relative abundance by BOEM wind energy planning/lease area

To facilitate comparisons of predicted relative density among BOEM wind energy planning/lease areas the predicted relative abundance (density × area) in each BOEM area as a proportion of the total relative abundance in the entire study area was tabulated by BOEM area and season for each species. These calculations accounted for any partial coverage of study grid cells. Computer files defining the BOEM areas for this analysis were downloaded from https://www.boem.gov/Renewable-Energy-GIS-Data/, https://www.boem.gov/OCS-A-502/, and https://www.boem.gov/OCS-A-503/ in September 2017. It is important to recognize that these proportional relative abundance results are relative to the study area. They do not account for birds outside of the study area. If the entire range of a species were to be considered then the proportional relative abundance in BOEM areas could decrease.

3. Results

3.1 Model selection and performance

The final selected models varied across species and seasons (Table 6). ZINB models were selected more frequently than ZIP models (85 versus 55 models), and models with boosting offsets derived from a

generalized additive model were selected more frequently than models with boosting offsets derived from a simple intercepts-only model (104 versus 36 models). A higher proportion of selected ZINB models had boosting offsets derived from a generalized additive model than did selected ZIP models. Models with different likelihoods and different boosting offset methods were often selected for different seasons for the same species.

The statistical performance of the final selected models was highly variable among species and seasons (Table 6). Over half of the models had an optimal number of boosting iterations >19,000, close or equal to the maximum of 20,000. PDE ranged from 14-86%. AUC ranged from 0.81 to 1.00. Spearman and Gaussian rank correlation coefficients ranged from 0.05-0.59 and 0.06-0.60, respectively. The median and mean absolute residual error ranged from 0-56% and 39-262% of the mean count, respectively. The median and mean residual error (bias) ranged from 0-56% and -100 to 122% of the mean count, respectively. RMSE ranged from 0.05-426.

Performance metrics were often correlated with each other, usually in the expected direction, although the correlations were often not very strong. The Spearman and Gaussian rank correlation performance metrics were very strongly correlated with each other (Spearman rank correlation coefficient $r_s = 0.99$) as were the median residual error and median absolute residual error ($r_s = 0.98$). PDE was strongly correlated ($|r_s| > 0.5$) with AUC (positive), median/mean absolute residual error (negative), and median residual error (negative). AUC was strongly negatively correlated with median absolute residual error and median residual error. Spearman/Gaussian rank correlation coefficient were strongly negatively correlated with mean absolute residual error. Mean absolute residual error was strongly positively correlated with median residual error and median absolute residual error. Unexpectedly, Spearman/Gaussian rank correlation were positively correlated with RMSE and to a lesser extent negatively correlated with AUC.

The best performing models overall were Black-capped Petrel fall and winter, which had 7 of 9 performance metrics in the top 10 across all species and seasons. Audubon Shearwater winter had 5 performance metrics in the top 10. These three models were all ZIP models with boosting offsets derived from a generalized additive model. The models with the worst performance overall were Parasitic Jaeger spring and Pomarine Jaeger summer which had 7 of 9 performance metrics in the bottom 10 across all species and seasons. Parasitic Jaeger summer and fall had 6 performance metrics in the bottom 10, and Red-breasted Merganser winter and Roseate Tern fall had 5 metrics in the bottom 10. Some models had performance metrics in the bottom 10 and top 10. For example, Parasitic Jaeger spring and summer and Pomarine Jaeger summer had RMSE in the top 10. It is possible that low sample size contributed to the poor performance of some models. For example, Parasitic Jaeger spring had the lowest number of segments with sightings, the lowest number of individuals counted, and the lowest count per segment when sighted (Table 2). Parasitic Jaeger summer had the second lowest total count.

3.2 Predicted spatial distributions

3.2.1 Spatial and seasonal patterns

Given the large number of species modeled the predicted spatial distributions of relative density varied widely (Appendix C). Broad patterns in predicted distributions generally aligned with observed sighting locations and densities and usually matched what is known about the distributions of these marine bird species. Predicted distributions of Brown Pelican, Double-crested Cormorant, Horned Grebe, loons, Red-breasted Merganser, sea ducks, and several gull and tern species were relatively coastal with highest relative density near shore. Black-capped Petrel, Bridled Tern, Northern Fulmar, shearwaters, Sooty Tern,

and storm-petrels had highest densities further offshore. Alcids tended to have offshore distributions except during the summer (June-August) for species that breed in the study area (Atlantic Puffin, Black Guillemot, and Razorbill). Jaegers and skuas also had offshore distributions except Parasitic Jaeger during summer when the highest density was nearer to shore overlapping with the area of highest density for some breeding species (e.g., Arctic Tern, alcids). Areas of highest density for Black-legged Kittiwake, Great Black-backed Gull, Herring Gull, and Northern Gannet generally spanned nearshore to offshore. Distributions of phalaropes tended to be closer to shore during summer than during spring (March-May) and fall (September-November).

The predicted distributions of some species within the study area were relatively restricted in area, at least seasonally. For example, most of the highest density areas for Arctic Tern, breeding alcids, and phalaropes during summer were relatively nearshore off Maine and Nova Scotia around the mouth of the Bay of Fundy. Distributions of sea ducks often exhibited localized areas of highest density especially during winter (December-February), for example in and around Nantucket Sound, and near the mouths of Delaware Bay and Chesapeake Bay. The distribution of the endangered Roseate Tern exhibited relatively small areas of highest density in and around Cape Cod and Nantucket Sound during spring-fall but also further south along the east coast of Florida during summer. Most other species' distributions were less restricted in size but their highest densities were usually still limited to parts of the study area. The bulk of many species' distributions was in the northern part of the study area within the Gulf of Maine and over surrounding shelf waters out to the shelf break or beyond and south as far as Cape Hatteras (e.g., Atlantic Puffin, Black-legged Kittiwake, Dovekie, Great Black-backed Gull, Great Shearwater, Herring Gull, Northern Fulmar, and Sooty Shearwater). Other species had more southerly distributions, either coastal (e.g., Brown Pelican, Royal Tern) or offshore (e.g., Black-capped Petrel, Sooty Tern).

The predicted spatial distributions of many species changed seasonally reflecting seasonal movements and migrations. As mentioned above, the seasonal distributions of alcids that breed in the study area were more concentrated nearshore around the colonies during summer transitioning to more widely dispersed offshore distributions during winter, although the area of highest density for Razorbill during winter and spring was around and to the south of Cape Cod and Nantucket Sound. Areas of relatively high density extended further north during the summer and/or further south during the winter for many species (e.g., Common Loon, Laughing Gull, Northern Fulmar, and Northern Gannet). The distributions of Great Black-backed Gull and Herring Gull were closer to shore, more concentrated, and more northerly during summer and were further from shore, more dispersed, and more southerly during winter. The distributions of both phalarope species exhibited similar seasonal changes with highest densities along the shelf break during spring, closer to shore off Maine and Nova Scotia during the summer, and from the mouth of the Bay of Fundy through the Gulf of Maine and the Northeast Channel between Georges Bank and Browns Bank extending along the shelf break during winter. Migrations of species that mostly leave the study area altogether were reflected in the absence of models for certain seasons (e.g., sea ducks during summer and jaegers, phalaropes, skuas, storm-petrels, and terns during winter).

Predicted relative abundance in individual BOEM wind energy planning/lease areas expressed as a proportion of total relative abundance in the study area reflected the broader predicted spatial distributions, but was additionally influenced by the size of individual BOEM areas with larger areas having higher relative abundance for the same density (Appendix D). Relative abundance in individual BOEM areas was usually a small proportion of the total relative abundance within the study area, although for 9 species this proportion was ≥1% for one or more BOEM areas in one or more seasons. Often these BOEM areas were New Jersey areas (Common Loon spring, Common Tern summer, Surf

Scoter spring) or the South Carolina Grand Strand area (Bonaparte's Gull spring, Common Loon winter, Red-throated Loon spring, Royal Tern spring-summer). Twenty-two species had total relative abundance across all BOEM areas that was ≥1% of total relative abundance in the study area for one or more seasons. The highest of these proportions was for Razorbill and Common Loon during spring where total relative abundance across all BOEM areas was >5% of the total relative abundance in the study area, mostly in Rhode Island and Massachusetts areas for Razorbill and in New Jersey areas and the South Carolina Grand Strand area for Common Loon.

3.2.2 Uncertainty

Generally speaking, the estimated uncertainty in the model predictions was high. The minimum CV for predictions in individual spatial grid cells ranged from 0.02-1.34 across species and seasons, and the maximum CV ranged from 1.23-14.14. Thus, all models had at least some predictions with CVs exceeding 1 indicating that the SE was greater than the mean. These CVs reflect multiple aspects of the data and model including the amount of survey effort (i.e., sample size), sampling variability and the degree to which birds of a given species aggregate, extrapolation to predictor variable values outside the range of values associated with the observed survey effort, and un-modeled variation in the spatial distributions of birds (e.g., changes in spatial distributions over time). It is difficult to quantify the contribution of each of these sources of variability to the CV of any particular prediction. The spatial patterns in the estimated CV of predictions varied widely across species and seasons (Appendix C). In some cases the CV was relatively lower in areas with predicted higher density (e.g., Northern Fulmar summer), but in other cases the CV was higher in areas with predicted higher density (e.g., Black Guillemot summer). Higher CVs sometimes reflected an absence of survey effort in areas with predicted low (Ring-billed Gull winter, offshore) or high relative density (Atlantic Puffin summer, off the coast of Nova Scotia). Many of the problematic predictions (see Section 3.2.3) were associated with relatively high CVs (e.g., Brown Pelican offshore in winter, Herring Gull over northeast seamounts in winter). The spatial patterns in the estimated CV often reflected the influence of particular predictor variables, even when that influence was not as apparent in relative density itself (e.g., Red-throated Loon winter, probability of anticyclonic eddies). The estimated SE and confidence interval widths of predicted relative density were highly correlated with the relative density values, usually resulting in very similar spatial patterns. As indicated by the magnitude of the CVs, the values of the SE and confidence interval widths were generally large relative to the corresponding predictions of relative density.

3.2.3 Problematic predictions

Predictions of relative density for some species in some areas were questionable, especially in areas without survey effort. These predictions were often associated with high CVs. There was much less survey effort beyond the shelf break than coastally and over the shelf, especially during winter (Fig. 3). The predicted densities of many species were relatively high in this offshore area, some of which are plausible but others of which are doubtful. For example, several coastal species had moderate relative densities extending far offshore during winter that are unrealistic (e.g., Brown Pelican, Horned Grebe, Red-breasted Merganser, Red-throated Loon). Predictions of even moderate relative density of sea ducks far offshore (e.g., Long-tailed Duck, Surf Scoter, and White-winged Scoter in fall) are biologically implausible given their benthic foraging habitat (White et al. 2009; Veit et al. 2016; White and Veit 2018). Even for species that are generally found far from shore, areas of moderate to high relative density offshore may be larger than is realistic given the limited survey coverage there (e.g., Black-capped Petrel, Audubon Shearwater, Manx Shearwater). Predicted moderate to high relative densities of other species in some offshore areas are also unrealistic or questionable at best (e.g., Common Murre in winter, Dovekie along the edge of the Blake Plateau in spring and fall, Leach's Storm-Petrel in fall, Least Tern in fall,

South Polar Skua in fall). The extreme southern part of the study area (Straits of Florida) had very little survey effort (Fig. 3). Several northern species had moderate to high relative densities in this area that are unrealistic (e.g., Black Scoter, Dovekie, Northern Fulmar, Surf Scoter, Thick-billed Murre). Several species had high relative densities close to the southern shore of Nova Scotia in an area without survey effort (Arctic Tern, Atlantic Puffin, Black Scoter, Razorbill, Surf Scoter). There was predicted moderate density of Brown Pelican in Canadian Bay of Fundy waters during summer that is further north than is realistic for this species' current distribution.

Predicted spatial distributions sometimes exhibited patterning or extremely localized areas of high relative density that are likely unrealistic. Unrealistic patterning often reflected the undue influence of individual predictor variables on model predictions, especially in areas with little or no survey effort. These predicted features were often associated with higher CVs. For example, it is apparent that the predicted distribution of Brown Pelican in winter was heavily influenced by the probability of anticyclonic eddies with large discrete patches of higher density offshore corresponding to areas with high eddy probabilities. The distribution of Black-legged Kittiwake in spring exhibits an obvious effect of distance to land resulting in a line of discrete change in relative density paralleling the coast. Neither of these patterns are realistic. The distribution of Bridled Tern in summer exhibits a circular area of high relative density in the South Atlantic Bight corresponding to an area of high probability of cyclonic eddies. Some predictions were clearly extrapolations of the relationship between bathymetric predictor variables and density to areas without survey effort. For example, the predicted distributions for Audubon Shearwater in fall, Cory's Shearwater in fall, Great Shearwater in spring, and Herring Gull in winter exhibit well-defined areas of high relative densities over seamounts in the northeast part of the study area. It is probable that at least the discreteness of these distribution features are unrealistic. Predictions for Parasitic Jaeger, Wilson's Storm-Petrel, and other species exhibit ribbons of moderate to high density that match high slope transitions extending from north to south throughout the entire study area. These predictions are more likely realistic along the shelf break in the north where there was more survey effort than they are further south along the edge of the Blake Plateau further offshore in an area with very little survey effort. The predicted distribution for Long-tailed Duck in the spring exhibited fairly high density over Georges Bank in an area with some survey effort but no sightings. That prediction was primarily a result of similarities in spring chlorophyll-a and turbidity between Georges Bank and the area of observed high Long-tailed Duck density in Nantucket Sound and over Nantucket Shoals.

The very highest densities were sometimes limited to one or a few very small areas suggesting localized long-term concentrations of abundance that are almost certainly unrealistic. These predictions were sometimes associated with higher CVs but not always. Some example species and seasons exhibiting this behavior were Arctic Tern (summer, spot over Georges Bank), Black-Legged Kittiwake (fall), Common Murre (spring), Herring Gull (winter), Manx Shearwater (summer), Red-necked Phalarope (spring), and Thick-billed Murre (winter). It is difficult to ascribe these highly localized distribution features to a specific cause, but in at least some cases they may partially reflect large temporal and spatial aggregations of birds that coincided with survey effort rather than average long-term spatial patterns per se. It is unlikely that these are persistent areas of higher density than adjacent areas. While our spatial predictive modeling framework theoretically accounts for effort and attempts to account for the aggregated nature of bird distributions and sightings, limited sample size combined with extreme aggregations can unduly influence model predictions.

In addition to over-predictions of relative density, it is possible that the model predictions underrepresented the relative density of some species in some areas. For several species that frequent

Stellwagen Bank and Cape Cod in the southwestern Gulf of Maine the models did not always indicate substantial relative density there (e.g., Common Murre in winter and spring, Cory's Shearwater in summer and fall, Common Tern in fall, Great Shearwater in summer, Pomarine Jaeger in fall, and Roseate Tern fall). If the models indeed underrepresented relative density in this area, it could have been a result of survey timing and limited sightings in the data analyzed here or an issue with model fit. It is also possible that in some cases the use of 3-month seasons diluted the signal from more short-term concentrations of abundance (e.g., migrating birds that are only present for the first month or so of fall). As another example, Razorbill are known to occur in high densities in the Bay of Fundy during winter (Huettmann et al. 2005), yet predicted relative density in that area during winter was low potentially suggesting an under-prediction. There was no survey effort in that area during winter, which possibly explains the predicted low relative density.

Some of the predicted distributions for sea duck species were flatter than expected with moderate relative density extending further offshore and further north or south than the sighting data would suggest. The distributions for Common Eider in spring and winter most clearly manifested this issue. The areas of highest relative density corresponded with the highest observed densities in and around Nantucket Sound, but moderate relative densities extended offshore throughout the Gulf of Maine (winter) or the entire study area (spring) where there were few if any sightings. The predicted relative density values in these problematic areas were quite high (e.g., as high as 10 birds per km^2 or more in winter), emphasizing that the model predictions should not be interpreted in absolute terms. Other sea duck distributions exhibited the same issue to a lesser extent (e.g., Long-tailed Duck winter). This issue was likely a result of the highly skewed distributions of observed counts for these species. For example, the maximum observed density on a single transect segment was >40,000 birds/km^2 for Common Eider in winter and spring and Long-tailed Duck in spring while the mean observed densities when sighted ranged from only 73-313 birds/km^2. Although the model likelihoods allowed for overdispersion in the count data they might not have been sufficient for species and seasons with extremely large aggregations.

These problematic predictions sometimes affected the predicted proportional relative abundance by BOEM wind energy planning/lease area. For example, the relative abundance of Common Eider in individual BOEM areas was a small proportion of the total relative abundance within the study area (Appendix D), but the proportional relative abundance values for Common Eider during spring were more evenly distributed across BOEM areas from north to south than is realistic. There were no sightings south of New Jersey.

3.3 Predictor variable relative importance

The modeling framework used in this study was designed to provide accurate predictions. It was not designed to identify which environmental predictors were most ecologically relevant in determining the distribution of birds. Ecological inferences from the variable importance results should be cautious. Nevertheless, these results may suggest interesting hypotheses for future research. Also, as discussed in Section 3.2.3 extrapolations of the predicted relationships between density and predictor variables to areas with little or no survey effort were often questionable or unrealistic.

The most important predictor variables varied across species and seasons (Fig. 6a-d). Day of year, mean sea surface temperature, mean chlorophyll-a, turbidity, and distance to land were in the top eight most important predictor variables averaged across all species in all four seasons for both the p and μ model components. Year was almost always in the top eight except for the p model component of fall models. Day-of-year was the most important predictor on average in spring and fall models likely reflecting the

movement of migratory species in and out of the study area during the transitions between summer and winter. The importance of the year effect reflects inter-annual variability in species' seasonal abundance within the study area. Mean sea surface temperature was a relatively important predictor for most models, reflecting its ability to capture broad latitudinal and Gulf Stream-related patterns in distribution. For example, all seasonal Sooty Shearwater models predicted an increase in density as sea surface temperature decreased corresponding to the occurrence of this species mainly in the northern part of the study area. The effects of mean chlorophyll-a and turbidity tended to be most important in models for coastal species (e.g., Brown Pelican, Double-crested Cormorant, Horned Grebe, some gull species, loons, Red-breasted Merganser, sea ducks, and some tern species), reflecting these predictors' ability to capture coastal distributions, especially concentrations of abundance in certain areas (e.g., in and around Nantucket Sound). For example, Black Scoter models usually predicted a strong increase in density as chlorophyll-a and turbidity increased. Distance to land was often an important predictor for coastal species but was also often important for species with more offshore distributions (e.g., shearwaters).

Other predictor variables that were relatively important for multiple species in multiple seasons were transect ID, sea surface temperature standard deviation (SD), and wind stress (particularly in the east-west direction). Transect ID was an especially important predictor in the μ model component, and its importance indicates substantial variation in the count data that was not explained by the temporal and spatial predictor variables. Sea surface temperature SD was highly correlated with mean sea surface temperature (Table 4) so it is difficult to separate the effects of these two predictors. Wind stress was more eastward and/or stronger further north and further offshore (Appendix B), so some seasonal models with more southern spatial distributions predicted a negative relationship between density and wind stress in the east-west direction (e.g., Brown Pelican winter, Least Tern fall, Royal Tern fall) while some seasonal models with more northern spatial distributions predicted a positive relationship between density and wind stress in the east-west direction (e.g., Common Murre winter, Leach's Storm-Petrel fall). Wind stress was more often important in fall and winter models when the westerlies are stronger and the north-south gradient in east-west wind stress is greater.

Generally speaking the climate index predictor variables were relatively unimportant. They were more important in the spring and fall models than in the summer and winter models. The Atlantic Multidecadal Oscillation (AMO) index and the Trans-Niño Index (TNI) were the most important of the four indices on average including their 1-year-lagged versions, although the Multivariate El Niño-Southern Oscillation Index (MEI) and the North Atlantic Oscillation (NAO) index were important in some models.

4. Discussion

4.1 Interpretation of maps

This report presents maps of the seasonal spatial distributions of 47 marine bird species in U.S. Atlantic OCS waters (Appendix C) that can be used to inform marine spatial planning in the region. The maps of predicted relative density are accompanied by corresponding maps of the estimated CV of model predictions. It is important that these uncertainty maps are considered alongside the relative density maps. In many cases the CVs are very large indicating substantial statistical uncertainty and variability associated with the corresponding predictions, and those predictions should be interpreted cautiously. Although model predictions are at a 2-km resolution, interpretation of the maps presented here to inform spatial planning is probably more reliable at scales of 10-100 km. The maps of predicted relative density are also accompanied by inset maps of observed relative density. These inset maps indicate where species

were seen during a given season by the surveys analyzed here, and this information should also be considered when interpreting model predictions.

The maps represent spatial predictions of long-term average relative density. They do not provide predictions of the actual number of individuals of a given species that would be expected in a given area; they only indicate where a given species may be more or less abundant. Also, the maps do not provide predictions of density at a specific time; they only indicate seasonal distributions averaged across the timeframe of the survey dataset (1978-2016). The spatial distributions of marine birds often change during the course of a season and from year to year in response to fluctuations in environmental conditions, prey distributions, and fisheries (Oedekoven et al. 2001; Ballance et al. 2006; Renner et al. 2013; Nisbet and Veit 2015; Gjerdrum and Bolduc 2016; Goyert et al. 2016; Suryan et al. 2016; Veit et al. 2016; White and Veit 2018), so it is likely that the spatial distributions of many if not all of the modeled species have changed over time. Furthermore, long-term average spatial distributions do not necessarily highlight areas that are consistently used by a large number of birds but only for a short period during the year (e.g., hours or days); for example, movement corridors. By definition, areas of high long-term relative density should reflect relatively large numbers of birds using those areas for longer periods.

The maps represent predicted density relative to the study area only. The study area excluded very nearshore waters and coastal sounds and bays (e.g., Bay of Fundy, Long Island Sound, Delaware Bay, Chesapeake Bay) that are used by multiple marine bird species, sometimes with large numbers of birds occurring in these areas at certain times of year (e.g., wintering waterfowl). More generally, areas of high density occur adjacent to the study area for some species, and these areas are not represented on the maps. Thus, the areas with the highest predicted relative densities are not necessarily the areas of highest density for a species were its entire range to be considered. Depending on data availability, habitat-based predictive modeling could theoretically be extended to very nearshore waters and coastal sounds and bays, but such modeling would entail additional considerations. For example, relationships between bird density and environmental predictors may be different in these areas than in more offshore areas. Another consideration would be an appropriate spatial modeling technique for complex coastlines (Scott-Hayward et al. 2014).

4.2 Data limitations and information gaps

The maps presented here represent model predictions that ultimately rely on the underlying survey data that the models were fit to. The distribution of survey effort was highly uneven across the study area and over time (Figs 2 and 3), so some regions and years were much better sampled than others. For example, there were many fewer data offshore than nearshore. Model predictions in areas with no survey effort are indicated by hatched overlays on the maps. Predictions in these areas should be interpreted with caution, and we recommend additional field surveys to validate them. More generally, additional survey effort in under-sampled areas (e.g., the southern part of the study area; Fig. 3) would help to improve future model predictions. In order for future survey data to be amenable to an analysis such as that presented here, surveys should adhere to standardized survey protocols for marine birds at sea and document key information related to survey effort (e.g., complete spatial descriptions of transects, duration of observation, strip width, etc.).

Future habitat-based predictive modeling could also benefit from data on additional environmental predictor variables. Most of the environmental predictors used in this study would be indirect drivers of marine bird distributions. Data on variables that birds are responding to more directly (e.g., prey) would likely improve model predictions, particularly in areas with little or no survey effort. Unfortunately,

comprehensive climatologies of prey densities across the entire study area were not available for this study.

4.3 Combining seasonal maps

The seasonal maps presented in Appendix C represent periods of three months of the year for individual species. For some applications it may be of interest to consider an annual average distribution for individual species or a seasonal/annual average distribution across species. Such combining of seasonal maps should be done cautiously while acknowledging important assumptions.

To derive an annual map for a single species, we suggest averaging the seasonal predicted grids for that species assuming zero relative density for seasons that were not modeled. Ideally for bootstrapped predictions, a bootstrapped sample of annual predicted grids would be derived first and then desired quantities calculated from that sample (e.g., median, quantiles, etc.). The averaging of seasonal grids entails several important assumptions. First, species are often present in the study area at low density during seasons that were not modeled, so the assumption of zero density during those seasons is an approximation. Second, the predictions in each seasonal grid correspond to the average year of the survey data for that season which varied across seasons (spring – 2002, summer – 2003, fall – 2004, winter – 2006). Thus, the seasonal maps represent predictions for different years, so any variation in relative density across years will influence predictions averaged across seasons. Third, as discussed previously the predictions are of relative density and do not explicitly account for several potential biases (e.g., detectability). Any variation in these biases across seasons will influence predictions averaged across seasons. Fig. 7 shows annual maps for an example species, Atlantic Puffin. By averaging the seasonal predicted grids the annual map most reflects the seasons with the highest predicted relative density values, in this case summer and winter.

To derive multi-species maps, we suggest first normalizing the predicted grids for individual species and then averaging grids across species. Predicted relative density values are not comparable between species, so it would be inappropriate to directly average predicted grids across species. Normalization scales each grid the same, which makes averaging of grids across species more appropriate. Predicted grids can be normalized by dividing the predicted relative density value for each grid cell by the sum of predicted relative density values in all grid cells. If the grid dimensions are identical among species, as they are here, dividing by the mean predicted density value will achieve an equivalent normalization. Averaged normalized predicted values do not have a straightforward interpretation, so as with all predictions of relative density presented in this report it is the relative differences in predictions across space that are relevant, not the actual numbers themselves. It is important to note that because of normalization each species will essentially contribute equally to the average grid. Such equal weighting for all species may be desirable in some applications, but in others it may be desirable to weight species differently, for example by their population abundance. The results presented here could theoretically be used to derive weighted averages, but such an approach would require supplementary information to inform the weighting (e.g., independent estimates of population abundance). Fig. 8 shows an example multi-species winter map for a ‘coastal waterfowl’ species group as defined by Curtice et al. (2016). The group includes Black Scoter, Common Eider, Common Loon, Long-tailed Duck, Red-throated Loon, Surf Scoter, and White-winged Scoter.

4.4 Species identification

A fundamental assumption of the analysis presented here is that all species, when present, were recorded. This assumption might have been violated on one or more surveys if observers were focused on particular groups of species and failed to record occurrences of other species. A related issue is the identification of observed birds to the species level. From some survey platforms, or again if observers were more focused on some species than others, some birds might have been less likely to be identified to species. Birds that can be difficult to identify to species include but are not limited to alcids (e.g., Common Murre and Razorbill), gulls, jaegers, loons, phalaropes, scoters, storm-petrels, and terns. Birds that were not identified to species were not included in the main analysis presented here.

Our statistical modeling framework allowed for differences in the expected count of a given species among survey platforms and transects, so theoretically the models could account for some differences arising from failure to record or identify species. However, if a geographic area was covered by a limited number of surveys or platforms, then it would have been difficult or impossible for the model to determine whether differences in counts in that area were because of fewer birds in that area or because of differences in species recording and identification in that area.

Phalaropes provide an illustrative example of the effect of species identification on predicted relative density. Phalaropes are relatively small birds that can be difficult to identify to species from typical aerial surveys. Unidentified phalaropes accounted for 18%, 33%, and 44% of all phalaropes counted in spring, summer, and fall, respectively. A 'multi-species' model fit to pooled sighting data for Red Phalarope, Red-necked Phalarope, and unidentified phalaropes predicted areas of high relative density similar to those predicted by the individual species' models but also predicted areas of high relative density that were not evident in the individual species' maps. The spring multi-species model predicted a band of moderate to high relative density off South Carolina and North Carolina and the fall multi-species model predicted a band of moderate relative density off the east coast of northern Florida and Georgia (Fig. 9), neither of which were apparent in the spring and fall maps for Red Phalarope and Red-necked Phalarope (Appendix C). These areas of predicted moderate to high relative density corresponded to multiple sightings of phalaropes that were not identified to species, almost entirely from three aerial surveys: AMAPPS_FWS_Aerial_Spring2012, AMAPPS_FWS_Aerial_Fall2012, and AMAPPS_FWS_Aerial_Fall2013 (Table 1). The areas of predicted moderate to high relative density in spring ran along and between BOEM areas for South Carolina and North Carolina, with particularly high predicted relative density along the eastern edge of the South Carolina Grand Strand area. The results of this example multi-species model for phalaropes highlights that models fit to individual species data may fail to identify an area of high relative density when the number of surveys in that area is limited and identification to species is difficult. Pooling data across species, as was done in this example, is one option for identifying these areas, but inference is then restricted to the group of species as a whole. Alternative modeling techniques in combination with appropriate survey data may provide some ability to make individual species inferences from sightings of unidentified species (e.g., Johnston et al. 2015).

4.5 Comparison to other marine bird distribution models

A wealth of information is available about the distribution of marine birds in US Atlantic waters (e.g., see Nisbet et al. 2013 for a recent review). Here we compare our model predictions to results of other recent habitat-based modeling studies in this region. Habitat-based modeling of the spatial distributions of marine birds is an active field of research (Tremblay et al. 2009). Multiple studies have developed habitat-based distribution models for some of the species modeled here in parts of our study area often using

some of the same survey data (Zipkin et al. 2010; Winiarski et al. 2013, 2014a, b; Goyert 2014; Lieske et al. 2014; Flanders et al. 2015; Balderama et al. 2016; Goyert et al. 2016; Sollmann et al. 2016). By focusing on a smaller area, fewer predictor variables, fewer species, or a subset of the survey data with more homogenous sampling protocols these studies were able to employ alternative modeling techniques like distance sampling (e.g., Winiarski et al. 2013), occupancy modeling (Flanders et al. 2015), hierarchical multi-species community models (e.g., Goyert et al. 2016), and temporally varying spatial distributions (e.g., Balderama et al. 2016). Many of these studies were more focused on inference about ecological drivers of marine bird distributions so they employed modeling techniques more appropriate for that objective, although one of the three techniques considered by Lieske et al. (2014) was a machine learning technique with some similarity to the framework used here. Goyert (2014) was able to use data on prey abundance that were not available for our entire study area and timeframe improving their ability to make ecological inferences. While the combination of geographical scope, spatial resolution, number and heterogeneity of survey data, and number of species modeled here precluded many of these alternative modeling techniques, there are some elements that could theoretically be incorporated into the modeling framework used here. For example, there are statistical likelihood distributions that may better capture the extremely skewed count distributions for some species than the negative binomial likelihood used here (Zipkin et al. 2014, 2015; Balderama et al. 2016). More fundamental changes to the modeling framework would require sacrificing other aspects. For example, allowing spatial distributions to vary over time would limit either the number of predictor variables that could be used or the timespan of survey data that could be analyzed because most predictors do not have complete data from the entire timespan of the survey data (Mannocci et al. 2017). Fewer predictors or fewer survey data could reduce the predictive ability of the models.

Despite methodological differences, there were some similarities between the predicted spatial distributions of marine birds presented here and those found by other studies, but there were also differences especially at a fine spatial scale. Winiarski et al. (2013, 2014a) predicted higher Common Loon wintering densities in the western part of the Rhode Island Ocean Special Area Management Plan (RISAMP) area than in the eastern part, similar to the predictions presented here, although there are fine scale differences. The predicted winter distribution of Northern Gannet density in this area presented by Winiarski et al. (2014b) was less similar to our predicted distribution. Predicted spring distributions of Common Tern and Roseate Tern in Massachusetts waters presented by Goyert (2014) were quite different from those presented here, although there was an area of predicted high density of Roseate Tern east of Martha's Vineyard in both studies. Goyert (2014) predicted areas of high density west of Martha's Vineyard for both species, at the north end of Cape Cod for Common Tern, and inside Cape Cod Bay for Roseate Tern that were not apparent in our model predictions. Predicted seasonal density distributions for several species in the lower Mid-Atlantic Bight presented by Goyert et al. (2016) were qualitatively similar to the predicted distributions presented here. For example, predicted distributions of Common Tern (summer), Royal Tern (summer), Laughing Gull (fall), Dovekie (winter), Red-throated Loon (winter and spring), and Wilson's Storm-Petrel (summer) all exhibited similar inshore-offshore gradients in density. However some of the predicted distributions presented by Goyert et al. (2016) exhibited finer scale patterning that was not evident in the predictions presented here (e.g., Common Tern summer 2013, Razorbill winter 2013-2014). Broad similarities between the predicted distributions presented here and predicted distributions from other modeling studies in the same area are perhaps not surprising especially when there is overlap in the data analyzed. It is more difficult to ascribe the observed differences to specific causes. One of the likely common causes of differences is the shorter timespan of data analyzed in other studies combined with intra-seasonal and inter-annual variation in marine bird distributions. For

example, the spring survey data analyzed by Goyert (2014) came from a 10-day period in May over two years, whereas our predicted spring distributions reflect the average distribution from March, April, and May over many years.

4.6 Comparison to tracking studies

Electronic tracking of marine birds and habitat-based modeling of their distributions from tracking data is a burgeoning field of research (Tremblay et al. 2009; Wakefield et al. 2009, 2017). By following individual animals for extended periods of time tracking studies produce dense longitudinal data on animal locations that provide information generally much more difficult if not impossible to obtain from at-sea surveys. For example, tracking data more easily allow for the identification of areas that are used by animals consistently but for only short periods of time (e.g., movement corridors). One can infer behavioral states (e.g., foraging or migration) from tracking data (Jonsen et al. 2005) and thereby partition space usage by behavior, although direct behavioral data are often collected during at-sea surveys. Many electronic tracking technologies monitor animals wherever they go and so are not limited in geographical coverage like many survey platforms. Common limitations of tracking data are that results can be unrepresentative at the population level due to small sample size and that some species can be difficult to track (e.g., too small to carry electronic devices), although as sample sizes continue to increase and technology continues to improve these limitations are becoming less of an issue. Electronic tracking studies provide valuable information on the spatial distribution of marine birds that is complementary to the information provided by the analysis of at-sea survey data.

Multiple species modeled in this study have been tracked within the study area. Spiegel et al. (2017) reported on tracking of Red-throated Loon, Surf Scoter, and Northern Gannet in mid-Atlantic U.S. waters and compared their estimated distributions to seasonal predicted distributions from an earlier phase of this project (Kinlan et al. 2016). There was general agreement between the distributions of all three species in winter, but the distributions were less similar in spring and fall. In at least one case, Red-throated Loon during fall, the predicted distribution presented here is a better match with the distribution presented by Spiegel et al. (2017), but differences remain for other species and seasons. Spiegel et al. (2017) outline several possible reasons for these differences, but perhaps the most obvious reason is our exclusion of coastal sounds and bays and the heavy usage of those areas by tracked individuals (e.g., Surf Scoter in Chesapeake Bay).

Loring et al. (2014) and Beuth et al. (2017) reported on tracking of sea ducks, Black Scoter and Common Eider, respectively, in waters off southern New England. The winter distribution of tracked Black Scoter individuals (Fig. 4 of Loring et al. 2014) bore some broad similarities with the predicted distribution presented here; for example, areas of high usage/relative density between Cape Cod and Nantucket, between Nantucket and Martha's Vineyard, and off the east end of Long Island, with lower usage/relative density in the eastern central part of the RISAMP area. The winter distribution of Common Eider tagged along the coast of Rhode Island (Fig. 2 of Beuth et al. 2017) was quite different from the predicted distribution presented here. Areas of high usage by tracked individuals along the coast and near Block Island were not evident in our model predictions which were fairly flat across the RISAMP area in comparison to localized areas of predicted high relative density further east in and around Nantucket Sound.

Hatch et al. (2016) and Powers et al. (2017) reported on tracking of Great Shearwater in the Gulf of Maine from June-December. Broadly speaking, the estimated distribution (Hatch et al. 2016; their Fig. 1b) and locations (Powers et al. 2017; their Fig. 3) of tracked individuals overlapped with areas of

predicted highest density presented here for summer and fall. However, Powers et al. (2017) identified a migration pathway out of the Gulf of Maine in August and September (their Fig. 4) that is not particularly evident in the predicted distributions presented here, highlighting the advantage of tracking data for identifying movement corridors.

Jodice et al. (2015) reported on tracking of Black-capped Petrel tagged at a breeding site in the Caribbean. During the post-breeding period (summer-fall) locations of tracked individuals overlapped with sighting locations from the at-sea survey data and corresponding areas of predicted highest density presented here, for example along the western edge of the Gulf Stream and in the South Atlantic Bight (see Fig. 4 of Jodice et al. 2015 for visual comparison). Tracked individuals also visited waters further offshore, east of the Gulf Stream and around and beyond the Blake Spur. There was little at-sea survey effort in these areas, but the models predicted high relative density of Black-capped Petrel there, especially during summer.

Several past and current studies have tracked Brown Pelican within and adjacent to our study area (Poli 2015; Lamb 2016; Smithsonian Migratory Connectivity Project http://www.migratoryconnectivityproject.org/livetracks/). The distribution of tracked individuals along the U.S. Atlantic coast (Poli 2015; their Fig. 2.2) exhibited localized areas of high usage that corresponded to areas of predicted high relative density in the seasonal distributions presented here (e.g., near Charleston, SC; near Cape Canaveral, FL; and along the coast of the Delmarva peninsula and the mouth of Chesapeake Bay, especially during the summer breeding season). The distribution of tracked individuals presented by Poli (2015) was highly coastal, further confirming the spuriousness of predicted areas of moderate density far offshore for this species during winter.

In addition to the studies discussed above, there are other past and current tracking projects of marine birds in and adjacent to our study area. For example, at the north end of our study area, alcids have been tracked from Machias Seal Island in the Gulf of Maine (e.g., Clarke et al. 2010). The movements of Common Tern and Roseate Tern along the northeast U.S. Atlantic coast have been studied using geolocators (Nisbet et al. 2011; Mostello et al. 2014) and using VHF transmitters and automated radio telemetry stations (Loring 2016). As tracking data continue to accumulate for marine bird species along the U.S. Atlantic coast they will provide an invaluable resource for describing and understanding the spatial distributions of these species, complementing the information provided by the analysis of at-sea survey data (Perrow et al. 2015). We echo the call by Spiegel et al. (2017) for better integration of these two types of information, especially the development of a rigorous analytical framework that can be used to inform management decisions.

4.7 Conclusion

The maps presented in this report can be used to inform planning for ocean activities such as offshore wind energy development. The maps identify areas where the densities of marine bird species are likely to be higher or lower on a seasonal basis. This information can contribute to assessments of relative risk exposure aimed at minimizing the impacts of activities on marine birds (Winiarski et al. 2014b; Fifield et al. 2017). As discussed in Section 4.2, the survey data analyzed here had some limitations. Any full assessments of risk exposure in specific areas at specific times should augment the information provided here with more targeted analyses and potentially additional survey (or tracking) data to inform those analyses, especially when there are few existing data. Nevertheless, our maps provide a starting point for assessing relative risk exposure, which when combined with information about other aspects of risk exposure and vulnerability (e.g., flight height, avoidance/attraction, demographic impacts), can inform

assessments of overall risk for marine birds in U.S. Atlantic OCS waters (Garthe and Hüppop 2004; Robinson Willmott et al. 2013; Bailey et al. 2014; Bradbury et al. 2014).

5. Literature Cited

Bailey, H., Brookes, K. L., and Thompson, P. M. 2014. Assessing environmental impacts of offshore wind farms: lessons learned and recommendations for the future. Aquatic Biosystems 10:8.

Balderama, E., Gardner, B., and Reich, B. J. 2016. A spatial–temporal double-hurdle model for extremely over-dispersed avian count data. Spatial Statistics 18:263-275.

Ballance, L. T., Pitman, R. L., and Fiedler, P. C. 2006. Oceanographic influences on seabirds and cetaceans of the eastern tropical Pacific: A review. Progress in Oceanography 69:360-390.

Barlow, J. 2015. Inferring trackline detection probabilities, g(0), for cetaceans from apparent densities in different survey conditions. Marine Mammal Science 31:923-943.

Bates, D. and Maechler, M. 2017. Matrix: Sparse and dense matrix classes and methods. R package version 1.2-8. URL: https://CRAN.R-project.org/package=Matrix (accessed March 1, 2018).

Becker, R. A., Wilks, A. R., Brownrigg, R., Minka, T. P., and Deckmyn, A. 2016. maps: Draw geographical maps. R package version 3.1.1. URL: https://CRAN.R-project.org/package=maps (accessed March 1, 2018).

Beuth, J. M., Mcwilliams, S. R., Paton, P. W., and Osenkowski, J. E. 2017. Habitat use and movements of common eiders wintering in southern New England. Journal of Wildlife Management 81:1276-1286.

Bivand, R., Keitt, T., and Rowlingson, B. 2015. rgdal: Bindings for the Geospatial Data Abstraction Library. R package version 1.0-4. URL: https://CRAN.R-project.org/package=rgdal (accessed March 1, 2018).

Bivand, R. and Lewin-Koh, N. 2015. maptools: Tools for reading and handling spatial objects. R package version 0.8-36. URL: https://CRAN.R-project.org/package=maptools (accessed March 1, 2018).

Bivand, R. and Rundel, C. 2015. rgeos: Interface to Geometry Engine - Open Source (GEOS). R package version 0.3-11. URL: https://CRAN.R-project.org/package=rgeos (accessed March 1, 2018).

Bodenhofer, U., Krone, M., and Klawonn, F. 2013. Testing noisy numerical data for monotonic association. Information Sciences 245:21-37.

Boudt, K., Cornelissen, J., and Croux, C. 2012. The Gaussian rank correlation estimator: robustness properties. Statistics and Computing 22:471-483.

Bradbury, G., Trinder, M., Furness, B., Banks, A. N., Caldow, R. W. G., and Hume, D. 2014. Mapping seabird sensitivity to offshore wind farms. PLoSOne 9:1-17.

Bühlmann, P. and Hothorn, T. 2007. Boosting algorithms: Regularization, prediction and model fitting. Statistical Science 22(4):477-505.

Canty, A. and Ripley, B. 2015. boot: Bootstrap R (S-Plus) functions. R package version 1.3-17. URL: https://cran.r-project.org/web/packages/boot/index.html (accessed March 1, 2018).

Clarke, T. C. R., Diamond, A. W., and Chardine, J. W. 2010. Origin of Canadian Razorbills (*Alca torda*) wintering in the outer Bay of Fundy confirmed by radio-tracking. Waterbirds 33:541-545.

Conn, P. B., Thorson, J. T., and Johnson, D. S. 2017. Confronting preferential sampling when analysing population distributions: diagnosis and model-based triage. Methods in Ecology and Evolution 8:1535-1546.

Curtice, C., Cleary J., Shumchenia E., and Halpin P.N. 2016. Marine-life Data and Analysis Team (MDAT) technical report on the methods and development of marine-life data to support regional ocean planning and management. Prepared on behalf of the Marine-life Data and Analysis Team (MDAT). URL: http://seamap.env.duke.edu/models/MDAT/MDAT-Technical-Report-v1_1.pdf (accessed March 1, 2018).

Fifield, D. A., Hedd, A., Avery-Gomm, S., Robertson, G. J., Gjerdrum, C., and McFarlane Tranquilla, L. 2017. Employing predictive spatial models to inform conservation planning for seabirds in the Labrador Sea. Frontiers in Marine Science 4:149.

Flanders, N. P., Gardner, B., Winiarski, K., Paton, P. W. C., Allison, T., and O'Connell, A. F. 2015. Key seabird areas in southern New England identified using a community occupancy model. Marine Ecology Progress Series 533:277-290.

Friedman, J. H. 2002. Stochastic gradient boosting. Computational Statistics & Data Analysis 38:367-378.

Furrer, R. and Sain, S. R. 2010. spam: A sparse matrix R Package with emphasis on MCMC methods for Gaussian Markov random fields. Journal of Statistical Software 36(10).

Garthe, S., and Hüppop, O. 2004. Scaling possible adverse effects of marine wind farms on seabirds: developing and applying a vulnerability index. Journal of Applied Ecology 41:724-734.

Genz, A., Bretz, F., Miwa, T., Mi, X., Leisch, F., Scheipl, F., and Hothorn, T. 2014. mvtnorm: Multivariate normal and *t* distributions. R package version 1.0-2. URL: http://CRAN.R-project.org/package=mvtnorm (accessed March 1, 2018).

Gjerdrum, C. and Bolduc, F. 2016. Non-breeding distribution of Herring Gull (*Larus argentatus*) and Great Black-backed Gull (*Larus marinus*) in Eastern Canada from ship-based surveys. Waterbirds (Special Publication 1):202-219.

Goyert, H. F. 2014. Relationship among prey availability, habitat, and the foraging behavior, distribution, and abundance of common terns *Sterna hirundo* and roseate terns *S. dougallii*. Marine Ecology Progress Series 506:291-302.

Goyert, H. F., Gardner, B., Sollmann, R., Veit, R. R., Gilbert, A. T., Connelly, E. E., and Williams, K. A. 2016. Predicting the offshore distribution and abundance of marine birds with a hierarchical community distance sampling model. Ecological Applications 26:1797-1815.

Grothendieck, G., Kates, L., and Petzoldt, T. 2012. proto: Prototype object-based programming. R package version 0.3-10. URL: https://CRAN.R-project.org/package=proto (accessed March 1, 2018).

Grothendieck, G. 2014a. gsubfn: Utilities for strings and function arguments. R package version 0.6-6. URL: https://CRAN.R-project.org/package=gsubfn (accessed March 1, 2018).

Grothendieck, G. 2014b. sqldf: Perform SQL selects on R data frames. R package version 0.4-10. URL: https://CRAN.R-project.org/package=sqldf (accessed March 1, 2018).

Hatch, J. M., Wiley, D., Murray, K. T., and Welch, L. 2016. Integrating Satellite-Tagged Seabird and Fishery-Dependent Data: A Case Study of Great Shearwaters (*Puffinus gravis*) and the U.S. New England Sink Gillnet Fishery. Conservation Letters 9:43-50.

Heinänen, S., Žydelis, R., Dorsch, M., Nehls, G., and Skov, H. 2017. High-resolution sea duck distribution modeling: Relating aerial and ship survey data to food resources, anthropogenic pressures, and topographic variables. Condor 119:175-190.

Hijmans, R. J. 2015. raster: Geographic data analysis and modeling. R package version 2.4-15. URL: https://CRAN.R-project.org/package=raster (accessed March 1, 2018).

Hofner, B., Mayr, A., Robinzonov, N., and Schmid, M. 2012. Model-based boosting in R: A hands-on tutorial using the R package mboost. Technical Report 120, Department of Statistics, University of Munich, Germany.

Hofner, B. and Hothorn, T. 2015. stabs: Stability selection with error control. R package version 0.5-1. URL: https://CRAN.R-project.org/package=stabs (accessed March 1, 2018).

Hothorn, T., Hornik, K., and Zeileis, A. 2006. Unbiased recursive partitioning: A conditional inference framework. Journal of Computational and Graphical Statistics 15:651-674.

Hothorn, T., Leisch, F., and Zeileis, A. 2013. modeltools: Tools and classes for statistical models. R package version 0.2-21. URL: https://CRAN.R-project.org/package=modeltools (accessed March 1, 2018).

Hothorn, T., Buehlmann, P., Kneib, T., Schmid, M., and Hofner, B. 2015. mboost: Model-based boosting. R package version 2.4-2. URL: https://CRAN.R-project.org/package=mboost (accessed March 1, 2018).

Huettmann, F., Diamond, A. W., Dalzell, B., and Macintosh, K. 2005. Winter distribution, ecology and movements of Razorbills *Alca torda* and other auks in the outer Bay of Fundy, Atlantic Canada. Marine Ornithology 33:161-171.

Jackman, S. 2015. pscl: Classes and methods for R developed in the Political Science Computational Laboratory, Department of Political Science, Stanford University. Stanford, CA. R package version 1.4.9. URL: https://CRAN.R-project.org/package=pscl (accessed March 1, 2018).

Jenness, J. 2013. DEM Surface Tools. Jenness Enterprises. URL: http://www.jennessent.com/arcgis/surface_area.htm (accessed March 1, 2018).

Jodice, P. G. R., Ronconi, R. A., Rupp, E., Wallace, G. E., and Satgé, Y. 2015. First satellite tracks of the Endangered black-capped petrel. Endangered Species Research 29:23-33.

Johnston, A., Thaxter, C. B., Austin, G. E., Cook, A. S., Humphreys, E. M., Still, D. A., Mackay, A., Irvine, R., Webb, A., and Burton, N. H. 2015. Modelling the abundance and distribution of marine birds accounting for uncertain species identification Journal of Applied Ecology 52:150-160.

Jonsen, I. D., Flemming, J. M., and Myers, R. A. 2005. Robust state-space modeling of animal movement data. Ecology 86:2874-2880.

Kinlan, B. P., Winship, A. J., White, T. P., and Christensen, J. 2016. Modeling at-sea occurrence and abundance of marine birds to support Atlantic marine renewable energy planning: Phase I report. U.S. Department of the Interior, Bureau of Ocean Energy Management, OCS Study BOEM 2016-039. Sterling, VA. 113 pp.

Lamb, J. S. 2016. Ecological drivers of brown pelican movement patterns and reproductive success in the Gulf of Mexico. Ph.D. thesis. Clemson University, Clemson, SC. 216 pp.

Lieske, D. J., Fifield, D. A., and Gjerdrum, C. 2014. Maps, models, and marine vulnerability: Assessing the community distribution of seabirds at-sea. Biological Conservation 172:15-28.

Loring, P. H., Paton, P. W., Osenkowski, J. E., Gilliland, S. G., Savard, J.-P. L., and Mcwilliams, S. R. 2014. Habitat use and selection of black scoters in southern New England and siting of offshore wind energy facilities. Journal of Wildlife Management 78:645-656.

Loring, P. H. 2016. Evaluating digital VHF technology to monitor shorebird and seabird use of offshore wind energy areas in the western North Atlantic. Ph.D. thesis. University of Massachusetts, Amherst, MA. 172 pp.

Mannocci, L., Boustany, A. M., Roberts, J. J., Palacios, D. M., Dunn, D. C., Halpin, P. N., Viehman, S., Moxley, J., Cleary, J., Bailey, H., Bograd, S. J., Becker, E. A., Gardner, B., Hartog, J. R., Hazen, E. L., Ferguson, M. C., Forney, K. A., Kinlan, B. P., Oliver, M. J., Perretti, C. T., Ridoux, V., Teo, S. L. H., and Winship, A. J. 2017. Temporal resolutions in species distribution models of highly mobile marine animals: Recommendations for ecologists and managers Diversity and Distributions 23:1098-1109.

Mayr, A., Fenske, N., Hofner, B., Kneib, T., and Schmid, M. 2012. Generalized additive models for location, scale and shape for high dimensional data---a flexible approach based on boosting. Applied Statistics 61(3):403-427.

Miller, P. I. and Christodoulou, S. 2014. Frequent locations of oceanic fronts as an indicator of pelagic diversity: Application to marine protected areas and renewables. Marine Policy 45:318-329.

Mostello, C. S., Nisbet, I. C. T., Oswald, S. A., and Fox, J. W. 2014. Non-breeding season movements of six North American Roseate Terns *Sterna dougallii* tracked with geolocators. Seabird 27:1-21.

Müller, K., Wickham, H., James, D. A., and Falcon, S. 2014. RSQLite: 'SQLite' interface for R. R package version 1.0.0. URL: https://CRAN.R-project.org/package=RSQLite (accessed March 1, 2018).

Nisbet, I. C. T., Mostello, C. S., Veit, R. R., Fox, J. W., and Afanasyev, V. 2011. Migrations and winter quarters of five Common Terns tracked using geolocators. Waterbirds 34:32-39.

Nisbet, I. C., Veit, R. R., Auer, S. A., and White, T. P. 2013. Marine birds of the eastern United States and the Bay of Fundy: Distribution, numbers, trends, threats, and management. Nuttall Ornithological Club, Cambridge, MA.

Nisbet, I. C. T. and Veit, R. R. 2015. An explanation for the population crash of Red-necked Phalaropes *Phalaropus lobatus* staging in the Bay of Fundy in the 1980s. Marine Ornithology 43:119-121.

Nychka, D., Furrer, R., Paige, J., and Sain, S. 2015. fields: Tools for spatial data. R package version 8.10. URL: https://CRAN.R-project.org/package=fields (accessed March 1, 2018).

O'Connell, A. F., Gardner, B., Gilbert, A. T., and Laurent, K. 2009. Compendium of Avian Occurrence Information for the Continental Shelf Waters along the Atlantic Coast of the United States, Final report (Database Section – Seabirds). U.S. Department of the Interior, Bureau of Ocean Energy Management, OCS Study BOEM 2012-076. Herndon, VA. 344 pp.

Oedekoven, C. S., Ainley, D. G., and Spear, L. B. 2001. Variable responses of seabirds to change in marine climate: California Current, 1985-1994. Marine Ecology Progress Series 212:265-281.

Pebesma, E. J., and Bivand, R. S. 2005. Classes and methods for spatial data in R. R News 5(2). URL: https://CRAN.R-project.org/doc/Rnews/ (accessed March 1, 2018).

Perrow, M. R., Harwood, A. J., Skeate, E. R., Praca, E., and Eglington, S. M. 2015. Use of multiple data sources and analytical approaches to derive a marine protected area for a breeding seabird. Biological Conservation 191:729 – 738.

Pinheiro, J., Bates, D., DebRoy, S., Sarkar, D., and R Core Team. 2017. nlme: Linear and nonlinear mixed effects models. R package version 3.1-131. URL: http://CRAN.R-project.org/package=nlme (accessed March 1, 2018).

Poli, C. 2015. Variability in movement patterns and habitat use of two species of Pelecaniformes. M.Sc. thesis. Clemson University, Clemson, SC. 104 pp.

Powers, K. D., Wiley, D. N., Allyn, A. J., Welch, L. J., and Ronconi, R. A. 2017. Movements and foraging habitats of great shearwaters Puffinus gravis in the Gulf of Maine. Marine Ecology Progress Series 574:211-226.

R Core Team. 2017. R: A language and environment for statistical computing. R Foundation for Statistical Computing, Vienna, Austria. URL: http://www.R-project.org/ (accessed March 1, 2018).

R Special Interest Group on Databases (R-SIG-DB), Wickham, H., and Müller, K. 2017. DBI: R Database Interface. R package version 0.6-1. URL: https://CRAN.R-project.org/package=DBI (accessed March 1, 2018).

Renner, M., Parrish, J. K., Piatt, J. F., Kuletz, K. J., Edwards, A. E., and Hunt Jr, G. L. 2013. Modeled distribution and abundance of a pelagic seabird reveal trends in relation to fisheries. Marine Ecology Progress Series 484:259-277.

Robin, X., Turck, N., Hainard, A., Tiberti, N., Lisacek, F., Sanchez, J.-C., and Müller, M. 2011. pROC: an open-source package for R and S+ to analyze and compare ROC curves. BMC Bioinformatics 12:77.

Robinson Willmott, J. C., G. Forcey, and A. Kent. 2013. The relative vulnerability of migratory bird species to offshore wind energy projects on the Atlantic Outer Continental Shelf: An assessment method and database. Final Report to the U.S. Department of the Interior, Bureau of Ocean Energy Management, Office of Renewable Energy Programs. OCS Study BOEM 2013-207. 275 pp.

Ryan, W. B. F., Carbotte, S. M., Coplan, J. O., O'Hara, S., Melkonian, A., Arko, R., Weissel, R.A., Ferrini, V., Goodwillie, A., Nitsche, F., Bonczkowski, J., and Zemsky, R. 2009. Global Multi-Resolution Topography synthesis. Geochemistry, Geophysics, Geosystems 10:Q03014.

Sarkar, D. 2008. Lattice: Multivariate data visualization with R. Springer, New York, NY.

Schmid, M., Potapov, S., Pfahlberg, A., and Hothorn, T. 2008. Estimation and regularization techniques for regression models with multidimensional prediction functions. Technical Report 42, Department of Statistics, University of Munich, Germany.

Scott-Hayward, L. A. S., Mackenzie, M. L., Donovan, C. R., Walker, C. G., and Ashe, E. 2014. Complex Region Spatial Smoother (CReSS). Journal of Computational and Graphical Statistics 23:340-360.

Sollmann, R., Gardner, B., Williams, K. A., Gilbert, A. T., and Veit, R. R. 2016. A hierarchical distance sampling model to estimate abundance and covariate associations of species and communities. Methods in Ecology and Evolution 7:529-537.

Spear, L.B., D.G. Ainley, and P. Pyle. 1999. Seabirds in southeastern Hawaiian waters. Western Birds 30:1-32.

Spiegel, C. S., Berlin, A. M., Gilbert, A. T., Gray, C. O., Montevecchi, W. A., Stenhouse, I. J., Ford, S. L., Olsen, G. H., Fiely, J. L., Savoy, L., Goodale, M. W., and Burke, C. M. 2017. Determining fine-scale use and movement patterns of diving bird species in federal waters of the mid-Atlantic United States using satellite telemetry. U.S. Department of the Interior, Bureau of Ocean Energy Management, OCS Study BOEM 2017-069. Sterling, VA. 260 pp.

Suryan, R. M., Kuletz, K. J., Parker-Stetter, S. L., Ressler, P. H., Renner, M., Horne, J. K., Farley, E. V., and Labunski, E. A. 2016. Temporal shifts in seabird populations and spatial coherence with prey in the southeastern Bering Sea. Marine Ecology Progress Series 549:199-215.

Tasker, M. L., Jones, P. H., Dixon, T., and Blake, B. F. 1984. Counting seabirds at sea from ships: a review of methods employed and a suggestion for a standardized approach. Auk 101:567-577.

Tremblay, Y., Bertrand, S., Henry, R. W., Kappes, M. A., Costa, D. P., and Shaffer, S. A. 2009. Analytical approaches to investigating seabird-environment interactions: a review. Marine Ecology Progress Series 391:153-163.

Veit, R. R., White, T. P., Perkins, S. A., and Curely, S. 2016. Abundance and distribution of seabirds off southeastern Massachusetts, 2011-2015. U.S. Department of the Interior, Bureau of Ocean Energy Management, OCS Study BOEM 2016-067. Sterling, VA. 82 pp.

Venables, W. N., and Ripley, B. D. 2002. Modern Applied Statistics with S. Fourth Edition. Springer, New York, NY.

Wakefield, E. D., Phillips, R. A., and Matthiopoulos, J. 2009. Quantifying habitat use and preferences of pelagic seabirds using individual movement data: a review. Marine Ecology Progress Series 391:165-182.

Wakefield, E. D., Owen, E., Baer, J., Carroll, M. J., Daunt, F., Dodd, S. G., Green, J. A., Guilford, T., Mavor, R. A., Miller, P. I., Newell, M. A., Newton, S. F., Robertson, G. S., Shoji, A., Soanes, L. M., Votier, S. C., Wanless, S., and Bolton, M. 2017. Breeding density, fine-scale tracking, and large-scale modeling reveal the regional distribution of four seabird species. Ecological Applications 27:2074-2091.

Weatherall, P., Marks, K. M., Jakobsson, M., Schmitt, T., Tani, S., Arndt, J. E., Rovere, M., Chayes, D., Ferrini, V., and Wigley, R. 2015. A new digital bathymetric model of the world's oceans. Earth and Space Science 2:331-345.

White, T. P., Veit, R. R., and Perry, M. C. 2009. Feeding ecology of Long-tailed Ducks *Clangula hyemalis* wintering on the Nantucket Shoals. Waterbirds 32:293-299.

White, T. P. and Veit. R. R. 2018. Spatial ecology of long-tailed ducks (*Clangula hyemalis*) and white-winged scoters (*Melanitta fusca*) wintering on Nantucket Shoals: persistent foraging areas stabilized by local enhancement. Unpublished manuscript.

Wickham, H. 2007. Reshaping data with the reshape package. Journal of Statistical Software 21(12).

Winiarski, K. J., Miller, D. L., Paton, P. W. C., and McWilliams, S. R. 2013. Spatially explicit model of wintering common loons: conservation implications. Marine Ecology Progress Series 492:273-283.

Winiarski, K. J., Burt, M. L., Rexstad, E., Miller, D. L., Trocki, C. L., Paton, P. W. C., and McWilliams, S. R. 2014a. Integrating aerial and ship surveys of marine birds into a combined density surface model: A case study of wintering Common Loons. Condor 116:149-161.

Winiarski, K. J., Miller, D. L., Paton, P. W., and McWilliams, S. R. 2014b. A spatial conservation prioritization approach for protecting marine birds given proposed offshore wind energy development. Biological Conservation 169:79-88.

Wood, S.N. 2006. Generalized additive models: An introduction with R. Chapman and Hall/CRC. Boca Raton, FL. 392 pp.

Yee, T. W. 2015. Vector generalized linear and additive models: With an implementation in R. Springer, New York, NY.

Zeileis, A., Leisch, F., Hornik, K., and Kleiber, C. 2002. strucchange: An R package for testing for structural change in linear regression models. Journal of Statistical Software 7(2).

Zeileis, A. and Grothendieck, G. 2005. zoo: S3 infrastructure for regular and irregular time series. Journal of Statistical Software 14(6).

Zeileis, A. 2006. Object-oriented computation of sandwich estimators. Journal of Statistical Software 16(9).

Zeileis, A., Kleiber, C., and Jackman, S. 2008. Regression models for count data in R. Journal of Statistical Software 27(8).

Zipkin, E. F., Gardner, B., Gilbert, A. T., O'Connell, A. F., Royle, J. A., and Silverman, E. D. 2010. Distribution patterns of wintering sea ducks in relation to the North Atlantic Oscillation and local environmental characteristics. Oecologia 163:893-902.

Zipkin, E. F., Leirness, J. B., Kinlan, B. P., O'Connell, A. F., and Silverman, E. D. 2014. Fitting statistical distributions to sea duck count data: Implications for survey design and abundance estimation. Statistical Methodology 17:67-81.

Zipkin, E. F., Kinlan, B. P., Sussman, A., Rypkema, D., Wimer, M., and O'Connell, A. F. 2015. Statistical guidelines for assessing marine avian hotspots and coldspots: A case study on wind energy development in the U.S. Atlantic Ocean. Biological Conservation 191:216-223.

Table 1. Survey datasets, sample sizes, and surveyed area analyzed. All datasets (and their ID codes) were extracted from the USFWS Northwest Atlantic Seabird Catalog except ECSAS which was provided by CWS-ECCC. Continuous data were segmented as described in Section 2.2. A description of each individual survey is presented in Appendix A. Area surveyed does not necessarily represent unique area surveyed; some surveys covered similar areas over multiple days, months, or years. Seasons were defined as spring (March-May), summer (June-August), fall (September-November), and winter (December-February). Sample sizes and surveyed area analyzed for corrected MassCEC datasets (see Section 2.2) are shown in parentheses.

Source Dataset ID	Platform	Method	Year		Number of transect segments					Area surveyed (km^2)				
			Start	End	Spring	Summer	Fall	Winter	Total	Spring	Summer	Fall	Winter	Total
AMAPPS_FWS_Aerial_Fall2012	aerial	continuous	2012	2012	0	0	2,986	0	2,986	0	0	4,765	0	4,765
AMAPPS_FWS_Aerial_Fall2013	aerial	continuous	2013	2013	0	0	4,629	0	4,629	0	0	7,395	0	7,395
AMAPPS_FWS_Aerial_Fall2014	aerial	continuous	2014	2014	0	0	2,876	0	2,876	0	0	4,608	0	4,608
AMAPPS_FWS_Aerial_Preliminary_ Summer2010	aerial	continuous	2010	2010	0	1,131	0	0	1,131	0	1,802	0	0	1,802
AMAPPS_FWS_Aerial_Spring2012	aerial	continuous	2012	2012	2,962	0	0	0	2,962	4,739	0	0	0	4,739
AMAPPS_FWS_Aerial_Summer2011	aerial	continuous	2011	2011	0	3,442	0	0	3,442	0	5,502	0	0	5,502
AMAPPS_FWS_Aerial_Winter2010-2011	aerial	continuous	2010	2011	0	0	0	513	513	0	0	0	823	823
AMAPPS_FWS_Aerial_Winter2014	aerial	continuous	2014	2014	0	0	0	3,073	3,073	0	0	0	4,914	4,914
AMAPPS_NOAA/NMFS_NEFSCBoat2011	boat	continuous	2011	2011	0	1,537	0	0	1,537	0	1,794	0	0	1,794
AMAPPS_NOAA/NMFS_NEFSCBoat2013	boat	continuous	2013	2013	0	1,577	0	0	1,577	0	1,853	0	0	1,853
AMAPPS_NOAA/NMFS_NEFSCBoat2014	boat	continuous	2014	2014	1,023	0	0	0	1,023	1,219	0	0	0	1,219
AMAPPS_NOAA/NMFS_NEFSCBoat2015	boat	continuous	2015	2015	0	261	0	0	261	0	308	0	0	308
AMAPPS_NOAA/NMFS_SEFSCBoat2011	boat	continuous	2011	2011	0	982	0	0	982	0	1,155	0	0	1,155
AMAPPS_NOAA/NMFS_SEFSCBoat2013	boat	continuous	2013	2013	0	701	277	0	978	0	823	326	0	1,149
BarHarborWW05	boat	continuous	2005	2005	0	876	181	0	1,057	0	1,048	217	0	1,265
BarHarborWW06	boat	continuous	2006	2006	0	821	331	0	1,152	0	994	399	0	1,393
CapeHatteras0405	boat	continuous	2004	2005	0	195	0	168	363	0	213	0	161	374
CapeWindAerial	aerial	continuous	2002	2004	1,117	1,112	1,176	1,271	4,676	1,788	1,782	1,881	2,041	7,492
CapeWindBoat	boat	continuous	2002	2003	117	109	29	0	255	748	712	184	0	1,644
CDASMidAtlantic	aerial	continuous	2001	2003	241	0	0	1,363	1,604	113	0	0	653	766
CSAP	boat	discrete	1980	1988	7,612	6,975	7,325	4,213	26,125	9,712	8,967	9,466	5,400	33,545
DOEBRIAerial2012	camera	continuous	2012	2012	1,486	832	1,515	763	4,596	1,190	661	1,208	610	3,669
DOEBRIAerial2013	camera	continuous	2013	2013	941	1,615	1,479	1,265	5,300	765	1,297	1,178	1,010	4,250
DOEBRIAerial2014	camera	continuous	2014	2014	1,029	0	0	1,341	2,370	822	0	0	1,074	1,896

Source Dataset ID	Platform	Method	Year		Number of transect segments					Area surveyed (km^2)				
			Start	End	Spring	Summer	Fall	Winter	Total	Spring	Summer	Fall	Winter	Total
DOEBRIBoatApr2014	boat	continuous	2014	2014	164	0	0	0	164	195	0	0	0	195
DOEBRIBoatApril2012	boat	continuous	2012	2012	165	0	0	0	165	197	0	0	0	197
DOEBRIBoatAug2012	boat	continuous	2012	2012	0	164	0	0	164	0	197	0	0	197
DOEBRIBoatAug2013	boat	continuous	2013	2013	0	166	0	0	166	0	199	0	0	199
DOEBRIBoatDec2012	boat	continuous	2012	2013	0	0	0	162	162	0	0	0	194	194
DOEBRIBoatDec2013	boat	continuous	2013	2013	0	0	0	170	170	0	0	0	202	202
DOEBRIBoatJan2013	boat	continuous	2013	2013	0	0	0	164	164	0	0	0	198	198
DOEBRIBoatJan2014	boat	continuous	2014	2014	0	0	0	164	164	0	0	0	197	197
DOEBRIBoatJune2012	boat	continuous	2012	2012	0	166	0	0	166	0	200	0	0	200
DOEBRIBoatJune2013	boat	continuous	2013	2013	0	168	0	0	168	0	200	0	0	200
DOEBRIBoatMar2013	boat	continuous	2013	2013	166	0	0	0	166	201	0	0	0	201
DOEBRIBoatMay2013	boat	continuous	2013	2013	168	0	0	0	168	201	0	0	0	201
DOEBRIBoatNov2012	boat	continuous	2012	2012	0	0	165	0	165	0	0	197	0	197
DOEBRIBoatOct2013	boat	continuous	2013	2013	0	0	170	0	170	0	0	201	0	201
DOEBRIBoatSep2012	boat	continuous	2012	2012	0	0	168	0	168	0	0	201	0	201
DOEBRIBoatSep2013	boat	continuous	2013	2013	0	0	168	0	168	0	0	201	0	201
DominionVirginia_VOWTAP	boat	continuous	2013	2014	24	18	12	24	78	77	58	38	77	250
EcoMonAug08	boat	continuous	2008	2008	0	480	0	0	480	0	575	0	0	575
EcoMonAug09	boat	continuous	2009	2009	0	458	0	0	458	0	547	0	0	547
EcoMonAug10	boat	continuous	2010	2010	0	480	12	0	492	0	573	15	0	588
EcoMonAug2012	boat	continuous	2012	2012	0	656	0	0	656	0	782	0	0	782
EcoMonFeb10	boat	continuous	2010	2010	0	0	0	334	334	0	0	0	398	398
EcoMonFeb2012	boat	continuous	2012	2012	0	0	0	549	549	0	0	0	661	661
EcoMonFeb2013	boat	continuous	2013	2013	0	0	0	521	521	0	0	0	620	620
EcoMonJan09	boat	continuous	2009	2009	0	0	0	391	391	0	0	0	474	474
EcoMonJun2012	boat	continuous	2012	2012	31	513	0	0	544	38	613	0	0	651
EcoMonMay07	boat	continuous	2007	2007	433	72	0	0	505	520	86	0	0	606
EcoMonMay09	boat	continuous	2009	2009	199	422	0	0	621	241	505	0	0	746
EcoMonMay10	boat	continuous	2010	2010	274	370	0	0	644	328	442	0	0	770

Source Dataset ID	Platform	Method	Year		Number of transect segments					Area surveyed (km^2)				
			Start	End	Spring	Summer	Fall	Winter	Total	Spring	Summer	Fall	Winter	Total
EcoMonNov09	boat	continuous	2009	2009	0	0	441	0	441	0	0	528	0	528
EcoMonNov10	boat	continuous	2010	2010	0	0	418	0	418	0	0	500	0	500
EcoMonNov2011	boat	continuous	2011	2011	0	0	454	0	454	0	0	542	0	542
EcoMonOct2012	boat	continuous	2012	2012	0	0	498	0	498	0	0	598	0	598
ECSAS	boat	discrete	2006	2016	5,993	2,810	3,700	513	13,016	3,068	1,425	2,004	230	6,727
FLPowerLongIsland_Aerial	aerial	continuous	2004	2006	104	49	158	0	311	154	75	237	0	466
FLPowerLongIsland_Boat	boat	continuous	2004	2006	497	159	346	211	1,213	566	188	385	235	1,374
FWS_MidAtlanticDetection_Spring2012	aerial	continuous	2012	2012	177	0	0	0	177	283	0	0	0	283
FWS_SouthernBLSC_Winter2012	aerial	continuous	2012	2012	0	0	0	904	904	0	0	0	1,500	1,500
FWSAtlanticWinterSeaduck2008	aerial	continuous	2008	2011	78	0	0	8,311	8,389	124	0	0	13,295	13,419
GeorgiaPelagic	boat	discrete	1982	1985	681	698	576	231	2,186	844	727	705	293	2,569
HatterasEddyCruise2004	boat	continuous	2004	2004	0	131	0	0	131	0	117	0	0	117
HerringAcoustic06	boat	continuous	2006	2006	0	0	287	0	287	0	0	341	0	341
HerringAcoustic07	boat	continuous	2007	2007	0	0	334	0	334	0	0	395	0	395
HerringAcoustic08	boat	continuous	2008	2008	0	0	822	0	822	0	0	990	0	990
HerringAcoustic09Leg1	boat	continuous	2009	2009	0	0	127	0	127	0	0	151	0	151
HerringAcoustic09Leg2	boat	continuous	2009	2009	0	0	289	0	289	0	0	341	0	341
HerringAcoustic09Leg3	boat	continuous	2009	2009	0	0	263	0	263	0	0	315	0	315
HerringAcoustic2010	boat	continuous	2010	2010	0	0	555	0	555	0	0	670	0	670
HerringAcoustic2011	boat	continuous	2011	2011	0	0	808	0	808	0	0	950	0	950
HerringAcoustic2012	boat	continuous	2012	2012	0	0	772	0	772	0	0	917	0	917
MassAudNanAerial	aerial	continuous	2002	2006	860	988	1,374	2,004	5,226	631	715	1,004	1,464	3,814
MassCEC2011-2012	aerial	continuous	2011	2012	668 (670)	503 (503)	845 (846)	495 (495)	2,511 (2,514)	1,068 (1,072)	804 (804)	1,354 (1,355)	790 (790)	4,016 (4,021)
MassCEC2013	aerial	continuous	2013	2013	498 (498)	499 (499)	921 (921)	330 (330)	2,248 (2,248)	797 (797)	798 (798)	1,473 (1,473)	528 (528)	3,596 (3,596)
MassCEC2014	aerial	continuous	2014	2015	167 (167)	500 (500)	171 (171)	674 (674)	1,512 (1512)	267 (267)	801 (801)	273 (273)	1,080 (1,080)	2,421 (2,421)
NewEnglandSeamount06	boat	discrete	2007	2007	61	4	0	0	65	34	2	0	0	36
NJDEP2009	boat	continuous	2008	2009	1,224	1,350	1,430	967	4,971	1,460	1,618	1,727	1,162	5,967
NOAA/NMFS_NEFSCBoat2004	boat	continuous	2004	2004	0	1,207	0	0	1,207	0	1,422	0	0	1,422

Source Dataset ID	Platform	Method	Year		Number of transect segments					Area surveyed (km^2)				
			Start	End	Spring	Summer	Fall	Winter	Total	Spring	Summer	Fall	Winter	Total
NOAA/NMFS_NEFSCBoat2007	boat	continuous	2007	2007	0	633	0	0	633	0	746	0	0	746
NOAAMBO7880	boat	discrete	1978	1979	1,677	2,458	2,043	787	6,965	1,597	2,360	1,779	681	6,417
PlattsBankAerial	aerial	continuous	2005	2005	0	869	0	0	869	0	1,178	0	0	1,178
RISAMPAerial	aerial	continuous	2009	2010	985	767	0	714	2,466	1,180	918	0	855	2,953
RISAMPBoat	boat	continuous	2009	2010	202	288	128	163	781	276	354	173	219	1,022
SEFSC1992	boat	continuous	1992	1992	0	0	0	783	783	0	0	0	938	938
SEFSC1998	boat	continuous	1998	1998	0	1,365	0	0	1,365	0	1,596	0	0	1,596
SEFSC1999	boat	continuous	1999	1999	0	730	524	0	1,254	0	852	623	0	1,475
StatoilMaine	boat	continuous	2012	2013	40	150	140	70	400	48	180	168	84	480
WHOIJuly2010	boat	continuous	2010	2010	0	86	0	0	86	0	102	0	0	102
WHOISept2010	boat	continuous	2010	2010	0	0	85	0	85	0	0	99	0	99
Total			1978	2016	32,064	42,543	42,008	33,606	150,221	35,491	50,866	51,722	43,061	181,140

Table 2. List of species-season combinations modeled with sample sizes and counts. Only combinations with ≥50 sightings were modeled. Seasons were defined as spring (March-May), summer (June-August), fall (September-November), and winter (December-February).

Species code	Common name	Scientific name	Family	Number of segments					Count				
				Spring	Summer	Fall	Winter	Total	Spring	Summer	Fall	Winter	Total
ARTE	Arctic Tern	*Sterna paradisaea*	Sternidae		170			170		524			524
ATPU	Atlantic Puffin	*Fratercula arctica*	Alcidae	362	287	124	342	1,115	723	639	174	589	2,125
AUSH	Audubon's Shearwater	*Puffinus lherminieri*	Procellariidae	134	916	297	170	1,517	449	2,709	982	340	4,480
BCPE	Black-capped Petrel	*Pterodroma hasitata*	Procellariidae	159	371	93	90	713	315	1,001	246	212	1,774
BLGU	Black Guillemot	*Cepphus grylle*	Alcidae		90			90		167			167
BLKI	Black-legged Kittiwake	*Rissa tridactyla*	Laridae	741		2,239	4,066	7,046	3,426		15,106	34,357	52,889
BLSC[1]	Black Scoter	*Melanitta americana*	Anatidae	516		443	1,330	2,289	19,582		10,224	64,882	94,688
BOGU	Bonaparte's Gull	*Chroicocephalus philadelphia*	Laridae	467		329	1,585	2,381	5,808		2,297	14,072	22,177
BRPE	Brown Pelican	*Pelecanus occidentalis*	Pelecanidae	66	127	164	76	433	307	567	815	316	2,005
BRSP[2]	Band-rumped Storm-Petrel	*Oceanodroma castro*	Hydrobatidae		276			276		558			558
BRTE	Bridled Tern	*Sterna anaethetus*	Sternidae		101	65		166		224	148		372
COEI[1]	Common Eider	*Somateria mollissima*	Anatidae	906	146	640	2,172	3,864	208,330	23,280	63,016	536,264	830,890
COLO[1]	Common Loon	*Gavia immer*	Gaviidae	2,932	211	1,472	3,825	8,440	7,086	283	3,199	9,770	20,338
COMU	Common Murre	*Uria aalge*	Alcidae	212			268	480	520			759	1,279
COSH[1]	Cory's Shearwater	*Calonectris diomedea*	Procellariidae	137	3,383	1,944		5,464	272	15,084	9,193		24,549
COTE[1]	Common Tern	*Sterna hirundo*	Sternidae	642	1,806	777		3,225	2,934	8,315	7,753		19,002
DCCO	Double-crested Cormorant	*Phalacrocorax auritus*	Phalacrocoracidae	158	187	278	157	780	4,282	1,430	5,710	2,134	13,556
DOVE	Dovekie	*Alle alle*	Alcidae	664	61	468	1,252	2,445	3,774	126	4,058	9,627	17,585
GBBG	Great Black-backed Gull	*Larus marinus*	Laridae	3,882	3,513	6,155	3,902	17,452	27,567	12,000	37,287	32,058	108,912
GRSH	Great Shearwater	*Puffinus gravis*	Procellariidae	682	7,351	7,531	140	15,704	6,047	186,133	102,183	591	294,954
GRSK	Great Skua	*Stercorarius skua*	Stercorariidae			196		196			223		223
HERG	Herring Gull	*Larus argentatus*	Laridae	6,384	3,202	8,612	5,300	23,498	55,681	11,147	63,122	32,945	162,895
HOGR	Horned Grebe	*Podiceps auritus*	Podicipedidae				103	103				200	200
LAGU	Laughing Gull	*Leucophaeus atricilla*	Laridae	742	1,750	1,871	134	4,497	1,767	5,769	10,339	354	18,229

Species code	Common name	Scientific name	Family	Number of segments					Count				
				Spring	Summer	Fall	Winter	Total	Spring	Summer	Fall	Winter	Total
LESP	Leach's Storm-Petrel	*Oceanodroma leucorhoa*	Hydrobatidae	279	2,540	591		3,410	920	10,336	1,496		12,752
LETE	Least Tern	*Sterna antillarum*	Sternidae		126	98		224		457	1,202		1,659
LTDU[1]	Long-tailed Duck	*Clangula hyemalis*	Anatidae	1,335		539	3,564	5,438	90,219		18,805	151,955	260,979
MASH	Manx Shearwater	*Puffinus puffinus*	Procellariidae	107	353	344		804	165	944	595		1,704
NOFU	Northern Fulmar	*Fulmarus glacialis*	Procellariidae	2,678	956	2,171	2,061	7,866	31,524	13,376	10,666	24,805	80,371
NOGA	Northern Gannet	*Morus bassanus*	Sulidae	6,729	1,358	5,532	7,932	21,551	41,213	2,951	24,453	61,036	129,653
PAJA	Parasitic Jaeger	*Stercorarius parasiticus*	Stercorariidae	53	77	191		321	59	103	236		398
POJA	Pomarine Jaeger	*Stercorarius pomarinus*	Stercorariidae	112	155	830		1,097	144	186	1,169		1,499
RAZO[1]	Razorbill	*Alca torda*	Alcidae	1,063	87	194	1,990	3,334	6,979	230	1,309	16,772	25,290
RBGU	Ring-billed Gull	*Larus delawarensis*	Laridae	211	53	414	745	1,423	451	145	1,532	3,357	5,485
RBME	Red-breasted Merganser	*Mergus serrator*	Anatidae	69			112	181	379			950	1,329
REPH	Red Phalarope	*Phalaropus fulicarius*	Scolopacidae	480	250	338		1,068	86,165	26,657	2,597		115,419
RNPH	Red-necked Phalarope	*Phalaropus lobatus*	Scolopacidae	143	182	201		526	2,452	2,354	1,372		6,178
ROST[1]	Roseate Tern	*Sterna dougallii*	Sternidae	59	212	83		354	203	805	533		1,541
ROYT	Royal Tern	*Sterna maxima*	Sternidae	270	289	352		911	752	648	937		2,337
RTLO[1]	Red-throated Loon	*Gavia stellata*	Gaviidae	1,746		412	2,607	4,765	5,219		1,608	8,484	15,311
SOSH	Sooty Shearwater	*Puffinus griseus*	Procellariidae	916	1,812	119		2,847	6,671	36,282	299		43,252
SOTE	Sooty Tern	*Sterna fuscata*	Sternidae	60	119			179	617	595			1,212
SPSK	South Polar Skua	*Stercorarius maccormicki*	Stercorariidae		92	142		234		108	191		299
SUSC[1]	Surf Scoter	*Melanitta perspicillata*	Anatidae	846		848	1,918	3,612	17,211		29,378	51,116	97,705
TBMU	Thick-billed Murre	*Uria lomvia*	Alcidae	315			151	466	1,324			422	1,746
WISP[1]	Wilson's Storm-Petrel	*Oceanites oceanicus*	Hydrobatidae	1,750	9,269	1,481		12,500	15,059	100,317	7,820		123,196
WWSC[1]	White-winged Scoter	*Melanitta fusca*	Anatidae	568		667	1,536	2,771	21,676		12,241	30,142	64,059
Total									678,272	466,450	454,514	1,088,509	2,687,745

[1] Models were re-run with the corrected MassCEC datasets (see Section 2.2)

[2] The American Ornithological Union four-letter species code is BSTP

Table 3. Predictor variables used in models with native resolutions, year ranges, and sources.

Predictor variable	Native spatial resolution	Native temporal resolution	Years	Source
Survey				
survey platform				survey data
survey ID				survey data
transect ID				survey data
Temporal				
year		yearly		
day of year		daily		
Atlantic Multidecadal Oscillation (AMO) index[1]		monthly	1978-2016	NOAA ESRL http://www.esrl.noaa.gov/psd/data/correlation/amon.us.data
Multivariate El Niño-Southern Oscillation Index (MEI)[1]		monthly	1978-2016	NOAA ESRL http://www.esrl.noaa.gov/psd/data/correlation/mei.data
North Atlantic Oscillation (NAO) index[1]		monthly	1978-2016	NOAA ESRL http://www.esrl.noaa.gov/psd/data/correlation/nao.data
Trans-Niño Index (TNI)[1]		monthly	1978-2016	NOAA ESRL http://www.esrl.noaa.gov/psd/data/correlation/tni.data
Geographic				
longitude projected[2]				
latitude projected[2]				
distance to land[3]	50 m			derived from Prototype Global Shoreline Data (http://msi.nga.mil/NGAPortal/DNC.portal?_nfpb=true&_pageLabel=dnc_portal_page_72)
Bathymetric				

Predictor variable	Native spatial resolution	Native temporal resolution	Years	Source
depth[4]	Okeanos Explorer: 25 m; ACUMEN: approx. 25 m; CCOM: approx. 100 m; GMRT: approx. 400 m; CRM: approx. 100 m; GEBCO: approx. 1 km			Okeanos Explorer (http://oceanexplorer.noaa.gov/okeanos/welcome.html) obtainable from NOAA National Centers for Environmental Information Bathymetry Data Viewer (https://maps.ngdc.noaa.gov/viewers/bathymetry/); NOAA Atlantic Canyons Undersea Mapping Expeditions (ACUMEN) (http://oceanexplorer.noaa.gov/okeanos/explorations/acumen12/summary/welcome.html); University of New Hampshire Center for Coastal and Ocean Mapping (CCOM) / Joint Hydrographic Center (http://ccom.unh.edu/theme/law-sea/law-of-the-sea-data/atlantic and https://www.ngdc.noaa.gov/ships/marcus_g_langseth/MGL1512_mb.html); Global Multi-Resolution Topography Data Synthesis (GMRT) (http://www.marine-geo.org/portals/gmrt/; Ryan et al. 2009); NOAA National Geophysical Data Center U.S. Coastal Relief Model (CRM) (http://www.ngdc.noaa.gov/mgg/coastal/crm.html); General Bathymetric Chart of the Oceans (GEBCO) GEBCO_2014 grid version 20150318 (http://www.gebco.net/data_and_products/gridded_bathymetry_data/gebco_30_second_grid/; Weatherall et al. 2015)
slope (2 km)				derived from depth[5,6]
slope (10 km)				derived from depth[5,6]
slope of slope (10 km)				derived from depth[5,6]
planform curvature (10 km)				derived from depth[6,7]
profile curvature (10 km)				derived from depth[6,7]
Oceanographic (seasonal climatologies)				
surface chlorophyll-a (reflectance inputs between 440 and 670 nm)	approx. 4 km	daily	1997-2017	NASA OceanColor (https://oceancolor.gsfc.nasa.gov/); SeaWiFS, MODIS Aqua, and VIIRS sensors/missions
turbidity (reflectance at 547 nm)	approx. 4 km	daily	2000-2017	NASA OceanColor (https://oceancolor.gsfc.nasa.gov/); MODIS Aqua and MODIS Terra sensors/missions

Predictor variable	Native spatial resolution	Native temporal resolution	Years	Source
surface current velocity (u direction)	approx. 9 km	daily	1992-2012	Hybrid vertical coordinate system ocean model (HYCOM) global reanalysis (GLBu0.08 grid, experiments 19.0 and 19.1), 1200 h (http://hycom.org/dataserver)
surface current velocity (v direction)	approx. 9 km	daily	1992-2012	Hybrid vertical coordinate system ocean model (HYCOM) global reanalysis (GLBu0.08 grid, experiments 19.0 and 19.1), 1200 h (http://hycom.org/dataserver)
surface current divergence	approx. 9 km	daily	1992-2012	derived from surface current velocity
surface current vorticity	approx. 9 km	daily	1992-2012	derived from surface current velocity
sea surface height	approx. 28 km	daily	1993-2016	AVISO Global 'DT all sat' MADT daily sea surface altimetry product (https://www.aviso.altimetry.fr/en/data/products/sea-surface-height-products/global/madt-h-uv.html)
sea surface height standard deviation	approx. 28 km	daily	1993-2016	derived from sea surface height
probability of anticyclonic eddy ring	approx. 28 km	daily	1993-2016	derived from sea surface height[8]
probability of cyclonic eddy ring	approx. 28 km	daily	1993-2016	derived from sea surface height[8]
sea surface temperature	approx. 1 km	daily	1985-2010	AVHRR Pathfinder (Peter Cornillon, University of Rhode Island; http://www.sstfronts.org/opendap/)
sea surface temperature standard deviation	approx. 1 km	daily	1985-2010	derived from sea surface temperature
probability of sea surface temperature front[9]	approx. 1 km	monthly	2002-2013	derived from monthly front presence/absence in turn derived from daily NASA MUR SST data (Peter Miller, Remote Sensing Group, Plymouth Marine Laboratory, UK; Miller and Christodoulou 2014)
upwelling index	approx. 28 km	monthly	1999-2009	NOAA CoastWatch grids derived from NASA Quick Scatterometer (QuikSCAT) data (http://coastwatch.pfeg.noaa.gov/erddap/griddap/erdQSstressmday.html)
Atmospheric (seasonal climatologies)				
wind stress (x direction)	approx. 28 km	monthly	1999-2009	NOAA CoastWatch grids derived from NASA Quick Scatterometer (QuikSCAT) data (http://coastwatch.pfeg.noaa.gov/erddap/griddap/erdQSstressmday.html)

Predictor variable	Native spatial resolution	Native temporal resolution	Years	Source
wind stress (y direction)	approx. 28 km	monthly	1999-2009	NOAA CoastWatch grids derived from NASA Quick Scatterometer (QuikSCAT) data (http://coastwatch.pfeg.noaa.gov/erddap/griddap/erdQSstressmday.html)
wind divergence	approx. 28 km	monthly	1999-2009	NOAA CoastWatch grids derived from NASA Quick Scatterometer (QuikSCAT) data (http://coastwatch.pfeg.noaa.gov/erddap/griddap/erdQSstressmday.html)

[1] Current and one-year lag

[2] Oblique Mercator projection: azimuth = 40, origin = 75°W 35°N, k = 0.9996, ellipse = GRS80, earth datum = NAD83

[3] Derived using ArcGIS 10.2 Spatial Analyst Tools

[4] Datasets were converted to a common 100-m grid then mosaicked in order of decreasing priority: Okeanos Explorer, ACUMEN, CCOM, GMRT, CRM, and GEBCO

[5] Derived using ArcGIS 10.4 Spatial Analyst Tools

[6] Calculated from mosaicked 100-m depth grids that were smoothed using a Gaussian low-pass filter for each spatial scale

[7] Derived using the ArcGIS 10.4 extension DEM Surface Tools (Jenness 2013)

[8] Derived using Duke University's Marine Geospatial Ecology Lab's Marine Geospatial Ecology Tools (MGET) 0.8a64 for ArcGIS 10.4.1 (Okubo-Weiss algorithm)

[9] A low-pass filter was applied to the climatologies to remove banding artifacts

Table 4a. Pairwise Spearman rank correlation coefficients for spatial predictor variables (spring – March-May). High correlations are highlighted in yellow (>0.7), orange (>0.8), and red (>0.9).

	projected latitude	distance to land	depth	slope (2 km)	slope (10 km)	slope of slope (10 km)	planform curvature (10 km)	profile curvature (10 km)	chlorophyll-a	turbidity	surface current velocity (u)	surface current velocity (v)	surface current divergence	surface current vorticity	sea surface height	sea surface height SD	anticyclonic eddy probability	cyclonic eddy probability	sea surface temperature	sea surface temperature SD	SST front probability	upwelling index	wind stress (x)	wind stress (y)	wind divergence
projected longitude	0.84	0.30	-0.26	0.08	0.04	-0.02	0.02	0.12	0.49	0.02	-0.16	-0.36	0.12	0.00	-0.38	0.10	0.16	-0.27	-0.73	0.44	0.03	0.26	0.53	-0.50	0.00
projected latitude		-0.18	0.21	0.01	-0.03	-0.03	0.02	0.05	0.82	0.32	-0.22	-0.38	0.18	0.02	-0.65	-0.20	-0.17	-0.56	-0.90	0.66	0.10	0.35	0.30	-0.65	0.12
distance to land			-0.90	0.18	0.17	0.05	-0.03	0.15	-0.53	-0.41	0.17	-0.03	-0.14	-0.08	0.41	0.67	0.63	0.52	0.24	-0.24	0.01	-0.14	0.61	0.20	-0.19
depth				-0.27	-0.25	-0.07	0.07	-0.29	0.59	0.46	-0.21	-0.02	0.12	0.06	-0.46	-0.70	-0.67	-0.54	-0.29	0.29	0.00	0.17	-0.63	-0.21	0.26
slope (2 km)					0.90	0.64	0.01	0.19	-0.21	-0.21	0.17	0.16	-0.08	0.19	-0.08	0.22	0.29	0.10	0.17	0.05	0.44	0.00	0.24	-0.17	-0.05
slope (10 km)						0.75	0.02	0.17	-0.22	-0.19	0.17	0.17	-0.08	0.21	-0.09	0.19	0.28	0.10	0.21	0.08	0.54	-0.01	0.23	-0.19	-0.01
slope of slope (10 km)							0.01	0.10	-0.16	-0.17	-0.01	0.06	-0.10	0.22	-0.13	-0.02	0.13	0.04	0.14	-0.02	0.35	0.00	0.00	-0.11	0.05
planform curvature (10 km)								-0.22	0.03	0.03	0.01	0.00	0.03	-0.01	-0.03	-0.02	-0.03	-0.02	-0.01	0.00	0.01	0.05	0.01	-0.06	0.01
profile curvature (10 km)									-0.07	-0.10	0.11	0.05	0.07	-0.06	0.00	0.16	0.23	0.02	0.01	0.05	-0.01	0.06	0.15	-0.06	-0.06
chlorophyll-a										0.65	-0.27	-0.36	0.22	0.13	-0.73	-0.42	-0.43	-0.60	-0.86	0.77	0.08	0.30	-0.02	-0.64	0.27
turbidity											-0.25	-0.28	0.01	0.22	-0.47	-0.24	-0.28	-0.20	-0.49	0.59	0.16	0.01	-0.11	-0.37	0.32
surface current velocity (u)												0.62	0.04	0.02	0.18	0.49	0.14	0.09	0.45	-0.01	0.30	0.16	0.34	-0.10	-0.26
surface current velocity (v)													0.07	0.04	0.22	0.27	0.01	0.01	0.58	-0.24	0.21	0.11	0.05	0.04	-0.29
surface current divergence														-0.01	-0.21	-0.05	-0.06	-0.23	-0.14	0.17	-0.06	0.29	0.01	-0.27	-0.02
surface current vorticity															-0.39	0.02	-0.06	0.12	-0.08	0.28	0.35	-0.05	-0.08	-0.37	0.21
sea surface height																0.41	0.24	0.54	0.67	-0.76	-0.33	-0.36	0.13	0.82	-0.43
sea surface height SD																	0.56	0.55	0.37	-0.06	0.16	-0.04	0.65	0.08	-0.37
anticyclonic eddy probability																		0.38	0.22	-0.09	0.09	-0.05	0.38	0.05	-0.10
cyclonic eddy probability																			0.49	-0.36	-0.02	-0.38	0.15	0.45	-0.11
sea surface temperature																				-0.66	0.07	-0.23	-0.07	0.55	-0.29
sea surface temperature SD																					0.47	0.32	0.18	-0.78	0.34
SST front probability																						0.13	0.29	-0.47	0.16
upwelling index																							0.13	-0.43	0.05
wind stress (x)																								-0.20	-0.23
wind stress (y)																									-0.29

Table 4b. Pairwise Spearman rank correlation coefficients for spatial predictor variables (summer – June-August). High correlations are highlighted in yellow (>0.7), orange (>0.8), and red (>0.9).

	projected latitude	distance to land	depth	slope (2 km)	slope (10 km)	slope of slope (10 km)	planform curvature (10 km)	profile curvature (10 km)	chlorophyll-a	turbidity	surface current velocity (u)	surface current velocity (v)	surface current divergence	surface current vorticity	sea surface height	sea surface height SD	anticyclonic eddy probability	cyclonic eddy probability	sea surface temperature	sea surface temperature SD	SST front probability	upwelling index	wind stress (x)	wind stress (y)	wind divergence
projected longitude	0.84	0.30	-0.26	0.08	0.04	-0.02	0.02	0.12	0.33	0.31	-0.15	-0.30	0.08	0.00	-0.34	0.11	0.16	-0.22	-0.84	0.81	0.50	0.38	0.55	-0.22	-0.13
projected latitude		-0.18	0.21	0.01	-0.03	-0.03	0.02	0.05	0.72	0.65	-0.22	-0.34	0.22	0.01	-0.65	-0.25	-0.15	-0.52	-0.94	0.90	0.70	0.51	0.33	-0.51	-0.03
distance to land			-0.90	0.18	0.17	0.05	-0.03	0.15	-0.70	-0.58	0.17	-0.02	-0.27	-0.07	0.51	0.75	0.57	0.57	0.11	-0.07	-0.28	-0.16	0.56	0.58	-0.23
depth				-0.27	-0.25	-0.07	0.07	-0.29	0.74	0.65	-0.18	-0.05	0.26	0.05	-0.54	-0.77	-0.65	-0.57	-0.16	0.13	0.32	0.18	-0.58	-0.60	0.28
slope (2 km)					0.90	0.64	0.01	0.19	-0.20	-0.23	0.21	0.20	-0.15	0.16	-0.01	0.26	0.32	0.10	0.07	-0.03	0.17	0.09	0.22	-0.05	-0.14
slope (10 km)						0.75	0.02	0.17	-0.20	-0.21	0.23	0.20	-0.18	0.18	-0.02	0.24	0.31	0.10	0.11	-0.05	0.21	0.07	0.21	-0.08	-0.09
slope of slope (10 km)							0.01	0.10	-0.13	-0.13	0.03	0.10	-0.17	0.19	-0.11	0.03	0.12	0.01	0.07	-0.04	0.13	0.05	-0.01	-0.15	0.00
planform curvature (10 km)								-0.22	0.05	0.05	0.01	0.00	-0.01	0.04	-0.03	-0.02	-0.03	0.00	-0.02	0.02	0.03	-0.01	-0.01	-0.07	0.02
profile curvature (10 km)									-0.10	-0.11	0.12	0.10	0.04	-0.09	0.03	0.18	0.25	0.02	-0.03	0.03	-0.01	0.11	0.16	0.06	-0.14
chlorophyll-a										0.91	-0.22	-0.21	0.36	0.14	-0.79	-0.58	-0.51	-0.66	-0.66	0.64	0.67	0.40	-0.14	-0.72	0.21
turbidity											-0.23	-0.28	0.31	0.16	-0.70	-0.49	-0.44	-0.54	-0.63	0.63	0.64	0.29	-0.08	-0.63	0.20
surface current velocity (u)												0.66	0.00	0.02	0.22	0.43	0.15	0.06	0.42	-0.39	0.09	0.10	0.27	0.16	-0.24
surface current velocity (v)													0.10	0.05	0.21	0.24	0.09	-0.02	0.51	-0.50	0.01	0.08	-0.01	0.05	-0.21
surface current divergence														0.00	-0.29	-0.18	-0.18	-0.28	-0.15	0.17	0.19	0.27	0.01	-0.27	0.04
surface current vorticity															-0.32	0.06	-0.11	0.14	-0.02	0.07	0.22	-0.10	-0.08	-0.32	0.15
sea surface height																0.54	0.27	0.56	0.64	-0.67	-0.61	-0.44	0.20	0.85	-0.25
sea surface height SD																	0.53	0.63	0.30	-0.30	-0.15	-0.13	0.63	0.59	-0.33
anticyclonic eddy probability																		0.29	0.12	-0.08	-0.20	-0.03	0.36	0.28	-0.17
cyclonic eddy probability																			0.43	-0.42	-0.45	-0.43	0.20	0.59	-0.06
sea surface temperature																				-0.96	-0.55	-0.39	-0.23	0.49	-0.07
sea surface temperature SD																					0.60	0.41	0.24	-0.54	0.11
SST front probability																						0.45	0.24	-0.58	-0.06
upwelling index																							0.16	-0.37	-0.09
wind stress (x)																								0.39	-0.25
wind stress (y)																									-0.27

Table 4c. Pairwise Spearman rank correlation coefficients for spatial predictor variables (fall – September-November). High correlations are highlighted in yellow (>0.7), orange (>0.8), and red (>0.9).

	projected latitude	distance to land	depth	slope (2 km)	slope (10 km)	slope of slope (10 km)	planform curvature (10 km)	profile curvature (10 km)	chlorophyll-a	turbidity	surface current velocity (u)	surface current velocity (v)	surface current divergence	surface current vorticity	sea surface height	sea surface height SD	anticyclonic eddy probability	cyclonic eddy probability	sea surface temperature	sea surface temperature SD	SST front probability	upwelling index	wind stress (x)	wind stress (y)	wind divergence
projected longitude	0.84	0.30	-0.26	0.08	0.04	-0.02	0.02	0.12	0.29	-0.25	0.02	-0.19	0.10	0.00	-0.35	0.11	0.14	-0.20	-0.75	0.47	0.29	0.25	0.91	0.23	0.16
projected latitude		-0.18	0.21	0.01	-0.03	-0.03	0.02	0.05	0.70	0.16	0.00	-0.30	0.18	0.02	-0.65	-0.23	-0.15	-0.52	-0.93	0.67	0.52	0.29	0.94	-0.07	0.26
distance to land			-0.90	0.18	0.17	0.05	-0.03	0.15	-0.71	-0.67	0.10	0.14	-0.17	-0.09	0.50	0.71	0.54	0.57	0.24	-0.25	-0.35	-0.04	0.05	0.42	-0.15
depth				-0.27	-0.25	-0.07	0.07	-0.29	0.77	0.71	-0.16	-0.22	0.14	0.07	-0.53	-0.73	-0.57	-0.59	-0.29	0.31	0.40	0.05	-0.01	-0.45	0.18
slope (2 km)					0.90	0.64	0.01	0.19	-0.20	-0.33	0.20	0.27	-0.14	0.19	-0.07	0.21	0.25	0.12	0.15	-0.13	0.19	0.05	0.07	-0.13	-0.08
slope (10 km)						0.75	0.02	0.17	-0.20	-0.32	0.20	0.27	-0.15	0.21	-0.08	0.19	0.23	0.12	0.18	-0.12	0.26	0.03	0.04	-0.20	-0.07
slope of slope (10 km)							0.01	0.10	-0.12	-0.19	0.01	0.15	-0.13	0.23	-0.15	-0.02	0.08	0.05	0.13	-0.10	0.20	0.01	-0.01	-0.13	0.00
planform curvature (10 km)								-0.22	0.04	0.06	0.03	0.00	0.01	0.00	-0.03	-0.01	0.00	-0.01	-0.01	-0.01	0.04	0.02	0.02	-0.05	0.01
profile curvature (10 km)									-0.11	-0.24	0.13	0.12	0.05	-0.08	0.02	0.16	0.19	0.03	0.00	0.00	-0.06	0.09	0.09	0.04	-0.03
chlorophyll-a										0.65	-0.03	-0.32	0.23	0.14	-0.77	-0.54	-0.47	-0.68	-0.74	0.68	0.62	0.15	0.53	-0.44	0.25
turbidity											-0.11	-0.24	0.10	0.19	-0.41	-0.45	-0.49	-0.33	-0.29	0.32	0.32	-0.13	-0.04	-0.43	0.09
surface current velocity (u)												0.59	0.07	0.03	0.07	0.40	0.08	-0.03	0.23	-0.20	0.26	0.11	0.02	-0.29	-0.26
surface current velocity (v)													0.01	0.03	0.25	0.34	0.14	0.08	0.53	-0.54	0.03	0.09	-0.26	-0.20	-0.34
surface current divergence														0.01	-0.17	-0.06	-0.04	-0.18	-0.14	0.15	0.15	0.10	0.11	-0.16	0.01
surface current vorticity															-0.39	0.04	-0.02	0.16	-0.04	0.20	0.32	-0.31	-0.02	-0.32	-0.01
sea surface height																0.48	0.24	0.55	0.67	-0.72	-0.67	-0.11	-0.53	0.49	-0.28
sea surface height SD																	0.52	0.64	0.35	-0.31	-0.20	-0.13	-0.05	0.19	-0.32
anticyclonic eddy probability																		0.34	0.19	-0.12	-0.20	-0.02	0.00	0.15	-0.07
cyclonic eddy probability																			0.48	-0.39	-0.42	-0.37	-0.38	0.27	-0.17
sea surface temperature																				-0.81	-0.40	-0.18	-0.85	0.01	-0.37
sea surface temperature SD																					0.48	0.06	0.60	-0.26	0.39
SST front probability																						0.14	0.45	-0.59	0.05
upwelling index																							0.28	-0.04	0.04
wind stress (x)																								0.01	0.21
wind stress (y)																									-0.04

Table 4d. Pairwise Spearman rank correlation coefficients for spatial predictor variables (winter – December-February). High correlations are highlighted in yellow (>0.7), orange (>0.8), and red (>0.9).

	projected latitude	distance to land	depth	slope (2 km)	slope (10 km)	slope of slope (10 km)	planform curvature (10 km)	profile curvature (10 km)	chlorophyll-a	turbidity	surface current velocity (u)	surface current velocity (v)	surface current divergence	surface current vorticity	sea surface height	sea surface height SD	anticyclonic eddy probability	cyclonic eddy probability	sea surface temperature	sea surface temperature SD	SST front probability	upwelling index	wind stress (x)	wind stress (y)	wind divergence
projected longitude	0.84	0.30	-0.26	0.08	0.04	-0.02	0.02	0.12	0.16	-0.51	-0.05	-0.39	0.11	-0.02	-0.31	0.12	0.11	-0.24	-0.69	0.53	-0.20	0.27	0.84	-0.53	-0.03
projected latitude		-0.18	0.21	0.01	-0.03	-0.03	0.02	0.05	0.61	-0.18	-0.10	-0.47	0.15	0.00	-0.61	-0.18	-0.19	-0.52	-0.89	0.73	0.07	0.41	0.71	-0.76	0.12
distance to land			-0.90	0.18	0.17	0.05	-0.03	0.15	-0.78	-0.62	0.16	0.08	-0.12	-0.08	0.47	0.65	0.58	0.51	0.30	-0.23	-0.43	-0.22	0.42	0.32	-0.22
depth				-0.27	-0.25	-0.07	0.07	-0.29	0.81	0.63	-0.22	-0.17	0.12	0.05	-0.53	-0.68	-0.61	-0.53	-0.35	0.29	0.43	0.26	-0.37	-0.32	0.29
slope (2 km)					0.90	0.64	0.01	0.19	-0.22	-0.40	0.16	0.16	-0.09	0.25	-0.07	0.18	0.22	0.11	0.20	0.07	0.22	0.07	0.21	-0.17	-0.10
slope (10 km)						0.75	0.02	0.17	-0.21	-0.39	0.16	0.16	-0.08	0.26	-0.09	0.16	0.21	0.11	0.23	0.09	0.32	0.07	0.20	-0.18	-0.06
slope of slope (10 km)							0.01	0.10	-0.12	-0.22	-0.03	0.03	-0.06	0.26	-0.14	-0.06	0.06	0.00	0.16	0.00	0.22	0.06	0.04	-0.12	-0.04
planform curvature (10 km)								-0.22	0.04	0.02	0.02	-0.01	0.00	-0.01	-0.03	-0.01	-0.03	-0.01	-0.01	0.02	0.03	0.03	0.03	-0.05	0.00
profile curvature (10 km)									-0.13	-0.26	0.13	0.09	0.06	-0.04	0.01	0.15	0.21	0.02	0.02	0.05	-0.10	0.07	0.14	-0.04	-0.05
chlorophyll-a										0.44	-0.19	-0.32	0.19	0.15	-0.76	-0.52	-0.52	-0.59	-0.71	0.67	0.44	0.35	0.05	-0.62	0.38
turbidity											-0.26	-0.10	0.00	-0.01	-0.06	-0.41	-0.44	-0.10	-0.06	-0.12	0.13	-0.17	-0.63	0.19	0.19
surface current velocity (u)												0.67	0.09	0.02	0.14	0.48	0.13	0.02	0.34	0.03	0.15	0.10	0.17	-0.08	-0.16
surface current velocity (v)													0.09	0.03	0.31	0.34	0.11	0.07	0.66	-0.29	0.13	0.04	-0.23	0.19	-0.26
surface current divergence														-0.03	-0.15	0.02	-0.01	-0.19	-0.12	0.20	0.02	0.19	0.04	-0.16	0.06
surface current vorticity															-0.36	0.06	-0.01	0.14	-0.04	0.22	0.34	-0.10	-0.03	-0.25	0.21
sea surface height																0.42	0.23	0.53	0.65	-0.73	-0.52	-0.35	-0.23	0.80	-0.43
sea surface height SD																	0.49	0.53	0.33	-0.05	-0.17	-0.15	0.37	0.14	-0.21
anticyclonic eddy probability																		0.30	0.25	-0.09	-0.18	-0.12	0.17	0.16	-0.08
cyclonic eddy probability																			0.46	-0.39	-0.20	-0.46	-0.13	0.53	-0.05
sea surface temperature																				-0.71	-0.04	-0.28	-0.48	0.64	-0.31
sea surface temperature SD																					0.48	0.40	0.54	-0.77	0.39
SST front probability																						0.21	-0.05	-0.44	0.33
upwelling index																							0.27	-0.45	0.05
wind stress (x)																								-0.58	-0.06
wind stress (y)																									-0.20

Table 5. Base-learners employed in the boosted generalized additive modeling framework. Base-learner names are from the 'mboost' package for R (Hothorn et al. 2015; R Core Team. 2017).

Name	Description	Predictor variables	Model component
bols	linear	intercept	p, μ, θ
bols	linear	survey platform	p, μ, θ
brandom	random effect	survey ID	θ
brandom	random effect	transect ID	p, μ
bbs	penalized regression spline[1]	year	p, μ
bbs	penalized regression spline[1]	day of year	p, μ
btree	tree[2]	all climate indices	p, μ
bspatial	penalized tensor product[1]	projected longitude projected latitude	p, μ
brad	penalized radial basis[3]	projected longitude projected latitude	p, μ
btree	tree[4]	distance to land and all bathymetric, oceanographic, and atmospheric variables	p, μ

[1] P-spline basis

[2] Maximum depth = 1

[3] Matern correlation function

[4] Maximum depth = 5

Table 6. Best models with model performance metrics.

Species	Season	Distribution	Start values[1]	Number of boosting iterations	Percent deviance explained[2]	AUC[3]	Spearman rank correlation	Gaussian rank correlation[4]	Median absolute error[5]	Mean absolute error[5]	Median bias[5]	Mean bias[5]	Root mean square error
ARTE	summer	ZINB	GAM	19,537	0.49	0.95	0.10	0.14	0.08	1.66	0.08	-0.11	0.36
ATPU	spring	ZINB	GAM	18,622	0.41	0.92	0.15	0.19	0.14	1.69	0.14	-0.09	0.27
ATPU	summer	ZIP	simple	19,991	0.49	0.98	0.14	0.18	0.08	1.58	0.08	0.01	0.24
ATPU	fall	ZIP	GAM	19,998	0.46	0.96	0.09	0.13	0.15	1.76	0.15	0.07	0.08
ATPU	winter	ZINB	GAM	19,928	0.41	0.95	0.15	0.20	0.12	1.59	0.11	-0.05	0.22
AUSH	spring	ZINB	simple	17,476	0.71	0.98	0.11	0.17	0.09	1.06	0.09	-0.31	0.33
AUSH	summer	ZINB	GAM	14,710	0.52	0.95	0.22	0.28	0.06	1.40	0.06	-0.11	1.39
AUSH	fall	ZINB	GAM	17,610	0.64	0.98	0.14	0.20	0.16	1.36	0.16	-0.21	0.82
AUSH	winter	ZIP	GAM	7,332	0.78	1.00	0.12	0.20	0.00	0.88	0.00	-0.10	0.11
BCPE	spring	ZIP	GAM	14,891	0.74	1.00	0.12	0.19	0.00	0.75	0.00	-0.01	0.12
BCPE	summer	ZINB	GAM	17,498	0.67	0.99	0.16	0.22	0.00	1.35	0.00	-0.19	0.59
BCPE	fall	ZIP	GAM	6,766	0.83	1.00	0.08	0.14	0.00	0.49	0.00	-0.01	0.07
BCPE	winter	ZIP	GAM	9,734	0.86	0.99	0.09	0.16	0.00	0.39	0.00	-0.01	0.05
BLGU	summer	ZIP	simple	19,954	0.59	0.99	0.08	0.13	0.15	1.50	0.15	0.09	0.09
BLKI	spring	ZINB	GAM	19,122	0.51	0.91	0.22	0.25	0.05	1.43	0.05	-0.32	2.82
BLKI	fall	ZINB	simple	18,020	0.56	0.95	0.35	0.40	0.02	1.17	0.02	-0.28	14.91
BLKI	winter	ZIP	GAM	17,973	0.58	0.93	0.48	0.51	0.10	1.07	0.06	-0.07	9.05
BLSC	spring	ZINB	GAM	19,910	0.59	0.95	0.19	0.24	0.02	1.24	0.02	-0.53	24.71
BLSC	fall	ZINB	GAM	19,858	0.48	0.96	0.16	0.21	0.13	1.63	0.13	-0.12	6.34
BLSC	winter	ZIP	simple	9,897	0.58	0.91	0.25	0.26	0.16	1.67	0.14	-0.10	71.51
BOGU	spring	ZINB	GAM	18,906	0.39	0.92	0.17	0.18	0.12	1.63	0.11	-0.27	8.79
BOGU	fall	ZINB	simple	19,892	0.46	0.90	0.11	0.14	0.19	1.95	0.19	0.14	1.49
BOGU	winter	ZIP	GAM	6,819	0.52	0.87	0.25	0.29	0.23	1.40	0.20	-0.15	5.08
BRPE	spring	ZIP	simple	17,205	0.45	0.99	0.08	0.13	0.20	1.51	0.20	-0.01	0.45
BRPE	summer	ZIP	GAM	18,954	0.28	0.99	0.09	0.14	0.00	1.11	0.00	-0.40	0.48
BRPE	fall	ZIP	GAM	16,244	0.43	0.99	0.10	0.16	0.02	1.25	0.02	-0.24	0.67

Species	Season	Distribution	Start values[1]	Number of boosting iterations	Percent deviance explained[2]	AUC[3]	Spearman rank correlation	Gaussian rank correlation[4]	Median absolute error[5]	Mean absolute error[5]	Median bias[5]	Mean bias[5]	Root mean square error
BRPE	winter	ZIP	GAM	17,807	0.59	0.98	0.08	0.12	0.00	1.43	0.00	-0.29	0.51
BRSP	summer	ZIP	GAM	19,249	0.53	0.96	0.13	0.19	0.08	1.42	0.08	-0.07	0.18
BRTE	summer	ZINB	GAM	19,970	0.60	0.95	0.08	0.11	0.10	1.66	0.10	-0.21	0.19
BRTE	fall	ZIP	simple	19,987	0.60	1.00	0.07	0.12	0.30	1.70	0.30	0.33	0.10
COEI	spring	ZIP	simple	4,941	0.43	0.98	0.25	0.31	0.20	1.82	0.19	0.17	260.83
COEI	summer	ZINB	simple	19,997	0.62	0.99	0.10	0.15	0.00	2.62	0.00	1.22	29.83
COEI	fall	ZIP	GAM	8,979	0.64	0.95	0.16	0.21	0.00	1.00	0.00	-1.00	109.23
COEI	winter	ZINB	simple	19,988	0.37	0.94	0.37	0.40	0.03	1.56	0.02	-0.20	425.86
COLO	spring	ZIP	GAM	19,981	0.40	0.91	0.41	0.44	0.19	1.24	0.13	-0.07	1.09
COLO	summer	ZINB	GAM	19,988	0.45	0.94	0.11	0.14	0.08	1.77	0.08	-0.08	0.10
COLO	fall	ZIP	GAM	19,980	0.44	0.95	0.28	0.34	0.11	1.31	0.09	-0.05	0.53
COLO	winter	ZINB	GAM	19,518	0.32	0.82	0.35	0.37	0.50	1.39	0.33	-0.16	3.80
COMU	spring	ZIP	GAM	18,023	0.38	0.92	0.12	0.15	0.22	1.64	0.22	-0.22	0.38
COMU	winter	ZIP	GAM	19,994	0.49	0.95	0.14	0.19	0.02	1.42	0.02	-0.09	0.37
COSH	spring	ZINB	GAM	19,522	0.56	0.98	0.11	0.15	0.07	1.65	0.07	-0.13	0.18
COSH	summer	ZINB	GAM	18,254	0.34	0.84	0.31	0.33	0.32	1.40	0.23	-0.29	5.42
COSH	fall	ZINB	GAM	19,994	0.43	0.89	0.28	0.32	0.15	1.38	0.12	-0.21	3.01
COTE	spring	ZINB	GAM	18,997	0.52	0.97	0.23	0.29	0.02	1.51	0.02	0.03	1.31
COTE	summer	ZIP	GAM	16,732	0.35	0.94	0.30	0.34	0.14	1.47	0.13	-0.02	2.51
COTE	fall	ZIP	simple	13,236	0.53	0.94	0.20	0.24	0.17	1.46	0.15	-0.02	3.60
DCCO	spring	ZINB	GAM	19,171	0.46	0.95	0.11	0.13	0.06	1.48	0.06	-0.43	7.43
DCCO	summer	ZIP	simple	13,180	0.53	0.91	0.09	0.11	0.24	1.79	0.24	-0.10	2.45
DCCO	fall	ZINB	simple	19,999	0.37	0.89	0.10	0.13	0.23	1.54	0.22	-0.42	4.77
DCCO	winter	ZINB	GAM	8,179	0.65	0.91	0.10	0.13	0.09	1.22	0.09	-0.73	3.57
DOVE	spring	ZIP	GAM	16,947	0.53	0.94	0.21	0.28	0.08	1.21	0.07	-0.18	1.39
DOVE	summer	ZINB	GAM	20,000	0.67	0.98	0.06	0.10	0.01	1.36	0.01	-0.30	0.10
DOVE	fall	ZINB	simple	19,792	0.62	0.98	0.18	0.25	0.02	1.07	0.02	-0.20	1.85

Species	Season	Distribution	Start values[1]	Number of boosting iterations	Percent deviance explained[2]	AUC[3]	Spearman rank correlation	Gaussian rank correlation[4]	Median absolute error[5]	Mean absolute error[5]	Median bias[5]	Mean bias[5]	Root mean square error
DOVE	winter	ZINB	GAM	18,923	0.43	0.91	0.27	0.33	0.08	1.17	0.07	-0.34	4.18
GBBG	spring	ZINB	GAM	19,978	0.48	0.86	0.41	0.43	0.13	1.24	0.10	-0.33	18.20
GBBG	summer	ZINB	GAM	19,074	0.47	0.90	0.38	0.40	0.09	1.35	0.05	-0.12	4.36
GBBG	fall	ZINB	GAM	16,719	0.40	0.88	0.46	0.47	0.15	1.30	0.09	-0.13	12.13
GBBG	winter	ZIP	GAM	16,954	0.66	0.89	0.42	0.45	0.10	1.12	0.07	-0.04	11.69
GRSH	spring	ZINB	GAM	19,995	0.72	0.98	0.24	0.32	0.00	1.00	0.00	-0.22	3.36
GRSH	summer	ZIP	GAM	11,197	0.78	0.90	0.50	0.50	0.08	1.03	0.06	-0.04	129.86
GRSH	fall	ZINB	simple	19,961	0.50	0.95	0.59	0.60	0.03	1.08	0.01	-0.13	22.02
GRSH	winter	ZINB	GAM	19,432	0.59	0.98	0.11	0.16	0.02	1.21	0.02	-0.33	0.71
GRSK	fall	ZIP	simple	19,994	0.33	0.95	0.11	0.13	0.20	1.92	0.20	0.01	0.08
HERG	spring	ZINB	simple	17,970	0.42	0.86	0.48	0.51	0.20	1.20	0.13	-0.21	22.70
HERG	summer	ZINB	GAM	17,602	0.50	0.90	0.37	0.40	0.07	1.35	0.04	-0.13	3.92
HERG	fall	ZINB	GAM	17,790	0.42	0.87	0.51	0.52	0.20	1.21	0.10	-0.12	14.84
HERG	winter	ZIP	simple	14,194	0.46	0.85	0.43	0.45	0.30	1.25	0.18	-0.04	10.69
HOGR	winter	ZIP	simple	19,993	0.41	0.94	0.09	0.12	0.26	1.71	0.26	-0.08	0.15
LAGU	spring	ZINB	GAM	17,678	0.52	0.95	0.23	0.29	0.08	1.43	0.07	-0.15	0.75
LAGU	summer	ZINB	GAM	19,997	0.58	0.95	0.30	0.36	0.06	1.24	0.05	-0.13	1.38
LAGU	fall	ZIP	GAM	15,380	0.55	0.94	0.31	0.36	0.06	1.34	0.05	0.00	3.41
LAGU	winter	ZINB	GAM	19,978	0.58	0.97	0.10	0.16	0.09	1.42	0.09	-0.17	0.24
LESP	spring	ZIP	simple	18,370	0.52	0.96	0.15	0.19	0.14	1.47	0.13	-0.06	0.81
LESP	summer	ZINB	GAM	19,925	0.50	0.94	0.36	0.40	0.05	1.21	0.04	-0.18	2.92
LESP	fall	ZINB	GAM	19,989	0.60	0.97	0.19	0.26	0.05	1.29	0.05	-0.23	0.59
LETE	summer	ZIP	GAM	13,589	0.36	0.94	0.08	0.11	0.18	1.76	0.18	-0.02	0.48
LETE	fall	ZINB	GAM	19,977	0.62	0.97	0.08	0.11	0.00	1.99	0.00	0.12	1.22
LTDU	spring	ZINB	GAM	18,504	0.57	0.98	0.33	0.40	0.00	1.11	0.00	-0.51	224.59
LTDU	fall	ZINB	GAM	19,850	0.66	0.99	0.19	0.27	0.03	1.27	0.03	-0.14	15.84
LTDU	winter	ZINB	GAM	14,859	0.61	0.97	0.49	0.53	0.02	1.18	0.01	-0.24	98.27

Species	Season	Distribution	Start values[1]	Number of boosting iterations	Percent deviance explained[2]	AUC[3]	Spearman rank correlation	Gaussian rank correlation[4]	Median absolute error[5]	Mean absolute error[5]	Median bias[5]	Mean bias[5]	Root mean square error
MASH	spring	ZIP	GAM	19,089	0.36	0.93	0.09	0.12	0.32	1.67	0.32	-0.10	0.11
MASH	summer	ZIP	simple	16,998	0.56	0.84	0.10	0.11	0.39	1.68	0.38	-0.26	1.97
MASH	fall	ZINB	simple	19,995	0.29	0.89	0.12	0.15	0.26	1.73	0.25	-0.18	0.27
NOFU	spring	ZINB	GAM	19,994	0.66	0.94	0.43	0.48	0.01	1.08	0.01	-0.26	24.71
NOFU	summer	ZINB	simple	19,619	0.68	0.98	0.24	0.32	0.01	0.94	0.00	-0.45	21.93
NOFU	fall	ZINB	GAM	19,836	0.62	0.96	0.35	0.42	0.00	1.18	0.00	0.13	9.88
NOFU	winter	ZINB	GAM	19,175	0.67	0.98	0.39	0.46	0.01	0.98	0.00	-0.28	15.23
NOGA	spring	ZINB	GAM	19,547	0.44	0.85	0.50	0.52	0.24	1.13	0.12	-0.24	14.42
NOGA	summer	ZIP	GAM	19,934	0.45	0.94	0.27	0.32	0.07	1.39	0.06	-0.07	0.58
NOGA	fall	ZINB	GAM	19,962	0.51	0.91	0.48	0.51	0.12	1.09	0.05	-0.13	4.10
NOGA	winter	ZINB	GAM	18,330	0.41	0.81	0.46	0.47	0.29	1.19	0.16	-0.33	20.58
PAJA	spring	ZIP	GAM	18,341	0.14	0.86	0.05	0.06	0.51	2.01	0.50	0.02	0.05
PAJA	summer	ZINB	GAM	18,311	0.23	0.87	0.05	0.06	0.56	1.97	0.56	-0.01	0.06
PAJA	fall	ZINB	GAM	19,997	0.25	0.83	0.08	0.08	0.51	1.97	0.50	-0.01	0.11
POJA	spring	ZINB	GAM	18,347	0.53	0.96	0.09	0.13	0.27	1.68	0.27	-0.15	0.08
POJA	summer	ZINB	simple	19,991	0.23	0.84	0.07	0.08	0.53	1.96	0.53	-0.02	0.08
POJA	fall	ZINB	GAM	19,998	0.37	0.90	0.19	0.21	0.13	1.77	0.11	-0.06	0.22
RAZO	spring	ZIP	GAM	17,136	0.43	0.94	0.27	0.32	0.08	1.40	0.07	-0.04	1.72
RAZO	summer	ZIP	simple	19,812	0.45	0.98	0.07	0.11	0.16	1.78	0.16	0.14	0.15
RAZO	fall	ZINB	GAM	19,999	0.58	0.97	0.11	0.15	0.09	1.91	0.09	0.29	1.05
RAZO	winter	ZIP	GAM	17,825	0.46	0.91	0.33	0.36	0.12	1.39	0.10	-0.06	4.74
RBGU	spring	ZINB	GAM	19,449	0.46	0.94	0.12	0.16	0.21	1.70	0.21	-0.08	0.36
RBGU	summer	ZINB	GAM	19,580	0.54	0.96	0.06	0.08	0.20	1.44	0.20	-0.54	0.21
RBGU	fall	ZINB	GAM	18,878	0.41	0.90	0.14	0.17	0.15	1.49	0.15	-0.34	1.20
RBGU	winter	ZIP	simple	6,421	0.41	0.88	0.19	0.23	0.30	1.71	0.29	-0.02	2.24
RBME	spring	ZINB	GAM	19,998	0.51	0.93	0.07	0.10	0.11	1.59	0.11	-0.33	0.43
RBME	winter	ZINB	GAM	19,649	0.31	0.89	0.07	0.07	0.53	1.68	0.53	-0.31	1.48

Species	Season	Distribution	Start values[1]	Number of boosting iterations	Percent deviance explained[2]	AUC[3]	Spearman rank correlation	Gaussian rank correlation[4]	Median absolute error[5]	Mean absolute error[5]	Median bias[5]	Mean bias[5]	Root mean square error
REPH	spring	ZIP	GAM	15,470	0.74	0.96	0.19	0.23	0.01	1.23	0.01	-0.27	90.82
REPH	summer	ZINB	simple	18,496	0.31	0.94	0.11	0.16	0.22	1.29	0.22	-0.63	96.77
REPH	fall	ZINB	GAM	19,241	0.38	0.95	0.14	0.17	0.19	1.69	0.19	-0.16	1.45
RNPH	spring	ZIP	simple	17,426	0.31	0.93	0.10	0.13	0.21	1.86	0.20	-0.04	3.18
RNPH	summer	ZINB	GAM	19,999	0.36	0.94	0.10	0.13	0.15	1.56	0.15	-0.27	1.98
RNPH	fall	ZINB	GAM	19,998	0.32	0.89	0.09	0.11	0.48	1.93	0.48	-0.02	0.87
ROST	spring	ZINB	GAM	19,999	0.57	0.98	0.07	0.10	0.12	1.59	0.12	-0.32	0.25
ROST	summer	ZINB	GAM	19,139	0.59	0.97	0.11	0.16	0.00	1.65	0.00	0.00	0.69
ROST	fall	ZIP	simple	12,530	0.46	0.96	0.07	0.10	0.36	2.38	0.36	0.89	0.53
ROYT	spring	ZINB	GAM	19,317	0.68	0.98	0.15	0.22	0.00	1.21	0.00	-0.28	0.58
ROYT	summer	ZINB	GAM	19,995	0.65	0.98	0.14	0.20	0.01	1.32	0.01	-0.15	0.23
ROYT	fall	ZINB	simple	19,985	0.53	0.97	0.15	0.20	0.05	1.61	0.05	-0.08	0.36
RTLO	spring	ZINB	GAM	19,564	0.48	0.93	0.34	0.39	0.08	1.25	0.06	-0.18	1.87
RTLO	fall	ZIP	GAM	17,216	0.45	0.96	0.16	0.21	0.05	1.47	0.05	-0.07	0.61
RTLO	winter	ZIP	GAM	17,073	0.42	0.87	0.33	0.37	0.27	1.42	0.19	-0.03	2.40
SOSH	spring	ZINB	GAM	18,420	0.53	0.95	0.26	0.32	0.02	1.22	0.02	-0.32	5.06
SOSH	summer	ZINB	simple	19,999	0.71	0.93	0.30	0.34	0.01	1.17	0.01	-0.52	57.21
SOSH	fall	ZINB	simple	17,594	0.39	0.92	0.08	0.09	0.27	1.85	0.27	-0.12	0.50
SOTE	spring	ZIP	GAM	11,468	0.63	1.00	0.07	0.13	0.00	1.14	0.00	-0.06	0.84
SOTE	summer	ZIP	GAM	18,403	0.56	0.98	0.09	0.12	0.03	1.67	0.03	-0.07	0.50
SPSK	summer	ZIP	simple	19,994	0.35	0.92	0.07	0.10	0.32	1.85	0.32	-0.02	0.06
SPSK	fall	ZIP	GAM	19,990	0.38	0.96	0.09	0.13	0.16	1.78	0.16	-0.07	0.09
SUSC	spring	ZINB	GAM	17,711	0.57	0.98	0.26	0.33	0.02	1.62	0.02	0.27	9.04
SUSC	fall	ZINB	GAM	19,811	0.55	0.97	0.23	0.31	0.01	1.04	0.01	-0.17	10.73
SUSC	winter	ZINB	simple	19,787	0.61	0.97	0.37	0.44	0.05	1.07	0.04	-0.18	16.31
TBMU	spring	ZINB	GAM	19,993	0.44	0.95	0.15	0.20	0.06	1.43	0.06	-0.20	0.90
TBMU	winter	ZIP	GAM	19,736	0.50	0.97	0.11	0.15	0.16	1.52	0.16	0.03	0.24

Species	Season	Distribution	Start values[1]	Number of boosting iterations	Percent deviance explained[2]	AUC[3]	Spearman rank correlation	Gaussian rank correlation[4]	Median absolute error[5]	Mean absolute error[5]	Median bias[5]	Mean bias[5]	Root mean square error
WISP	spring	ZINB	GAM	18,134	0.58	0.97	0.36	0.41	0.02	1.33	0.01	-0.10	10.65
WISP	summer	ZINB	GAM	19,033	0.38	0.86	0.50	0.52	0.18	1.18	0.10	-0.31	28.20
WISP	fall	ZIP	simple	18,090	0.25	0.96	0.29	0.35	0.08	1.46	0.07	-0.01	3.76
WWSC	spring	ZIP	GAM	9,376	0.49	0.94	0.19	0.24	0.20	1.34	0.20	-0.28	27.23
WWSC	fall	ZIP	GAM	11,397	0.56	0.97	0.20	0.27	0.02	1.23	0.02	-0.09	5.90
WWSC	winter	ZINB	GAM	19,906	0.53	0.95	0.32	0.37	0.05	1.25	0.05	-0.34	20.66

[1] See Section 2.5.5

[2] To calculate percent deviance explained, the saturated likelihood was assumed to be the maximum possible likelihood value, and the null likelihood was calculated from an intercepts-only zero-inflated model fit to the data (unpublished)

[3] Area under the receiver operating characteristic curve for classifying observed counts as 0 or >0

[4] Boudt et al. (2012) and Bodenhofer et al. (2013)

[5] Predicted values minus observed values expressed as a proportion of the mean observed value (i.e., mean count)

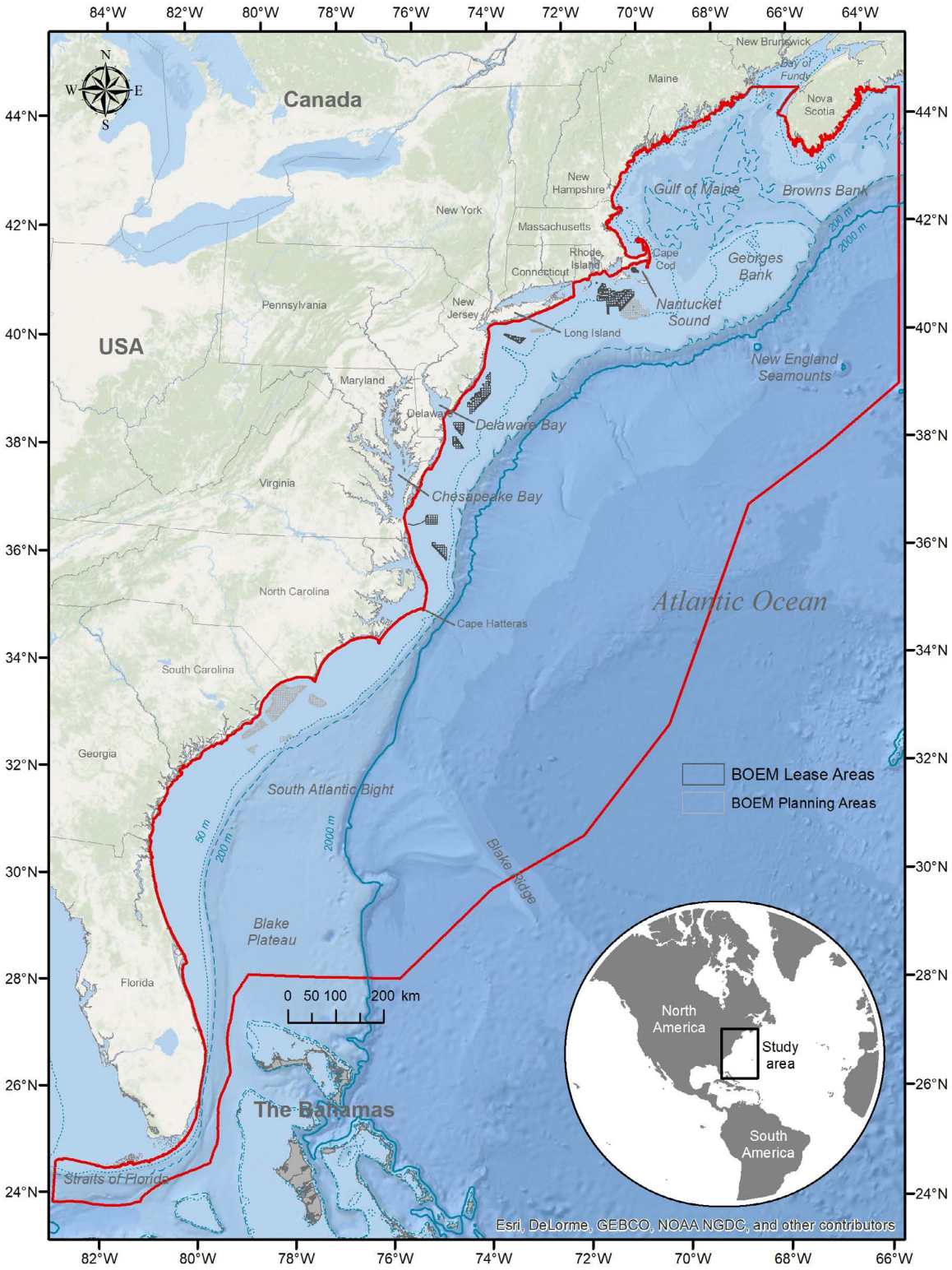

Figure 1. Study area with BOEM Wind Energy Lease and Planning Areas overlaid (approximate boundaries current as of 2017-04-10).

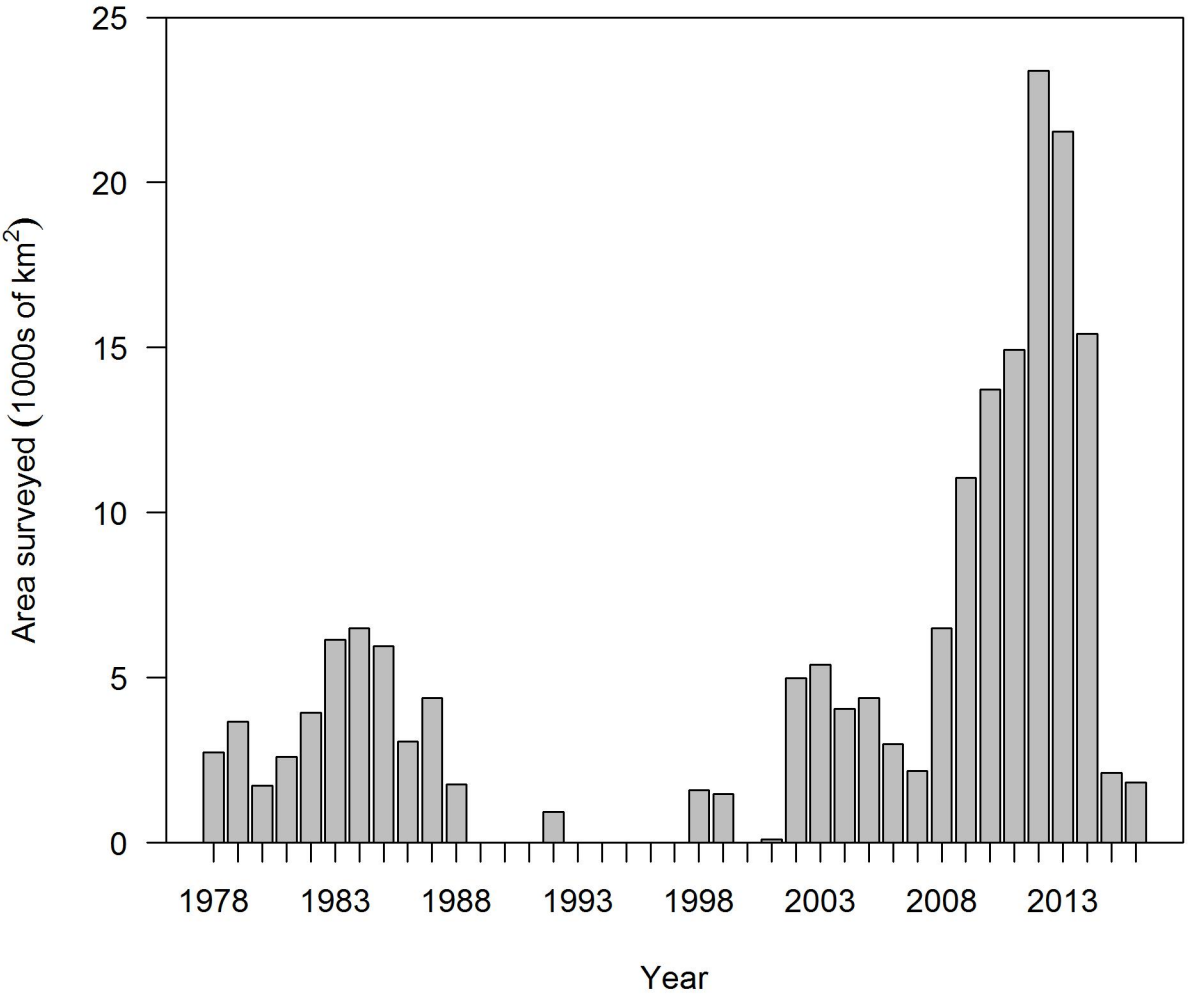

Figure 2. Area surveyed by year.

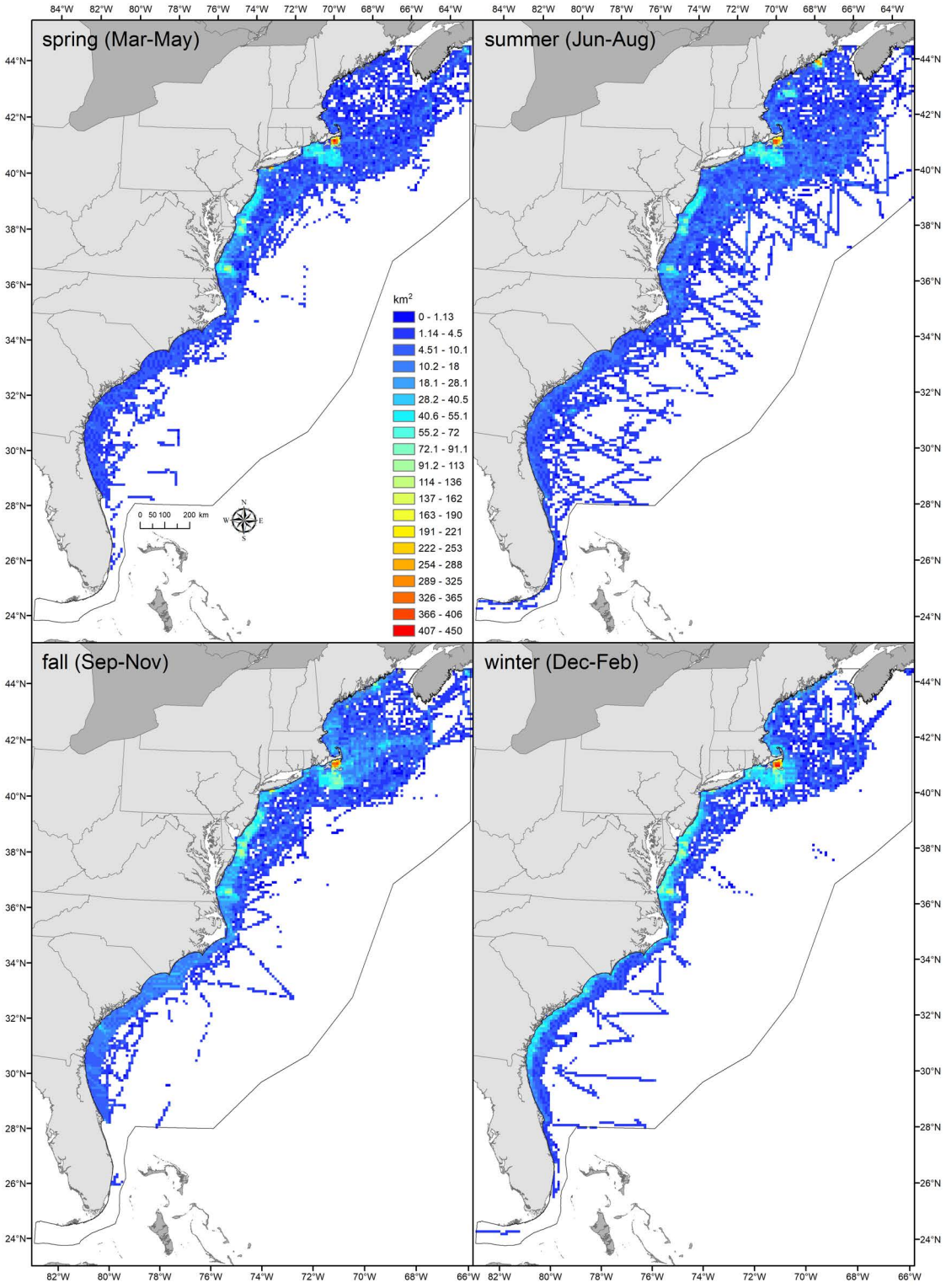

Figure 3. Total area surveyed each season within the study area, binned into 10 x 10 km cells. White areas represent no survey effort. See Appendix A for maps of individual survey effort.

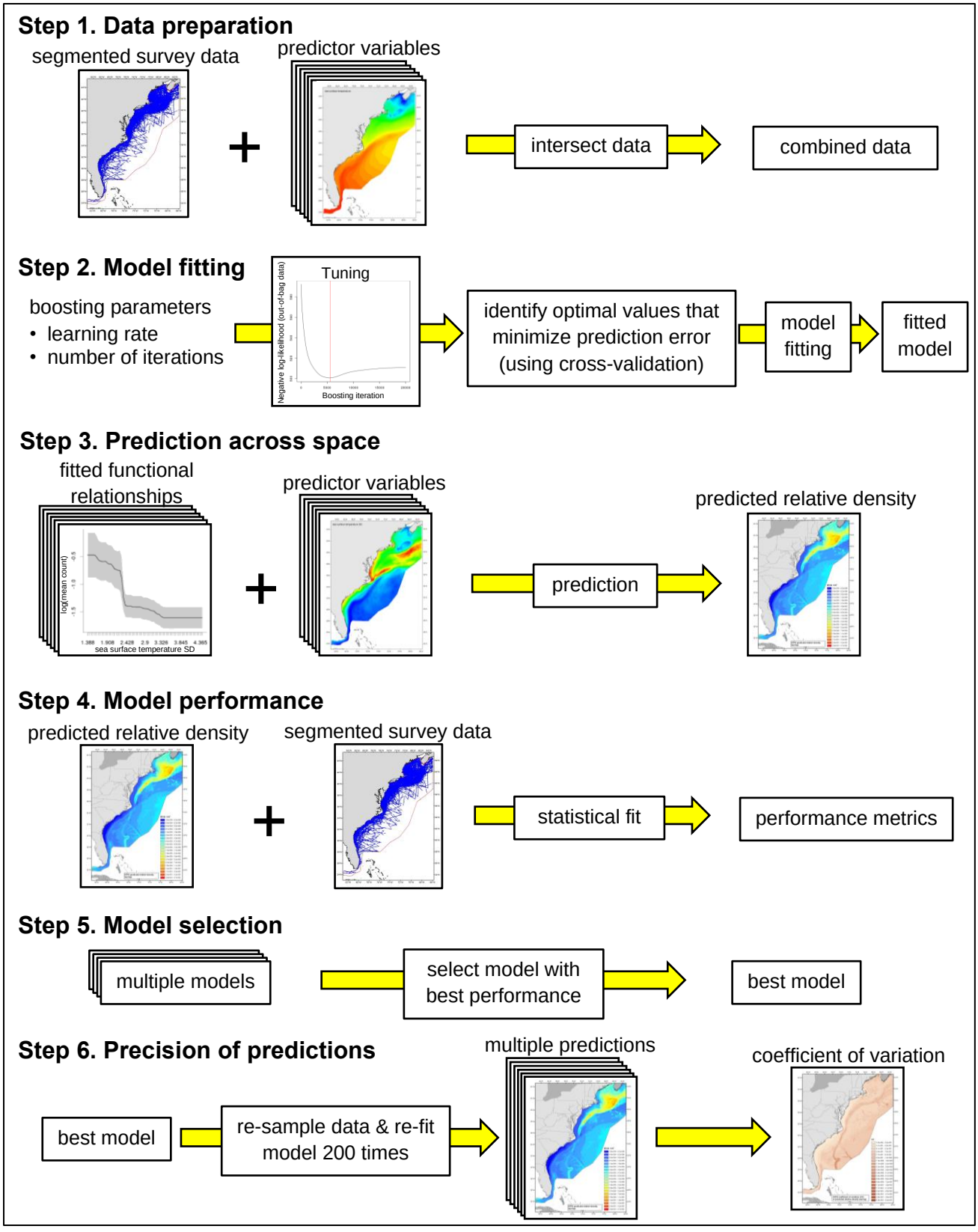

Figure 4. Schematic overview of statistical modeling process. See Section 2 Methods for details.

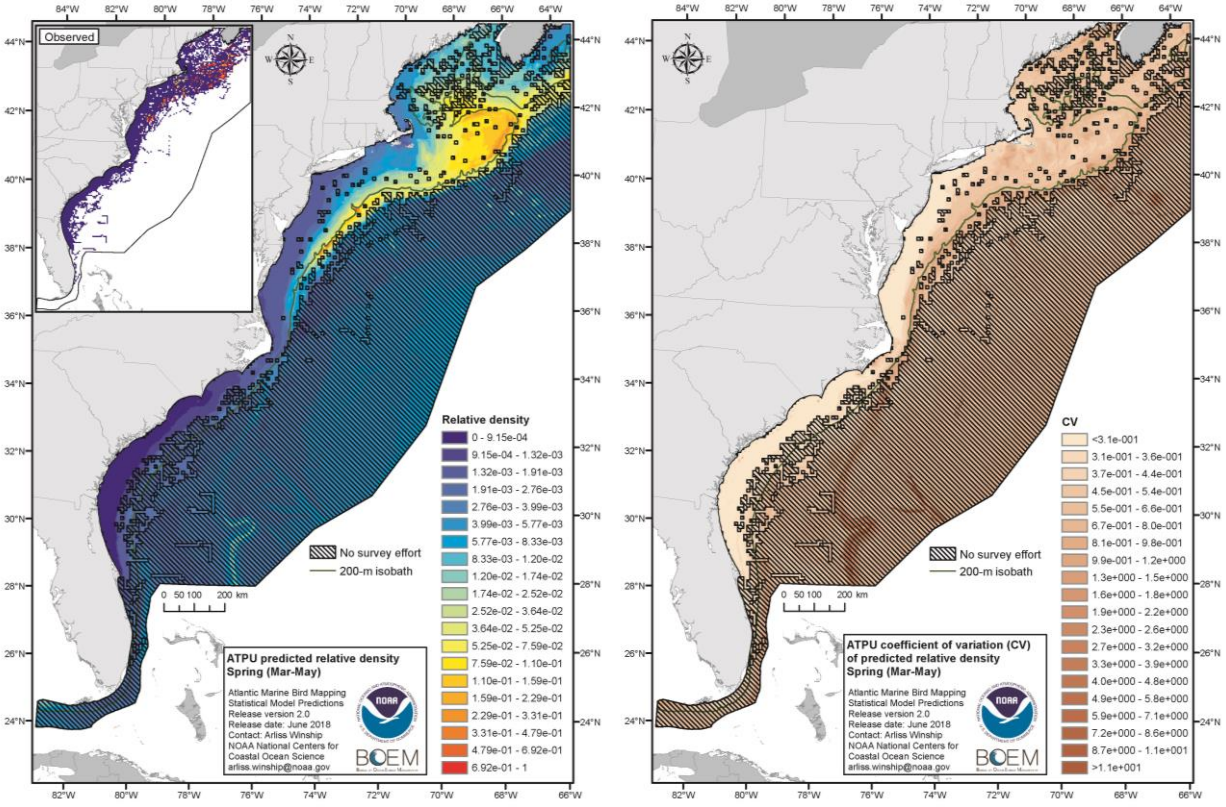

Figure 5. Example maps of predicted relative density and its coefficient of variation (CV) for one species (Atlantic Puffin) and season (spring).

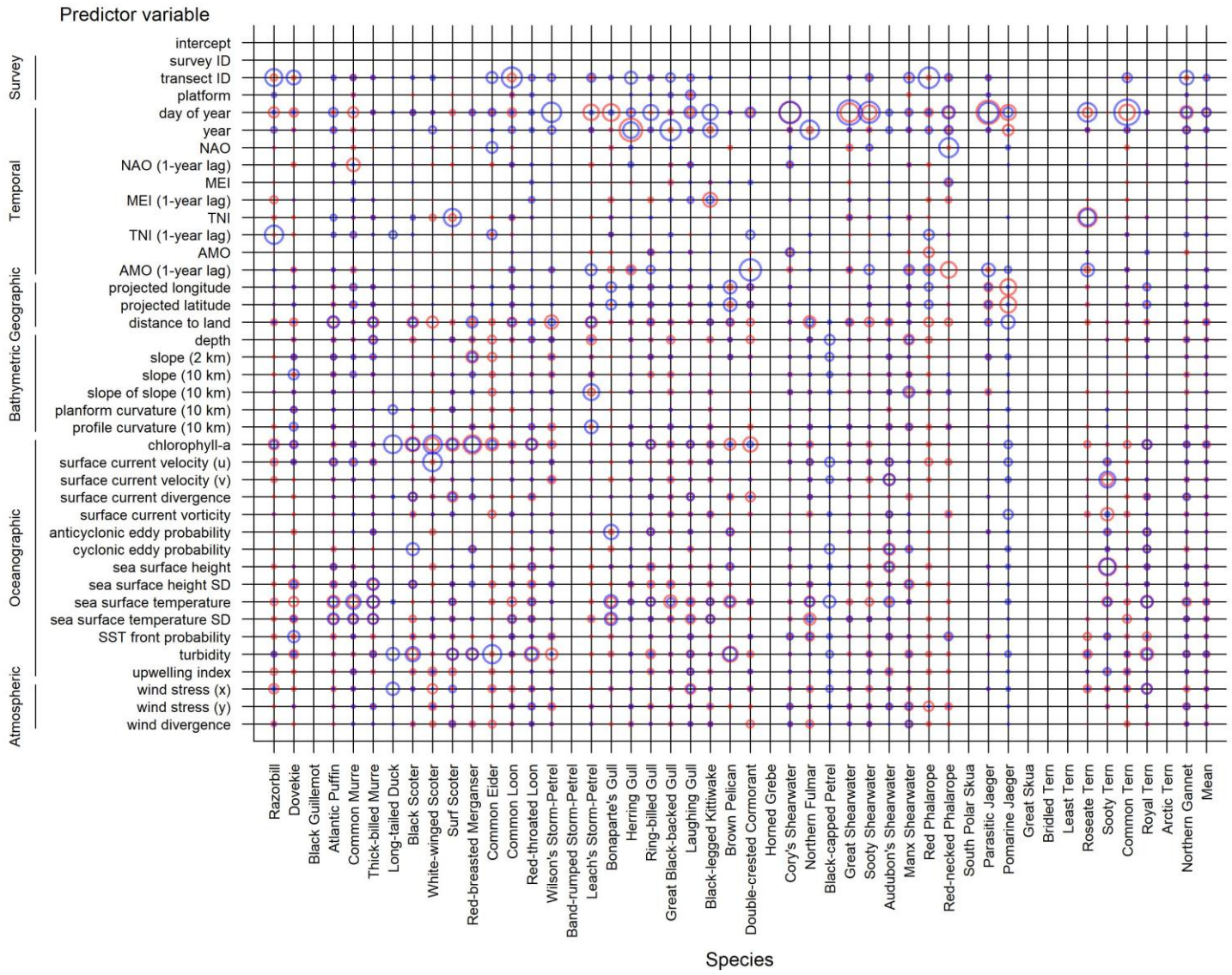

Figure 6a. Relative importance of predictor variables for p (red) and μ (blue) components of best spring (March-May) models. Areas of circles are proportional to importance.

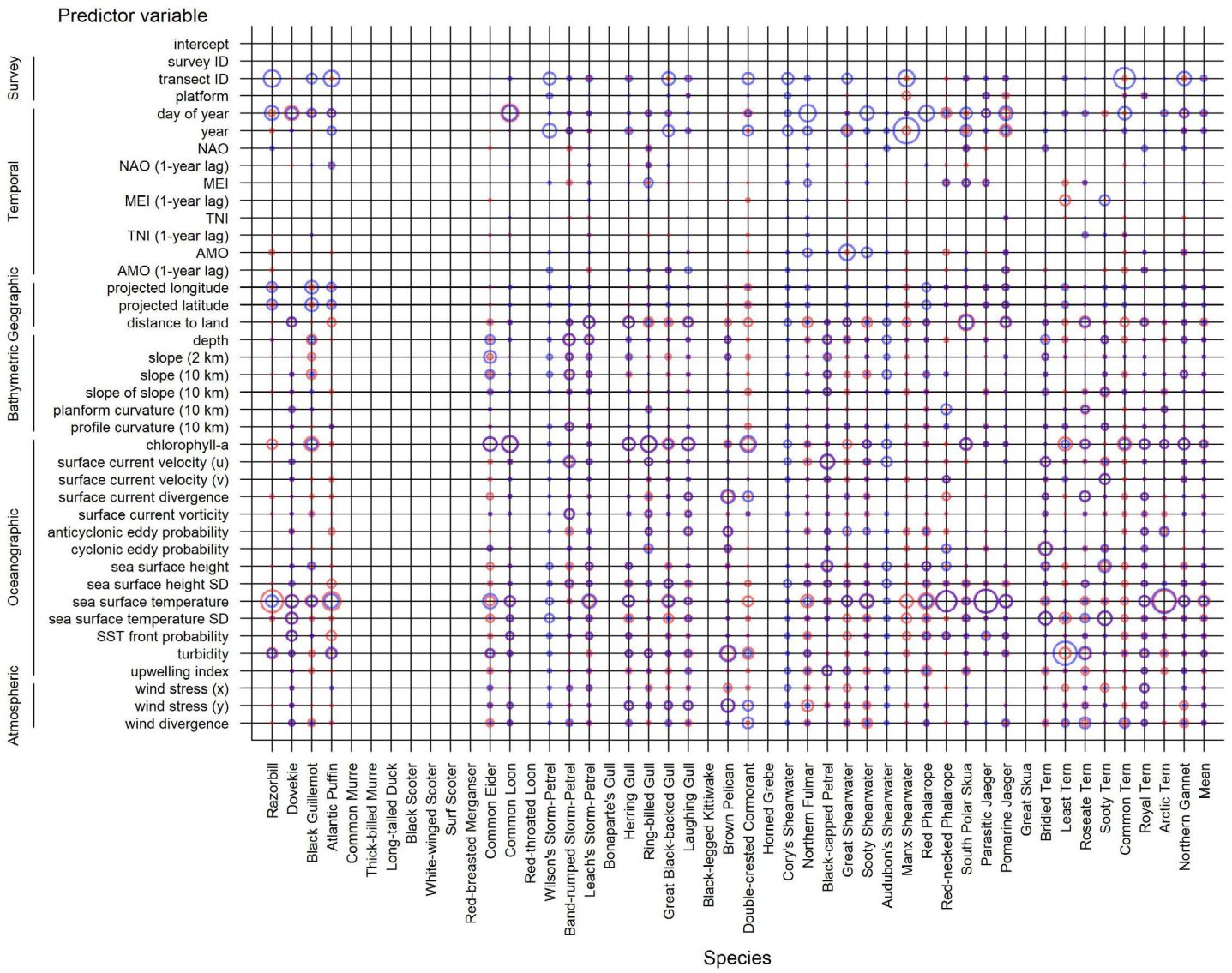

Figure 6b. Relative importance of predictor variables for p (red) and μ (blue) components of best summer (June-August) models. Areas of circles are proportional to importance.

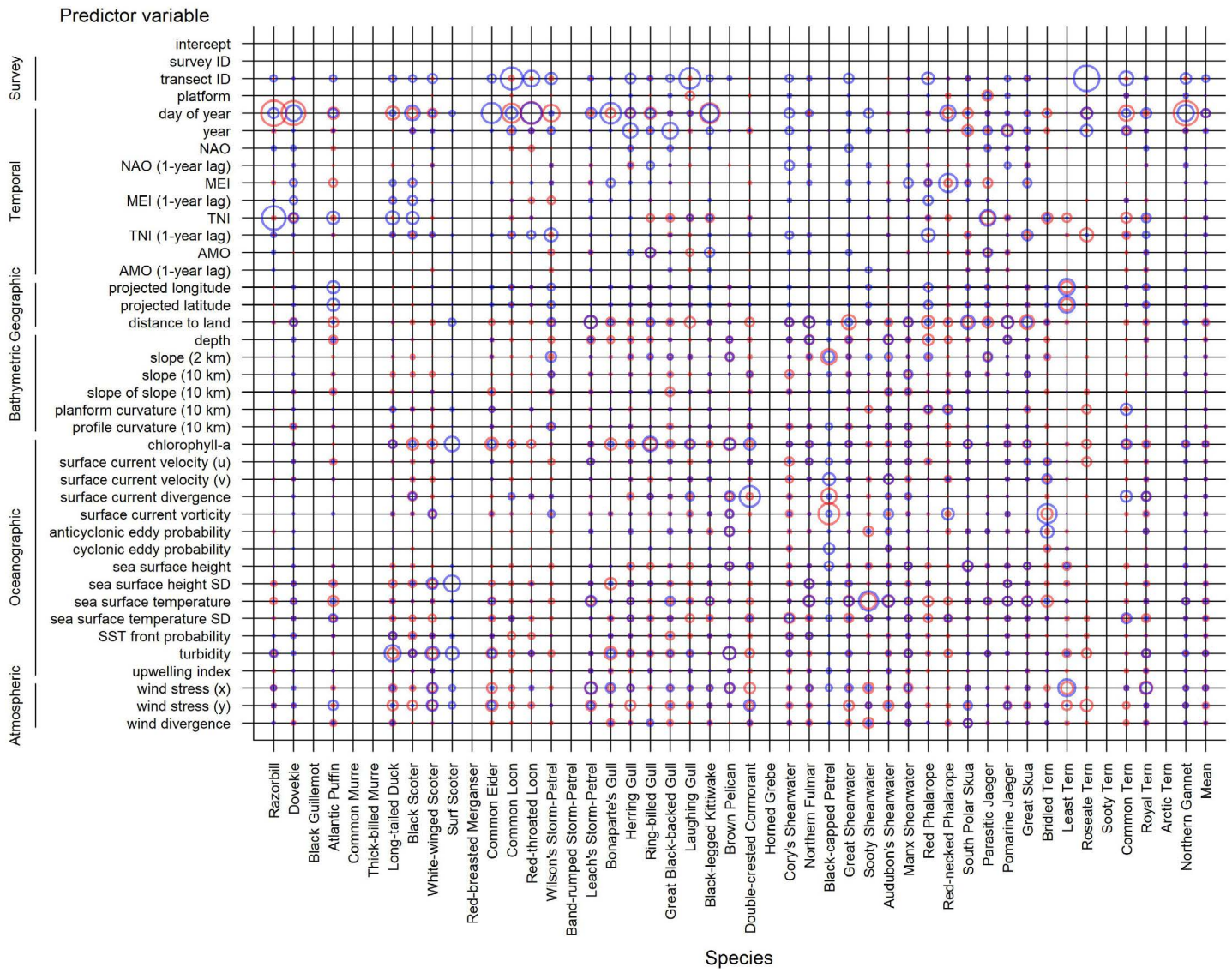

Figure 6c. Relative importance of predictor variables for p (red) and μ (blue) components of best fall (September-November) models. Areas of circles are proportional to importance.

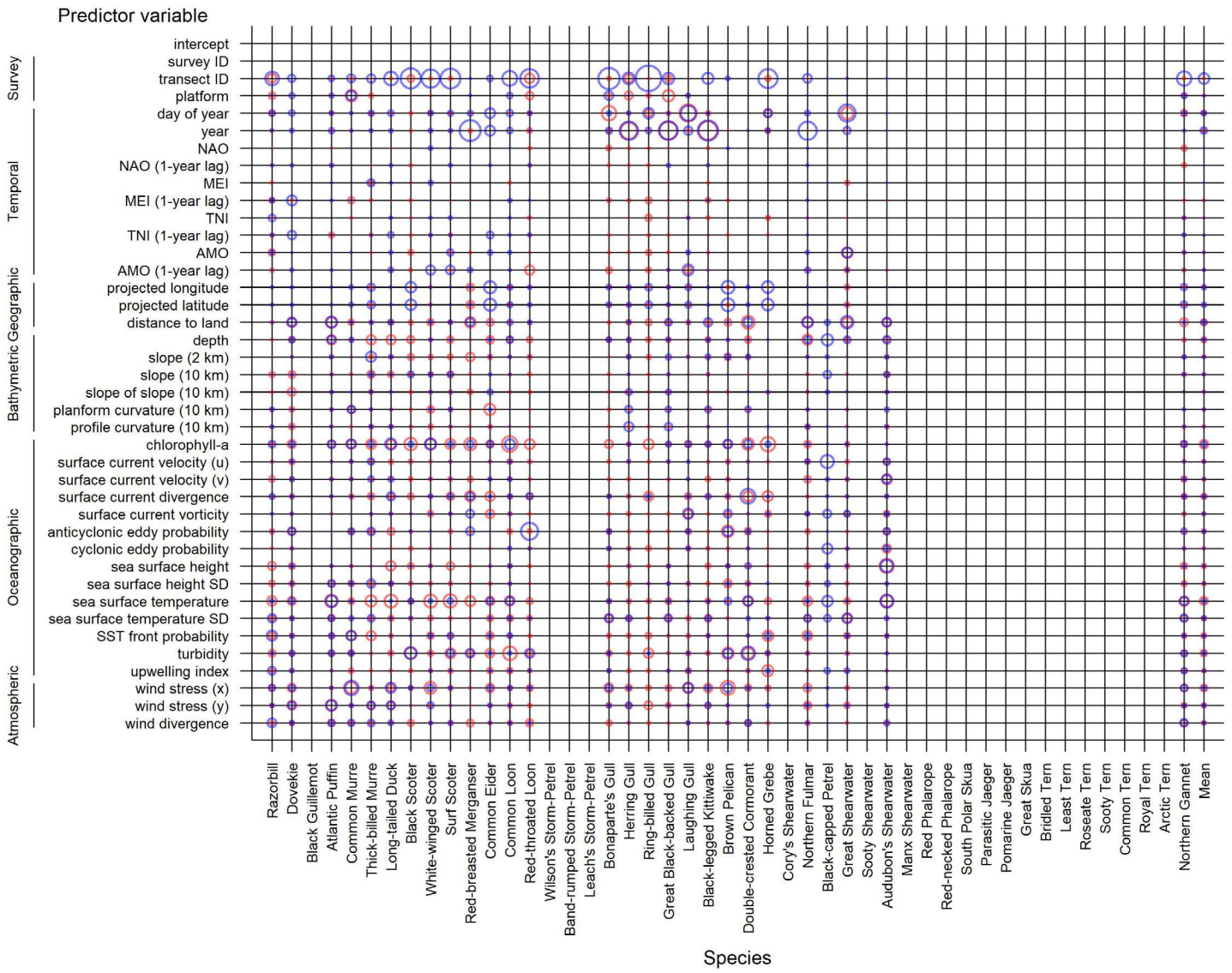

Figure 6d. Relative importance of predictor variables for p (red) and μ (blue) components of best winter (December-February) models. Areas of circles are proportional to importance.

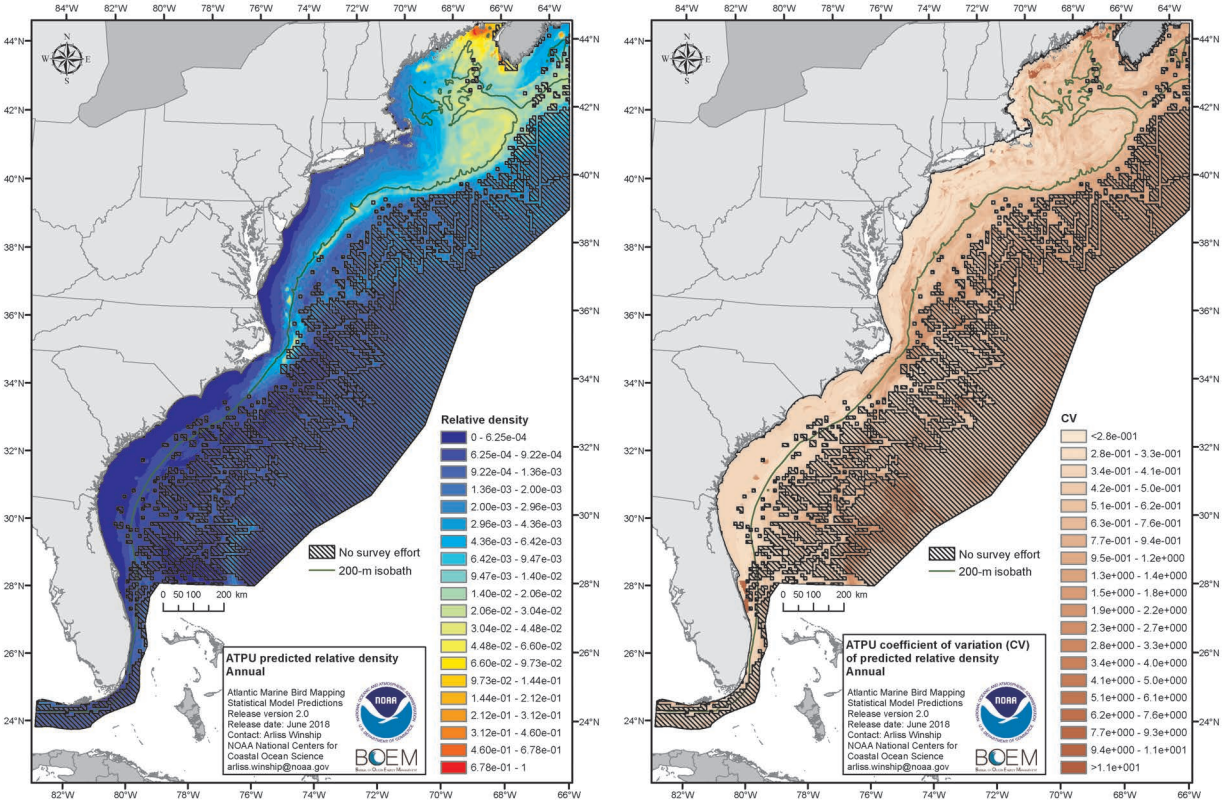

Figure 7. Example annual maps of predicted relative density and its coefficient of variation (CV) for one species (Atlantic Puffin).

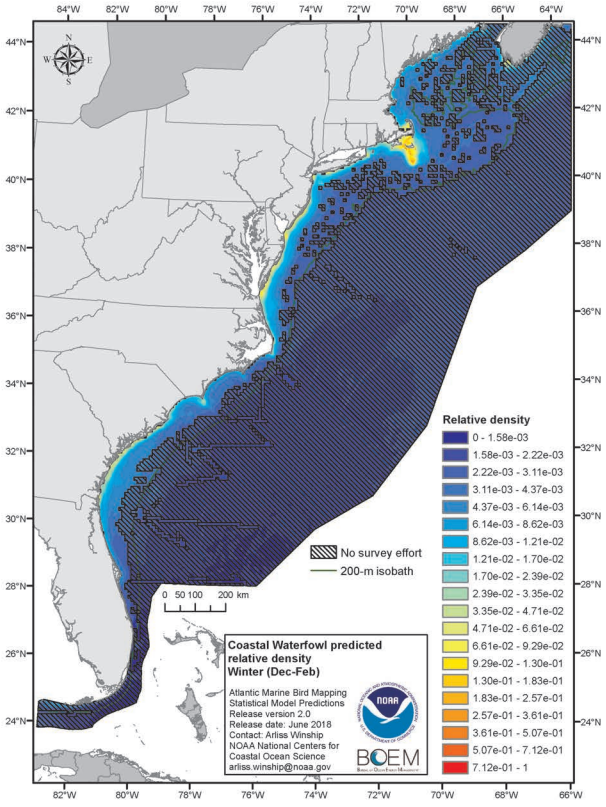

Figure 8. Example map of predicted relative density for Coastal Waterfowl species group during winter. Coastal Waterfowl included Black Scoter, Common Eider, Common Loon, Long-tailed Duck, Red-throated Loon, Surf Scoter, and White-winged Scoter.

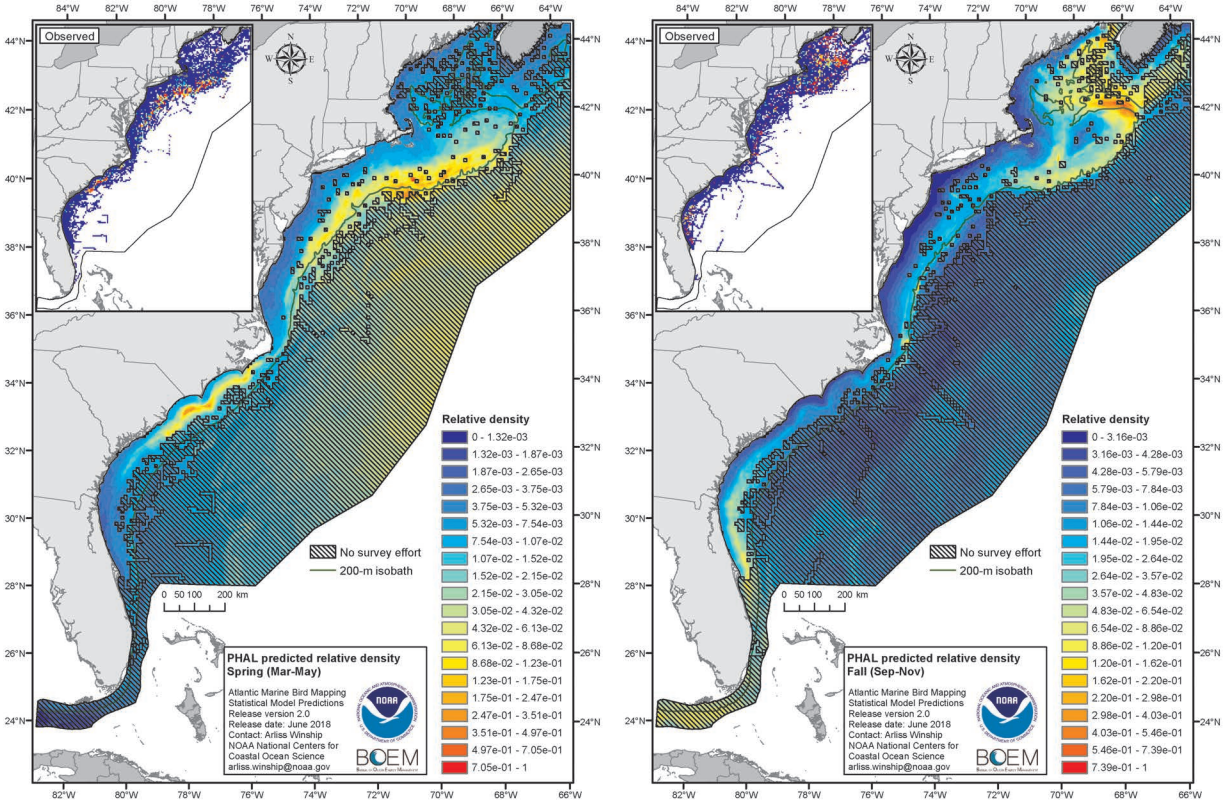

Figure 9. Maps of predicted relative density for phalarope multi-species models for spring and fall. These models were fit to pooled sighting data for Red Phalarope, Red-necked Phalarope, and unidentified phalaropes.

Glossary

Note: many of these definitions are specific to the context of this report.

Area under the receiver operating characteristic (ROC) curve (AUC) – An ROC curve is a graphical representation of how well a model can discriminate between (or predict) two categories of data (e.g., presence/absence), and the AUC is the integral of this curve. AUC values range from 0-1 where a value of 0.5 indicates model performance equivalent to random; a value >0.5 indicates performance better than random; and a value <0.5 indicates performance worse than random. Thus, higher AUC values indicate better model performance.

Autocorrelation – Correlation between data points or residual errors that are close in space and/or time. Spatial data often exhibit autocorrelation, and not accounting for it in predictive models can bias model predictions and artificially inflate statistical precision and significance.

Base-learner – In a boosted generalized additive modeling framework, a relatively simple model relating the response variable to a predictor variable(s). One base-learner is selected in each boosting iteration, and the final model is essentially the sum of modeled relationships across the selected base-learners.

Boosting – Iterative model fitting technique. In each iteration a single base-learner is selected. Each selected base learner's contribution to the final model is controlled by the learning rate.

Bootstrap (non-parametric) – A data re-sampling technique for estimating the statistical uncertainty in model predictions. A dataset of size n is re-sampled with replacement x times to derive x new datasets of size n. The model is fit to each new dataset to derive x predictions. The variability across these x predictions can then be used to evaluate their precision (e.g., coefficient of variation).

Climatology – Long-term spatial pattern in an environmental variable. For example, average values across years at different locations in space during a given annual time period (e.g., monthly, seasonal).

Coefficient of variation (CV) – Measure of dispersion for a distribution, representing the standard deviation (SD) as a proportion of the mean. In this report, CV is calculated from the mean and SD of distributions of bootstrapped model predictions, so the CV actually reflects the standard error (SE) of the prediction relative to the mean prediction. A larger CV indicates more variation (uncertainty) in the prediction relative to the mean prediction and thus lower precision and higher uncertainty.

Cross-validation – A technique for evaluating the predictive ability of a fitted model. The data are divided into in-bag data and out-of-bag data, the model is fit to the in-bag data, and then the fitted model's ability to predict the out-of-bag data is measured.

Ensemble model – A model created by combining multiple models into a single model. In the context of boosting, models are fit iteratively (i.e., after a model is fit, the remaining variation is used to fit the next model) and then combined.

Generalized additive model – A model whose response variable is the sum of multiple, potentially non-linear (e.g., smooth) functional relationships with predictor variables. A link function is employed for the response variable.

In-bag – In a cross-validation context, the subset of data, drawn at random without replacement from the full dataset, that the model is fit to in order to estimate the model parameters.

Learning rate – In a boosting context, the degree to which each base learner contributes to the final model. The optimal learning rate is one that results in well-defined model convergence sooner than later.

Offset (boosting) – In a boosting context, the initial values of each model component that are used to initialize the boosting algorithm.

Offset (effort) – In count models, a model term that accounts for survey effort by enforcing a proportional relationship between the expected count and effort (e.g., area surveyed).

Out-of-bag – In a cross-validation context, the subset of data, drawn at random without replacement from the full dataset, from which the predictive performance of the fitted model is assessed.

Percent deviance explained (PDE) – Measure of the percentage of variation in the data explained by a model beyond that explained by the simplest model without predictor variables. Values normally range from 0-100%, although negative values are possible. Higher values indicate better model performance. PDE is a generalized model analogue of the coefficient of determination (R^2).

Predictive performance – The ability of a model to explain variation in data that the model was not fit to (e.g., out-of-bag data in a cross-validation framework).

Predictor – An independent variable in a model that is used to explain variation in the response.

Rank correlation coefficient – Measure of the correspondence between observed and predicted values. Values range between -1 and 1 where a value of 0 indicates no correspondence between observed and predicted values; a value >0 indicates positive correspondence between observed and predicted values; and a value <0 indicates negative correspondence between observed and predicted values. Thus, positive values closer to 1 indicate better model performance.

Relative density – Model predicted values that are proportional to the expected number of birds per unit area, but that do not represent the actual expected number of birds per unit area. An index of density.

Relative variable importance – Measure of the importance of a predictor variable in terms of the frequency with which that predictor occurred in the selected base-learners across boosting iterations and that predictor's ability to explain variation in the data when it was selected. Relative variable importance was scaled so that it summed to 1 across predictors.

Re-sampling – A method of using randomly drawn subsets of data to estimate statistical precision (e.g., bootstrapping model predictions) or to perform model validation (e.g., cross-validation).

Residual error – Difference between observed data and corresponding model predictions. In this report, residual error is expressed as a percentage of the mean of the data.

Response – The dependent variable in a model representing the quantity of interest for which predictions are to be made.

Spatial predictive modeling – Modeling technique whereby relationships between environmental predictors and a response variable are estimated for areas with survey data, and then these relationships are used to predict the response as a function of the same environmental predictors in areas without survey data.

Stochastic gradient boosting – A type of boosting whereby the data are sub-sampled in each iteration before the base-learner(s) is fit to the gradient.

Tree depth – In a tree base-learner, a parameter that controls the number of allowable nodes in the tree, thereby controlling the number of possible interactions between predictor variables. Greater tree depth allows for more interactions.

Tuning – Procedure by which model fitting parameters are adjusted to maximize the predictive performance of a model. For example, in boosting the learning rate and number of boosting iterations are adjusted during tuning.

Zero-inflated negative binomial (ZINB) distribution – A statistical distribution used to model count data that accounts for a large number of zeroes and an overdispersed count distribution (e.g., because of aggregative behavior of animals).

Zero-inflated Poisson (ZIP) distribution – A statistical distribution used to model count data that accounts for a large number of zeroes.

The Department of the Interior Mission

As the Nation's principal conservation agency, the Department of the Interior has responsibility for most of our nationally owned public lands and natural resources. This includes fostering sound use of our land and water resources; protecting our fish, wildlife, and biological diversity; preserving the environmental and cultural values of our national parks and historical places; and providing for the enjoyment of life through outdoor recreation. The Department assesses our energy and mineral resources and works to ensure that their development is in the best interests of all our people by encouraging stewardship and citizen participation in their care. The Department also has a major responsibility for American Indian reservation communities and for people who live in island territories under US administration.

The Bureau of Ocean Energy Management

As a bureau of the Department of the Interior, the Bureau of Ocean Energy (BOEM) primary responsibilities are to manage the mineral resources located on the Nation's Outer Continental Shelf (OCS) in an environmentally sound and safe manner.

The BOEM Environmental Studies Program

The mission of the Environmental Studies Program (ESP) is to provide the information needed to predict, assess, and manage impacts from offshore energy and marine mineral exploration, development, and production activities on human, marine, and coastal environments.